Diagnosis of Gear Tooth Surface Damage by Analyzing Vibration Signal of Spur Gears

（平歯車の振動信号の解析による歯面損傷診断）

学位取得年月 **2015** 年 **3** 月

Qingrong Fan (范　青荣)

Abstract

Gear device is one of the most commonly used and important components in machine system. Minor gear damage may cause serious failures of the entire equipment even huge economic losses. Consequently, it is crucial to detect the gear damage as early as possible to prevent the system from malfunction. Analyzing the vibration signal on gear or gear box is one of the effective methods to diagnose gear failures. Researchers have done countless studies in this respect and have developed many diagnostic methods based on the analysis of vibration signal in time domain, frequency domain and time-frequency domain. However, the diagnosis of gear damage in most widely used methods is usually based on observing the variations of characteristics between the normal gear and damaged gear. The diagnostic result mainly depends on the experience of operators and is unstable. Therefore, it is important to develop some technique for diagnosing gear damage with satisfactory accuracy independent of artificial experience.

This study proposes an intelligent method for diagnosing gear tooth surface damage by analyzing the vibration accelerations on gear box and bearing box. To investigate the validity of the proposed method, damage contrast test has been carried out in this study. Three kinds of gears namely normal gear, spot damaged gear and pitted gear are tested under different loads and gear rotation speeds on the power circulating type gear testing machine. The vibration accelerations of gear box and bearing box are measured in the experiment. Moreover, in order to illustrate the progression of gear failures and to demonstrate the effectiveness of the proposed approach, the cyclic fatigue test also has been implemented on the power circulating type gear testing machine. A test gear is driven continually with the same rotation speed and load torque. During the cyclic fatigue test, the vibration accelerations on gear box and bearing box are measured at different cycles. Then, techniques of Fast Fourier Transform and discrete wavelet transform are employed to analyze the acquired vibration accelerations. Residual signal and processed signal are respectively acquired by these methods. In order to quantitatively illustrate the characters of vibration accelerations, statistical parameters and characteristic amplitude ratios of frequency bands are extracted from the vibration accelerations. Both of the characteristic amplitude ratios and statistical parameters are together served as failure feature vector for representing different gear conditions. Finally, the technique of support vector machine is employed to diagnose gear condition based on the extracted failure feature vector. The diagnostic results demonstrate the effectiveness of the proposed method. Although a diagnostic method for gear damage based on support vector machines has been proposed, I try to adopt another technique of empirical mode decomposition to

extract failure feature vector for gear damage diagnosis. By the technique of empirical mode decomposition, the original signal is decomposed into several intrinsic mode functions. Then, the characteristic energy ratios are extracted from the intrinsic mode functions as failure feature parameters to be input to the support vector machines classifiers for diagnosis. The validity of the proposed approach is demonstrated by experimental results of cyclic fatigue test.

In Chap. 1 [Introduction], the background of gear damage diagnosis, the objective of this study and the organization of this dissertation are introduced.

In Chap. 2 [Literature Review], literature reviews on diagnostic methods of gear damage are presented.

In Chap. 3 [Types of Gear Failures], the types of gear failures are introduced.

In Chap. 4 [Damage Contrast Test], the experimental method, apparatus and conditions are introduced. The specifications of test gears are presented. In addition, the experimental results are shown and discussed. The acquired data is analyzed using techniques of Fast Fourier Transform and discrete wavelet transform.

In Chap. 5 [Cyclic Fatigue Test], the cyclic fatigue test is introduced. The specifications of test gears and experimental conditions are presented. The experimental results are also shown and discussed. Moreover, the acquired vibration accelerations are also analyzed using techniques of Fast Fourier Transform and discrete wavelet transform.

In Chap. 6 [Diagnosis of Gear Damage Using Support Vector Machines], a method of diagnosing gear damage based on support vector machine is proposed. The algorithm of support vector machines is introduced. The characteristic amplitude ratios of frequency bands and statistical parameters are together served as failure feature vector of gear conditions. Finally, the gear condition is diagnosed by the classifiers of support vector machines based on the extracted feature vector. The diagnostic results are presented. In addition, another diagnostic method based on empirical mode decomposition is proposed to extract failure feature parameters. The algorithm of empirical mode decomposition is introduced. By this method, the obtained vibration signal is decomposed into a number of intrinsic mode functions. Then characteristic energy ratios extracted from intrinsic mode functions and statistical parameters are together served as failure feature vectors to be input into the classifiers for identifying gear conditions. The diagnostic results are shown in the paper.

In Chap. 7 [Conclusions], the conclusions of this study are summarized and the validity of this study is confirmed.

Table of Contents

List of Figures

List of Tables

Notation

$\mathbf{A}$	$m \times m$ orthogonal matrix
a_i	eigenvector of the sample covariance matrix
A_m	amplitude of harmonics
A_j	amplitude of frequency
$a_m(t)$	amplitude modulation function
Ac_i	sample amplitude of i-th intrinsic mode function
b	scalar threshold
$b_m(t)$	phase modulation function
C	penalty constant
c_i	intrinsic mode functions
$d(t)$	resonance signal
E	total energy of intrinsic mode functions
E_i	energy of i-th intrinsic mode function
E_R	characteristic energy ratios of intrinsic mode functions
f_m	frequency of harmonics
$f(\mathbf{x})$	function of separating hyper-plane
$g(t)$	general signal
$h(\mathbf{x})$	decision function for classification
$k(\mathbf{x}_i, \mathbf{x})$	kernel function
$L(\mathbf{w}, b, \alpha)$	Lagrange function
M	order of harmonics
m_1	mean value of the local maxima and minima
$n(t)$	noise signal
N	sampling number of residual signal
P_s	energy of residual signal
P_N	energy of noise
$\mathbf{P}_l$	transformed vector by principal component analysis
p_{m}	principal component
$\mathbf{R}$	vector of characteristic amplitude ratio
r_n	residual data
s	a scaling factor
$S(t)$	original signal

$S(t)_{max}$	local maxima of the signal
$S(t)_{min}$	local minima of the signal
$S_r(t)$	residual signal
$S_p(t)$	processed signal
sgn ( )	sign function
T_i	sum of squares of frequency amplitude
$\mathbf{V}$	transformed input vector for classifiers of SVMs
$\mathbf{w}$	weight vector
$\mathbf{x}$	input vector
$\overline{x}$	mean value of the processed signal
y_i	class label of samples
$\mathbf{Z}_l$	original feature vector
z_m	feature parameter
α_i	Lagrange multiplier
β_1	kurtosis
β_2	skewness
γ	root mean square
ε_i	slack variable
$\emptyset_m$	phase of harmonics
λ	signal to noise ratio
μ	width of Gaussian function
σ	standard deviation
ξ_i	Lagrange multiplier
$\psi(t)$	a wavelet

1 Introduction

1.1 Background

With the progress of science and technology, our life becomes more and more convenient. Meanwhile, machines also have become an indispensable part in people's life. The operation of machines must depend on power supply, such as motor, gasoline engine and so on. However, the machine directly driven by the power is less. Most of the machines are driven by transmitted power through some transmission mechanism. Therefore, the power transmission mechanism is crucial in machine system. There are many kinds of transmission method, including gear transmission, friction transmission, chain transmission, fluid transmission and so on. Because gear transmission has advantages of constant speed ratio, relatively smaller size and high efficiency, a considerable number of machines have adopted the method of gear transmission mechanism [1]. Therefore, gear device performs an important role in the whole machine system. The operation status of gear device can directly affect the working conditions of the whole machine. Consequently, it is crucial to detect the gear damage as early as possible to prevent the system from malfunction [2].

In order to keep the gear device in good condition, it is necessary to conduct maintenance work at appropriate regular intervals. State maintenance method is a commonly used technique to check the deterioration situation of the equipment without disassembling machines. Because of its high efficiency and lower cost, this technology has been widely applied in the field of damage detection in industrial production [3]. According to the state maintenance method, analyzing the vibration signal of gearbox is one of the effective methods to diagnose gear conditions. It is usually to measure the vibration or noise on gear box, and diagnose the device condition using the vibration characteristics. Although the research on gear vibration characteristics has been carried out for a long period, the developed vibration theory mainly applied to the normal gear condition, it is difficult to analyze the abnormal gear condition based on the existed theoretical acknowledgement. In practical application, the diagnosis of gear damage is usually based on observing the variations of characteristics between the normal gear and damaged gear, the diagnostic result mainly depends on the experience of operators. Therefore, it is important to develop some diagnostic techniques to precisely detect gear damage independent of manual experience.

Because of unsteady gear rotation, lubrication situation, tooth stiffness variations, and other reasons, the collected vibration signal on gear box is usually non-stationary, and the failure

symptoms are not obvious especially in the early stage of gear failure [4]. It is difficult to extract distinctive characters from the vibration signal. Hence, how to emphasize the failure characteristics in the measured signals and extract suitable failure features from collected data is crucial for gear failure diagnosis. To address this, researchers have done countless studies in this respect and a lot of methods have been developed in the time domain, frequency domain and time-frequency domain [5]. In addition, with the development of artificial intelligence, many intelligent technologies, such as expert system, neural network and so on, have been developed and applied to the failure diagnosis of machines. Comparing with the traditional methods, these techniques can identify the gear condition automatically by computer according to the quantitative characteristic parameters extracted from the vibration signal.

This study proposes an intelligent method for diagnosing gear tooth surface damage by analyzing the vibration accelerations on gear box and bearing box. To investigate the validity of the proposed method, damage contrast test has been carried out in this study. Moreover, the damage contrast test is used to investigate the influence of load torques, gear rotation speeds and size of gear damage on the vibration accelerations. Three kinds of gears namely normal gear, spot damaged gear and pitted gear are tested under different loads and gear rotation speeds on the power circulating type gear testing machine. The vibration accelerations of gear box and bearing box are measured in the experiment. Moreover, in order to illustrate the progression of gear failures and to demonstrate the effectiveness of the proposed approach, the cyclic fatigue test also has been implemented on the power circulating type gear testing machine. A test gear is driven continually with the same rotation speed and load torque. During the cyclic fatigue test, the vibration accelerations on gear box and bearing box are measured at different cycles. The technique of Fast Fourier Transform is employed to analyze the original signal, by which the frequency spectrum is obtained. Then, the characteristic amplitude ratios of frequency bands are computed from the frequency spectrum to represent the frequency-domain characteristics of the signal. Because the collected vibration signal is usually non-stationary, and the failure symptoms are not obvious especially in the early stage of gear failure. In order to emphasize the failure characteristics of the measured signals, the residual signal is extracted from the original vibration accelerations. Moreover, the method of discrete wavelet transform is adopted to reduce noise from the residual signal. The processed signal is obtained by reconstructing the coefficients of discrete wavelet transform. Additionally, statistical parameters are extracted from the processed signal. Both of the characteristic amplitude ratios and statistical parameters are together served as failure feature vector to quantitatively represent the distinctive features of different gear conditions. Then, the technique of support vector machine is employed to detect gear condition based on the extracted failure feature vector. The diagnostic results demonstrate the effectiveness of the developed method.

Although a diagnostic method for gear damage using support vector machines has been proposed, I try to adopt another technique of empirical mode decomposition to extract appropriate failure feature parameters to improve the diagnostic accuracy. Because of its excellent generation capability, the empirical mode decomposition has been proved for more effectively dealing with data from non-stationary and nonlinear processes. With the initial processing of empirical mode decomposition, the original signal is decomposed into several intrinsic mode functions. Then, the characteristic energy ratios of intrinsic mode functions and statistical parameters are combined as failure feature vectors to be input to the support vector machine classifiers for gear damage diagnosis. The validity of the proposed approach is demonstrated by experimental results of cyclic fatigue test.

1.2 Objectives

The main objective of this study is to develop an intelligent method for diagnosing gear tooth surface damage effectively by analyzing vibration accelerations on gear box or bearing box. Consequently, the following four tasks are to be performed in this study:

(1) To carry out experiments under different load torques and gear rotation speeds, through which the vibration accelerations of gear box and bearing box are acquired and analyzed.

(2) To present a method for emphasizing the failure characteristics in the obtained vibration signals, by which the noise and other interferences can be reduced from the original data. The evidence of damage can be visually detected from the signal as far as possible.

(3) To develop a method of extracting appropriate failure feature parameters from the vibration signals, by which the extracted feature parameters can quantitatively represent the distinctive features of different gear conditions.

(4) To develop a method for diagnosing gear damage automatically based on the extracted failure feature vector, by which the gear damage can be detected accurately independent of manual experience.

1.3 Organization

This dissertation consists of seven chapters. The specific arrangement of this paper is organized as follows.

In Chap. 1 **[Introduction]**, the background of gear damage diagnosis, the objective of this study and the organization of this dissertation are introduced.

In Chap. 2 **[Literature Review]**, literature reviews on diagnostic methods of gear damage are presented.

In Chap. 3 **[Types of Gear Failures]**, the types of gear failures are introduced.

In Chap. 4 **[Damage Contrast Test]**, the experimental method, apparatus and conditions are introduced. The specifications of test gears are presented. In addition, the experimental results are shown and discussed. The acquired data is analyzed using techniques of Fast Fourier Transform and discrete wavelet transform. The frequency spectrum, residual signal and processed signal are obtained and shown in the paper.

In Chap. 5 **[Cyclic Fatigue Test]**, the cyclic fatigue test is introduced. The specifications of test gears and experimental conditions are presented. The experimental results are also shown and discussed. Moreover, the acquired vibration accelerations are also analyzed using techniques of Fast Fourier Transform and discrete wavelet transform, by which the frequency spectrum, residual signal and processed signal are acquired.

In Chap. 6 **[Diagnosis of Gear Damage Using Support Vector Machines]**, a method of diagnosing gear damage based on support vector machine is proposed. The characteristic amplitude ratios of frequency bands are extracted from the frequency spectrum of original signal. Statistical parameters are also extracted from the processed signal. Then, the characteristic amplitude ratios of frequency bands and statistical parameters are together served as failure feature vector of gear conditions. Finally, the gear condition is diagnosed by the classifiers of support vector machines based on the extracted feature vector. The diagnostic results are presented. In addition, another method based on empirical mode decomposition is proposed to extract failure feature parameters. By this method, the obtained vibration signal is decomposed into a number of intrinsic mode functions. Then, characteristic energy ratios extracted from intrinsic mode functions and statistical parameters are together served as failure feature vectors to be input into the classifiers for identifying gear conditions. The algorithm of support vector machines, principal component analysis and empirical mode decomposition is also introduced in the chapter. The diagnostic results are shown in the paper.

In Chap. 7 **[Conclusions]**, conclusions of this study are summarized and the validity of this study is confirmed.

2 Literature Review

2.1 Diagnostic Methods of Gear Damage

Gear is one of the most important and commonly used components in machine system. Minor gear damage may cause fatal failures of the entire equipment, even huge economic losses. Consequently, failure diagnosis especially early detection of gear damage is crucial to prevent the mechanism from malfunction. However, because the motion of gear device is always inevitably affected by the motion of other components in the system or the environment disturbances, the failure symptoms are not obvious especially in the early stage of gear failures. Therefore, it is difficult to precisely diagnose gear failures in the early stage. In past years, researchers have done countless effort to study the characteristics of gear failures and have developed many methods to detect gear failures by using techniques of acoustic emission, stress wave analysis, laser scattering, vibration signal analysis and so on.

Acoustic emission is gaining ground as a non-destructive technique for health diagnosis on rotating machinery, including gearboxes [6]. Singh et al. performed three experiments to investigate the feasibility of applying acoustic emission to gear fault diagnosis [7,8]. It is concluded that the acoustic emission technique is a useful diagnostic tool in condition monitoring of gears. Al-Balushi and Samanta also developed a technique for early fault diagnosis of gears by using energy-based features extracted from time domain acoustic emission signals of a test gearbox [9]. In addition, the experimental results demonstrate the effectiveness of the proposed method in monitoring and diagnosis of machine conditions, with the capability of early fault detection. Stress wave analysis is able to provide real-time measurement of shock and friction in operating process of gear device, as well as filter out interference vibration signal and audible noise because of its high frequency acoustic sensing technology. Board [10] demonstrated the ability of stress wave analysis to accurately detect a broad range of discrepant gears conditions and to characterize the severity of damage, by carrying out experiments on several diverse types of aircraft and industrial gears. The fault diagnosis principle of laser scattering is comparing the variations of laser reflection data between initial and the current conditions. If the laser-scattering data varies over some threshold value, we can estimate conditions on the tooth surface and detect damages such as abnormal abrasion, pitting, spalling, etc. based on the results. Tanaka et al. proposed an in situ method to accurately diagnose gear tooth surface damage at the early stage using scattering of a laser beam [11]. In order to confirm the effectiveness of the proposed method, a cyclic fatigue test was performed. A tooth surface is first irradiated at oblique incidence by a zone-covering laser

beam, and the zone is scanned along the surface of the gear tooth by the rotation of the gear. By analyzing variations in laser scattering between benchmark data and the current data, the condition of the gear-tooth surface can be estimated. The technique of vibration signal analysis is to detect gear failures by studying the vibration characteristics of gear or gear box. In the operating process of gear device, comparing with the normal gear condition, the gear failures will intensify or change the vibration of gears. Therefore, the gear conditions will be comprehensively and effectively reflected in the vibration signal of gear or gear box. Especially, analyzing the vibration signal of gear or gear box is one of the most effective methods applied in the detection of gear failures because of its simple operation and availability.

For studying the characteristics of the vibration signal, researchers have done countless effort in this respect and various technologies in time domain, frequency domain and time-frequency domain have been developed and widely applied in condition monitoring and diagnosis of gear device. In the past years, a great of technologies are reported in the literatures.

In the field of time-domain analysis, time-synchronous averaging is an effective technique to reduce the effects of noise and environment disturbances by removing any uninterested non-periodic events from the original signal. Some processing techniques of time-synchronous averaging are satisfactorily developed for the early detection of gear failures. Mafadden extracted residual signal by subtracting the regular tooth meshing harmonics from the original time domain vibration signal using technique of time-synchronous averaging [12]. The residual signal is proved to have excellent capability and better sensitivity to the representation and modulation phenomenon of gear damage, which can contribute to the diagnosis of gear damage. The validity of the proposed method is confirmed by an application to the early detection of gear failures. Mafadden and Dalpiaz estimated the location of damage on tooth surface by calculating the amplitude and phase angle of the vibration function of residual signal which is acquired using technique of time-synchronous averaging [13-15].

Concerning frequency-domain analysis, it is well known that the fault condition of gears can be observed from the meshing frequency and its harmonics, together with sidebands due to modulation phenomenon. Damages on gear tooth surface will produce modulation effects during the meshing of failure teeth, repeated once each revolution of the gear. The increment in the number and amplitude of sidebands with interval space of the failure gear rotation frequency may indicate a fault condition. Therefore, gear damage can be detected with analyzing the frequency spectrum of vibration signals. Randall studied the effects of various types of faults on the spectrum of vibration signals, and presented an alternative approach which is capable to the monitoring and diagnosis of gearbox faults in 1982 [16]. Researchers also have developed many methods for

diagnosing gear failures with combining spectra analysis with other techniques. The spectra analysis may be incapable of detecting gear failures at an early stage. Because the vibration is usually disturbed by other mechanical components, it may be difficult to evaluate the spacing and evolution of sidebands. Therefore, many researchers have developed other analysis techniques, such as cepstrum analysis [17, 18], cyclostationary analysis [19-21], high-resolution spectral analysis techniques [22] and so on.

Local faults in gears always produce transient modifications in vibration signals. Therefore, these signals have to be considered as non-stationary. Most widely used traditional signal processing techniques are based on the assumption of stationary signal [18]. Thus, they are not fully suitable for the detection of short-duration dynamic phenomena. Besides, the time-domain map or the frequency-map can just represent the partial characteristics of the vibration signal. Because the time-frequency analysis not only can present time and frequency information of a signal simultaneously by time-frequency map but also enables the detection of transitory phenomena, the time-frequency methods (in particular wavelet transform) are currently favored in gear failure diagnosis [23]. The study of wavelets is started in the 1980's by Morlet, Grossmann, Meyer, Mallat and others [24-27], but it is well known in 1988 by the paper written by Daubechies [28] which caught the attention of larger applied mathematicians in signal processing, statistics and numerical analysis. Wang and McFadden [29] are the pioneers of analyzing the vibration signal analysis in gears using the technique of wavelet transform. Results show that wavelet transform has the capacity of detecting both mechanical incipient failures and different types of faults simultaneously. With the development of wavelet transform, many techniques, including continuous wavelet transform, discrete wavelet transform, wavelet packet transform, Hilbert transform and so on, have been proposed and successfully applied to the non-stationary vibration signal processing and failure diagnosis [30-32]. The discrete wavelet transform, which is based on sub-band coding, is known as its fast application and excellent capacity to concentrate information. Wu and Hsu [33] adopted the technique of discrete wavelet transform to analyze the vibration signals in a gear-set experimental platform. The feature vector for gear faults diagnosis is extracted based on discrete wavelet transform. Saravanan and Ramachandran [34] extracted feature parameters from the vibration signals for diagnosing different conditions of gear box by using discrete wavelet transform. The application of discrete wavelet transform to feature extraction is demonstrated by the vibration signal of a spur bevel gear box in different conditions. The results show that the discrete wavelet transform enables to represent all possible types of transients in vibration signals generated by gear faults and make a great contribution to condition monitoring and fault diagnosis of gears. Continuous wavelet transform can provide a finer scale resolution and excellent visual inspection for the analysis of vibration signals. Dalpiaz et al. [18] presented a method to deal with gear

condition monitoring with using the visual advantages of continuous wavelet transform. Particularly, the diagnostic capability of continuous wavelet transform is proved when the residual part of the time-synchronous averaged vibration signal is used. Zheng et al. [35] proposed an approach based on continuous wavelet transform to diagnose and localize the faults on tooth surface. Wavelet packet transform divides the frequency space of vibration signal into various parts and allows a better time-frequency localization of signals. It has been widely used as a diagnostic method recently [36, 37]. Nikolaou and Antoniadis [36] adopted energy analysis of coefficients of wavelet packet transform for fault detection. Yen and Lin [37] used the wavelet packet transform to decompose the vibration signal, and select the wavelet packet node energy as feature parameters for fault diagnosis. The proposed method is investigated by experiments on gearboxes with several types of faults in a helicopter. The results show that the wavelet packet-based method is more robust to the white noise. Hilbert transform, which is a time-domain convolution, has been demonstrated to be useful for demodulation of vibration signals [38]. Fan and Zuo [39] proposed a new diagnostic method for gear damage that combines Hilbert transform and wavelet packet transform. Using the wavelet packet transform, the failure features of frequency components are extracted from the processed signal which is obtained by removing carrier signals from the vibration signal by Hilbert transform. The vibration signals collected from a gear box are used to confirm the validity of the presented method. Results show that the proposed method is effective to extract modulating signal and help to detect the early gear fault.

Moreover, the statistical method is also an effective technique for detection gear damage diagnosis. The statistical parameters, including standard deviation, root mean square value, kurtosis, skewness, crest factor and so on, are sensitive to the variation in the vibration signal generated by the failure on gear tooth surface. The employ of statistical parameters have shown strong performance for diagnosing gear faults in several studies. Pachaud et al. [40] investigated the effect of crest factor and kurtosis in the monitoring of rotating machinery. By using a simple model, the properties and the limitations of these indicators are demonstrated and illustrated with real examples. Wang, et al. [41] presented an approach which explores the properties of kurtosis, mean, variance, form factor and crest factor of the mean amplitude of continuous wavelet transform coefficient as quantitative indicators of gear failure, with employing the method of the continuous wavelet transform to analyze the time synchronously averaged residual signals. The statistical parameters are proved to be insensitive to the gear conditions.

In most widely used methods, the diagnosis of gear faults is usually based on observing the differences in vibration signals between the normal gear and damaged gear, the diagnostic result mainly depends on the experience of operators. With the development of artificial intelligence, many intelligent diagnostics system based on technologies, such as artificial neural network,

pattern recognition and support vector machines, have been developed and applied to the failure diagnosis of machines. Comparing with the traditional methods, these techniques identify the gear condition automatically by computer according to the quantitative feature parameters extracted from the vibration signal. An intelligent diagnostic system often needs to combine several techniques of time-domain, frequency-domain or time-frequency domain.

Artificial neural network is one of the forecasting and validating methods using computer models with some of the architecture and processing capabilities of the human brain [42]. The technique trying to achieve such results is called neural computing or artificial neural networks. Artificial neural network mimics biological neurons by simulating the workings of the human brain. Researchers have developed many techniques for diagnosing gear faults based on this technology. Paya and Esat [43] adopted the neural network to detect gear faults and identify different kinds of faults based on the preprocessed data acquired by wavelet transform. The effectiveness of the proposed method is investigated by the real time domain vibration signals of the drive-line. The multiple faults were successfully detected and classified, which illustrates artificial neural network is effective and reliable in diagnosing faults without relying on the experience of operator. Saravanan et al. [44] presented a method for classifying gear faults using artificial neural networks with extracting features from the vibration data of a bevel gear box by Morlet wavelet technique.

The objective of pattern recognition is to distinguish different types of patterns on the basis of measurements [45]. The technology can classify the inputs into its patterns based on the extracted features of the measurements. Staszewski et al. [46] proposed an intelligent diagnostic system for detecting different spur gear fault conditions using technique of statistical and neural pattern recognition. The types of faults are correctly classified, which shows that the neural pattern recognition is capable of detecting local tooth faults in spur gears.

The support vector machines is a new generation learning system based on statistical learning theory. As a novel machine learning method proposed by Vapnik in early 1990s [47], the technology has been introduced for health monitoring of gear device, bearing and rotating machinery in recent investigations because of its high accuracy and good generalization capabilities. Especially, support vector machines are capable of effectively solving the learning problem of a small number of samples and avoid the over-fitting problem in artificial neural network. Therefore, support vector machines is considered as more suitable to the application of gear fault detection, Among the previous studies, Samanta [48] studied the performance of support vector machines on detection of gear faults, on a basis of calculating statistical parameters of vibration signals as failure features. Saravanan and Ramachandran [49] adopted the method of proximal support vector machines for fault diagnosis of spur bevel gear with extracting statistical feature vector from

Morlet wavelet coefficients of the signal.

2.2 Discrete Wavelet Transform

The discrete wavelet transform is a linear transformation that decomposes a signal into multi resolution representation with both low frequency coarse information and high frequency detail information. The original signal is decomposed into a compact wavelet series with different frequency bands, which provides the information of the signal in both time domain and frequency domain simultaneously. Therefore, the major advantage of the wavelet transform for analyzing the signal is that it possesses multi-resolutions for localizing short-time components so that all possible types of gear faults can be displayed by a single timescale distribution resulting from the transform. The advantages make it optimal for on line process monitoring of faults diagnosis in mechanical rotary parts by analyzing the measured signals. Comparing with the other techniques of wavelet transform, the discrete wavelet transform is characterized for its fast computation and strong capacity to concentrate information. Moreover, the time-frequency map by discrete wavelet transform enables the detection of transitory phenomena in non-stationary signals. Hence, the discrete wavelet transform is employed in this study.

The study of wavelets is started in the 1980's. In 1985, Meyer constructed an orthogonal wavelet base with satisfactory time and frequency localization properties. Later on, Daubechies [28] made the wavelet transform become well known and more generalization by constructing orthogonal wavelet bases compactly supported in a simple but ingenious way. Daubechies has done many researches on wavelet frames that allow more liberty in the choice of the basis wavelet functions at a little expense of some redundancy, and developed a series of orthogonal wavelet bases with great significance, which are called Daubechies wavelets later. In the past years, there are many reports about the application of discrete wavelet transform to the diagnosis of gear faults. Wang and McFadden [50, 51], for example, used orthogonal wavelets such as the Daubechies 4 and harmonic wavelets to detect abnormal transients generated by early gear damage based on the vibration signal of gearbox. Butler-Purry and Bagriyanik developed [52] an automatic detection method for internal incipient faults in the transformers using discrete wavelet transform. The detection method can provide information to predict failures ahead of time so that the necessary corrective actions are taken to prevent outages and reduce down times. Saravanan and Ramachandran [34] extracted feature parameters from the vibration signals for diagnosing different conditions of gear box by using discrete wavelet transform. The results show that the discrete wavelet transform enables to represent all possible types of transients in vibration signals generated by gear faults and make a great contribution to condition monitoring and fault diagnosis of gears.

Signals acquired from accelerometer mounted on gear box are often inevitably contaminated by the interference signal, which is caused by vibrations from shafts, bearings, and other components on the testing machine. In addition, the signals are also polluted with the white noise which is generated by the accelerometer or the environmental electromagnetic disturbances. Except for the signal of interest, the other unnecessary signal components are considered as noise in this study. The noise is usually random and unstable, which degrades the accuracy of detection of transients generated by gear faults. Therefore, it is necessary to reduce the noise from the original signal. The de-noisy function of discrete wavelet transform can effectively filter the noise so as to more accurately detect weak impulse in signals.

The denoising procedure of discrete wavelet transform includes the analysis signal decomposition, threshold estimation and signal reconstruction. The estimation method is to select the best decomposition level and the best wavelet filter. Hard thresholding and soft thresholding are the two main approaches commonly applying to denoising. The algorithm of hard thresholding method is setting all the wavelet coefficients below a given threshold value equal to zero, while in soft thresholding the wavelet coefficients are reduced by a quantity equal to the threshold value [53]. Sqtwolog, heursure, rigrsure and minimax are the widely employed calculating methods of threshold value in wavelet transform. The denoising capacity of various methods are investigated by the signal to noise, which is defined as a ratio of the power of analytical signal to the power of the noise [54]. The denoising of discrete wavelet has been applied in many studies. In 1999, Pasti et al. [55] proposed a method to optimize the parameters used in signal denoising in discrete wavelet transform. The method tries to search the most appropriate decomposition level and wavelet filter function for denoising in the discrete wavelet domain. The result confirms the effectiveness of the de-noisy technique in white noise signal. Littler and Morrow [56] presented the application of discrete wavelet transform to denoising disturbance signals in power system. The transient fault signals are enhanced, which demonstrates the validity of the denoising method. Menon et al. [57] employed the wavelet-based method to eliminate the background operational noises to detect small fatigue cracks in rotor head components.

2.3 Support Vector Machines

Support vector machines (SVMs), based on structural risk minimization principle in statistical learning theory, are a novel machine learning method developed by Vapnik in early 1990s [58]. Fundamentally, support vector machines are binary classification algorithm with strong theoretical foundations in statistical learning theory. It is initially dealt with linear classification problems by constructing an optimal separating hyper-plane for high classification accuracy. Based on a given

set of training examples with two classes, the SVMs build a classifier that predicts whether a new sample falls into one category or the other (this can be extended to multi-class problems). The SVMs try to search for an optimal linear boundary to separate the data precisely, and ensure the classification distance between two classes is maximum to improve the classification accuracy [59]. Substantially, support vector machine is a training algorithm for learning classification and regression rules from data.

The intelligent system for fault diagnosis and condition monitoring, developed with artificial neural networks, pattern recognition and so on, has been widely used in many areas [60]. Based on the structural risk minimization principle, SVMs can minimize the empirical risk of the training sample, ensure generalization capability of leaning process, and can successfully overcome the defects of over-fitting, local optimal solution and low-convergence rate existing in the neural network [61]. Therefore, SVMs have gained popularity in the machine learning community. The method has been successfully applied in many areas, such as computer vision [62], pattern recognition [63], industry process monitoring [64] and so on. During the recent past years, methods of intelligent system for diagnosing machine failures using SVMs are introduced [65, 66]. Especially, SVMs are capable of effectively solving the learning problem of a small number of samples [67]. Since it is difficult to obtain sufficient samples in practice, SVMs are introduced for health monitoring or fault diagnosis of gear device, bearing and rotating machinery in recent investigations. Researchers have developed many methods for fault detection using SVMs, with extracting failure features by various techniques.

In the reported studies, Samanta [48, 68] studied the performance of SVMs on fault detection of gear and bearing, on a basis of calculating statistical parameters of vibration signals as failure features. The study compares the performance of fault detection using two different classifiers, which are built using artificial neural networks and support vector machines separately. The presented method is investigated by the experimental vibration data on gear box and bearing. Based on the experimental results, it is found that the performance of SVMs on fault detection is substantially better than that of artificial neural network. Sugumaran, et al. [69] proposed an intelligent method for fault diagnosis of roller bearing using SVMs. The vibration signal from a piezoelectric transducer is captured for the following conditions: good bearing, bearing with inner race fault, bearing with outer race fault, and inner and outer race fault. A set of statistical features are extracted from the vibration signal as input vectors to classifier of SVMs for diagnosis. Different conditions of bearing are successfully identified, which confirms the effectiveness of the proposed method. Saravanan and Ramachandran [49] adopted the method of proximal SVMs for fault diagnosis of spur bevel gear with extracting a group pf statistical feature vector from Morlet wavelet coefficients of the time-domain vibration signal. The selected parameters are treated as

inputs to SVMs for classification. The satisfactory results for large classes of data are acquired using the developed method in less time. Xue, et al. [70] presented an intelligent diagnostic method for identifying structural faults in rotating machinery based on SVMs under varied operating conditions. The optimal distinctive frequency components are extracted from vibration signals as feature vectors input into the classifiers of SVMs to identify fault types of rotating machinery. The efficiency of the presented method has been investigated using practical examples.

Because the acquired original experimental data can't be directly inputted into classifier of SVMs, we need to extract appropriate feature parameters to represent the distinctive characters of the signal. The diagnostic accuracy of SVMs considerably depends on the extracted failure features. For ensuring excellent classification performance of SVMs, it is important to extract optimal feature parameters from the original signal. Recently, the use of feature extraction and feature selection for data preparation before inputting into classifier has received considerable attention [71]. Many diagnostic systems for fault detection have been developed based on combining SVMs with features extraction methods such as continuous wavelet transform, statistical technique, frequency analysis and so on. Because the investigated subjects are different, although all the studies adopt the same SVMs method for fault detection, the signal preprocessing techniques or the failure features extraction methods are different. For instance, Samanta and Sugumaran both extracted statistical features from the original vibration signals, while Saravanan firstly preprocessed the signal by wavelet transform, then extracted statistical features from Morlet wavelet coefficients. Essentially, all the techniques are aimed to improve the diagnostic accuracy. In this study, I try to employ SVMs to the application of gear damage diagnosis and classification with extracting optimal features from the vibration signal with different methods.

2.4 Empirical Mode Decomposition

Local faults in gears always produce transient modifications in vibration signals. Therefore, these signals have to be considered as non-stationary. Empirical mode decomposition (EMD) as a new data processing method was recently introduced by Huang et al. [72], especially for analyzing data from nonlinear and non-stationary processes. The algorithm is based on a simple assumption that any data consists of different simple intrinsic modes of oscillations which have the same number of extremas and zero-crossings. With the initial processing of EMD, any linear or nonlinear signal can be decomposed into a finite sum of components known as intrinsic mode functions, each of which represents a simple oscillatory mode as a counterpart to the simple harmonic function and varies with the variation of the original signal. In contrast to other traditional time-frequency analysis methods, the EMD approach does not use pre-specified basis functions or filters but

instead decomposes a signal with a posteriori defined basis which is directly derived from the analytical data [73]. Therefore, it is highly adaptive and consequently can well present the time – frequency characteristics of a signal.

With the recent development on EMD method, the technique has already been employed successfully in wide applications : earthquake, climate variability, analysis of daily surface air temperature data, nonlinear ocean waves, detection of structural damage, health-monitoring and so on [74]. Recently, literatures of its applications on the failure detection of gear [75-78], bearing [79-81] and rotary machine [82] have been reported. Loutridis [75] presented the application of condition monitoring and detection of gear faults using EMD. Experimental vibration signals from a test rig are decomposed into a set of intrinsic mode functions. The energy of the intrinsic modes is calculated as features for gear failure prediction. The experimental results show the extracted energy of intrinsic modes is sensitive to gear damage, and confirm the efficiency of the proposed method. Liu et al. [76] applied the EMD method to vibration signal analysis for diagnosing faults in gearbox. The vibration signals collected from an automobile gearbox are employed to investigate the effectiveness of the proposed method. The results show that the EMD method can successfully detect and locate damage on gearbox. In addition, comparing with the traditional continuous wavelet transform, it presents more effective in detection of the vibration signatures. Yu et al. [79] developed a method for fault diagnosis of roller bearing by combining the envelop analysis and EMD method. In the proposed method, the EMD method and Hilbert transform are applied to the envelop signal acquired using wavelet bases. Then the local Hilbert marginal spectrum can be obtained, from which the faults in a roller bearing can be diagnosed and fault patterns can be identified. Vibration signals collected from roller bearings with out-race faults or inner-race faults are adopted to investigate the proposed method. It is found that the presented method is effective in extracting fault features of roller bearings. Gao et al. [82] investigated the application of EMD based approach for rotating machine fault diagnosis. A practical vibration signal of a power generator from a thermal-electric plant is used to diagnose the faults. Fault features are extracted from the decomposed intrinsic mode functions acquired using EMD method. The results show that the EMD method can extract fault features of the rotating machine and identify the fault patterns effectively.

3 Types of Gear Failures

3.1 Introduction

There are many factors that can cause various gear failures [83]. The gear failure would be different because of the gear material, operating situation, environment, lubricant, loads and so on. This chapter introduces representative types of gear failures.

3.2 Tooth Fracture

a) Fatigue breakage

The fatigue breakage may be caused by excessive tooth loads which result in root stresses higher than the endurance limit of the material. When the teeth work under loads, the high stress concentration together with highest tensile stress is normally exist at the root of the tooth or at the fillet. Therefore, when gears are loaded in this manner and subjected to enough repeated stress cycles, the initiation of crack usually takes place at the root of the teeth. Then crack propagates fast and suddenly results in fracture of the tooth. Figure 3.1 shows the photograph of gear tooth with fatigue breakage [83].

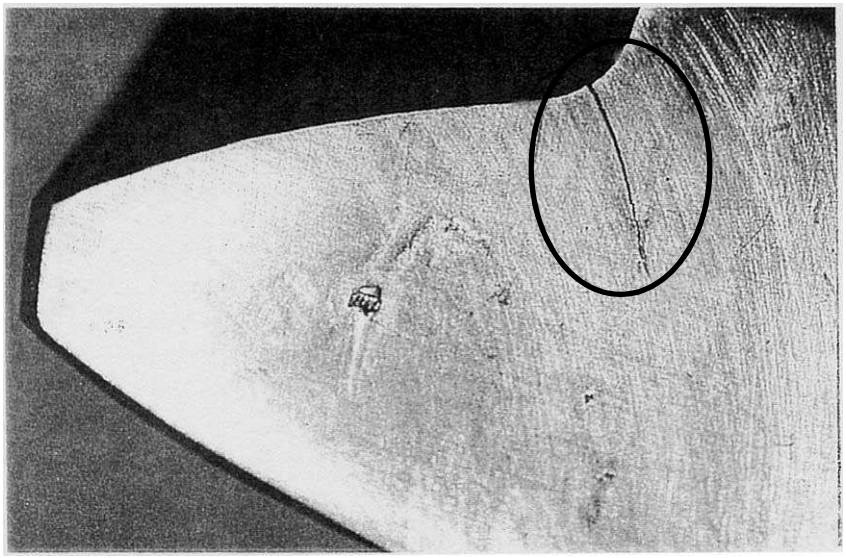

Fig. 3.1 Photograph of fatigue breakage [83]

b) Overload breakage

Overload breakage results from a short-cycle overload or impulsive load which exceeds the tensile strength of the gear material. Figure 3.2 shows the photograph of overload breakage [83].

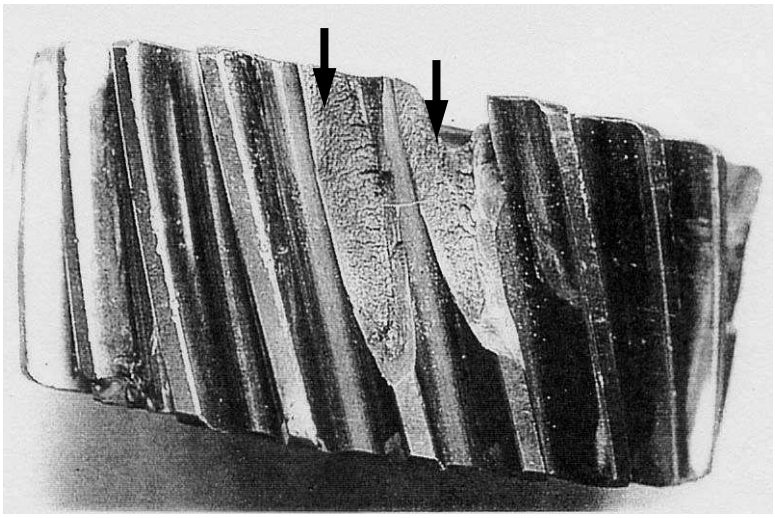

Fig. 3.2 Photograph of overload breakage [83]

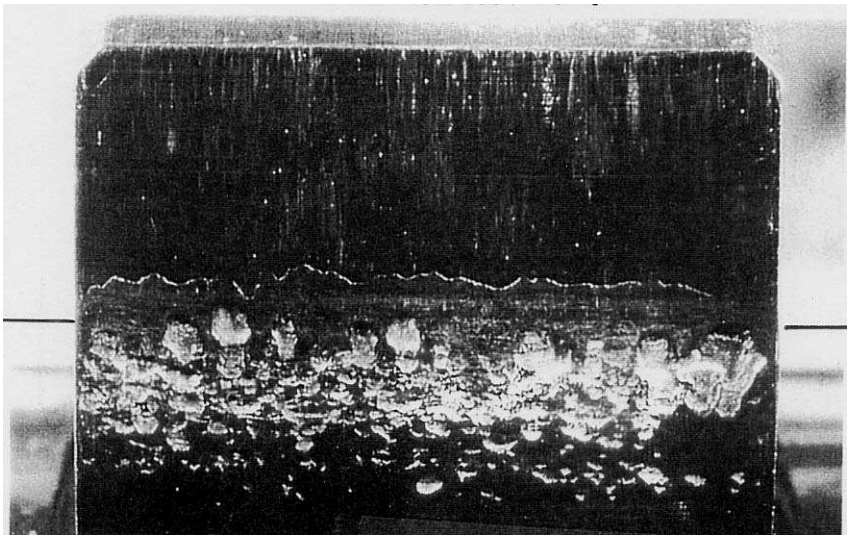

Fig. 3.3 Photograph of pitting [83]

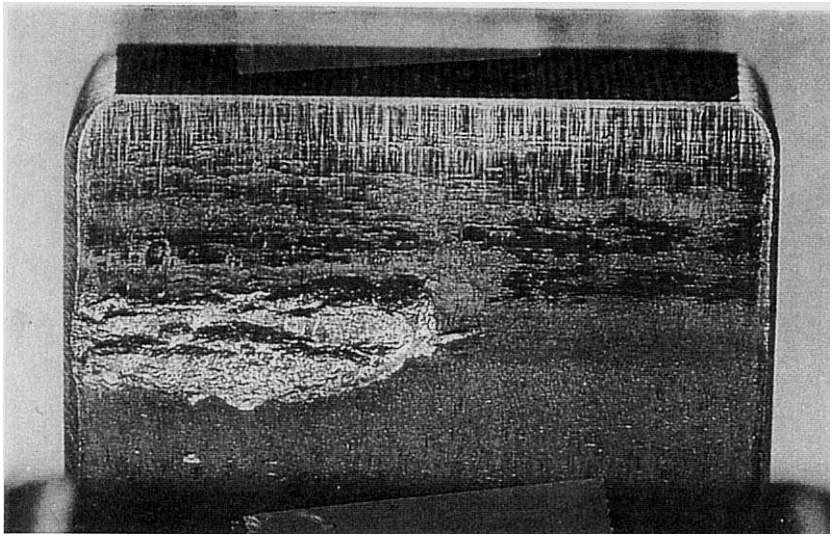

Fig. 3.4 Photograph of spalling [83]

3.3 Damage of Gear Tooth Surface

a) Surface fatigue

If the repeated contact stress exceeds the limited fatigue strength of the contact area, damage would occur because of the fatigue of tooth surface or the material under surface. This type of damage is called surface fatigue, which mainly includes pitting and spalling.

(1) Pitting

Pitting occurs due to repeated loading of tooth surface and the contact stress exceeding the surface fatigue strength of the material. Material in the fatigue region gets removed and a pit is formed. In the process of meshing, because the number of teeth is relatively few when mesh around the pitch line, the contact stress and friction force is large on the pitch line region. Therefore, pitting usually initially occurs on the pitch line region of a tooth. The failure of pitting is shown as Fig. 3.3[83].

(2) Spalling

Because of the high loading, the fatigue of material under the tooth surface would generate. Some larger sheet metals spall from the tooth surface, which is called spalling. Figure 3.4 shows the photograph of spalling [83].

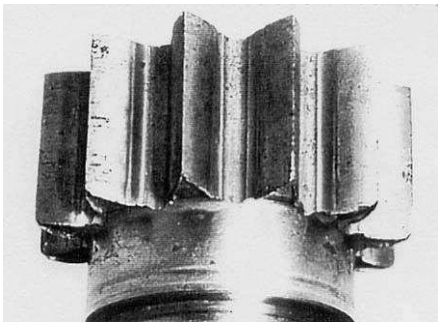

Fig. 3.5 Photograph of abrasive wear [83]

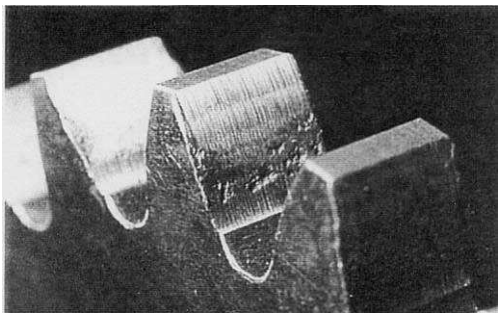

Fig. 3.6 Photograph of scratching [83]

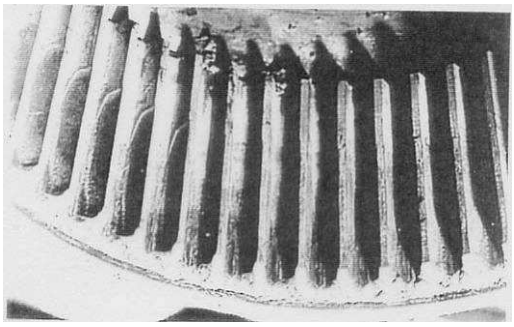

Fig. 3.7 Photograph of fretting corrosion [83]

b) Wear

Wear is a kind of tooth damage which generates during the sliding contact of metal surface. It would progressively remove metal from the surface. Wear is classified into abrasive wear, scratching and fretting corrosion.

(1) Abrasive wear

Abrasive wear is a main failure type in aspect of open gearing. The abrasive particles in the oil dust, sand grains, and iron fillings adhering on the meshing teeth surface may result in abrasive wear. Figure 3.5 shows the photograph of abrasive wear [83].

(2) Scratching

Scratching damage is larger and deeper than abrasive wear. The burr and protuberance of tooth surface, and larger foreign abrasive particles may cause the scratching damage. Figure 3.6 shows the photograph of scratching damage [83].

(3) Fretting corrosion

Because of the slight vibration between contact surface of gear coupling, the relative reciprocating motion is generated between meshing teeth surface, which may cause fretting corrosion. Figure 3.7 shows the photograph of fretting corrosion [83].

c) Plastic deformation

Plastic deformation is the permanent undulating distortion of materials, which is commonly caused by the excessive loads. Plastic deformation is classified as plastic flow, ripping and ridging.

(1) Plastic flow

Plastic flow of tooth surface occurs when it is subjected to high contact stress under rolling cum sliding action. Surface deformation takes place because of yielding of surface or subsurface material. Usually it occurs in softer gear materials. But it can occur on hardened gears in case of heavy loading. The damage of plastic flow is shown in Fig. 3.8 [83].

(2) Rippling

Ripping is a kind of wear which often occurs in operation of heavy load and low speed with very thin oil films. It has fish scale appearance and usually occurs on hardened gear surface. Figure 3.9 shows the photograph of rippling [83].

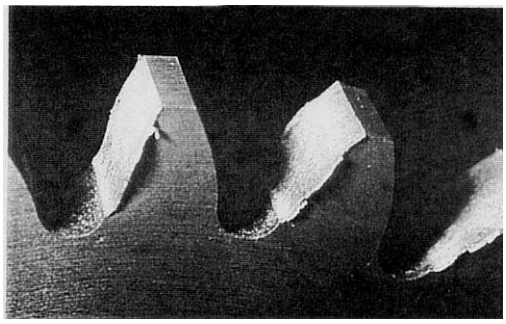

Fig. 3.8 Photograph of plastic flow [83]

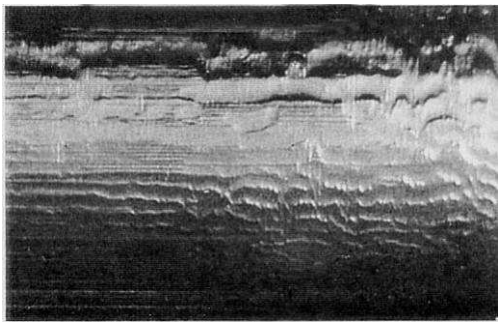

Fig. 3.9 Photograph of rippling [83]

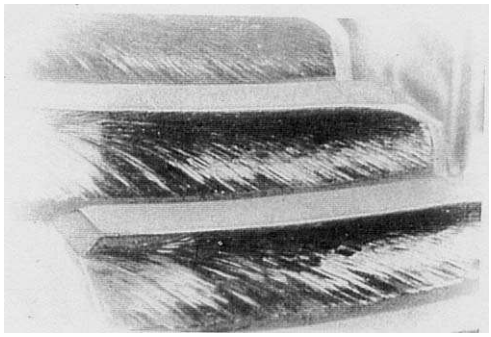

Fig. 3.10 Photograph of ridging [83]

(3) Ridging

After running for a longer time in the situation of inappropriate lubrication or heavier load, the pair of gears will often exhibit ridge along the pitch line of wheel and groove in the pitch line of the pinion. Figure 3.10 shows the photograph of ridging [83].

d) Thermal failure

Normally, thermal failure is caused by the higher temperature which is generated in the friction between teeth surface. The representative thermal failures are introduced as follows.

(1) Scoring

In the gear transmission with heavy load and low speed, the lubricating oil film may rupture in local contact region because of the overheating of friction. The lubrication failure will cause the direct contact of metal to metal. Later on, teeth surface agglutination and tearing action resulting from metallic contact removes the metal rapidly and continuously. Scoring usually occurs on the faster sliding region of the tip or root of tooth. Figure 3.11 shows the photograph of scoring [83].

(2) Burning

Because of the excessive speed, overload, and failure lubrication, the color of tooth surface will change for the friction overheating of local contact region. The failure of burning not only results in the hardness of material becoming lower, but also causes the endurance limit fatigue strength become weaker.

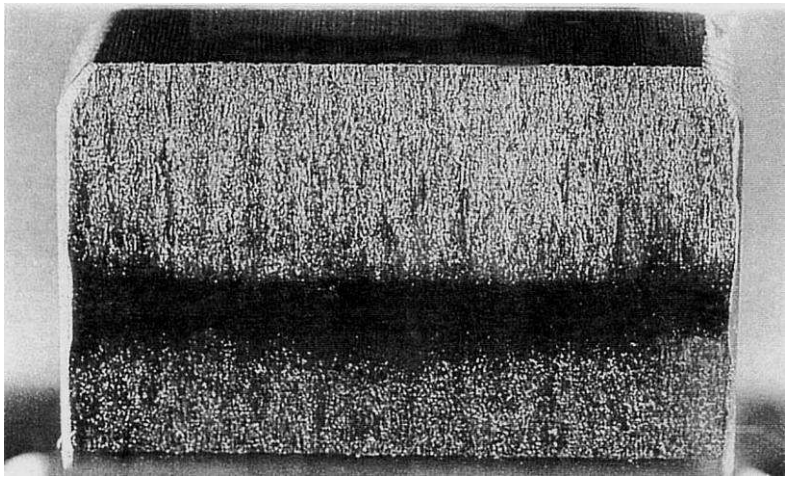

Fig. 3.11 Photograph of scoring [83]

4 Damage Contrast Test

4.1 Introduction

In order to investigate the influence of load torques, gear rotation speeds and size of gear damage on the vibration accelerations, the damage contrast test is carried out. Three kinds of gears, namely normal gear, spot damaged gear and pitted gear, are tested under different loads and gear rotation speeds on the power circulating type gear testing machine. The vibration accelerations of gear box and bearing box are measured in the experiment. The technique of Fast Fourier Transform is employed to analyze the original signal, by which the frequency spectrum is obtained. Because the collected vibration signal is usually non-stationary, and the failure symptoms are not obvious especially in the early stage of gear failure. In order to emphasize the failure characteristics of the measured signals, the residual signal is extracted from the original vibration accelerations. Moreover, the method of discrete wavelet transform is adopted to reduce noise from the residual signal. The processed signal is obtained by reconstructing the coefficients of discrete wavelet transform.

4.2 Experimental Apparatus

The vibration data analyzed in this chapter was measured on a power circulating type gear testing machine, whose photo is shown in Fig. 4.1. Figure 4.2 shows the scheme of the gear testing machine. The total length and total width of the power circulating type gear testing machine are about 2 meters and 1 meter respectively. It mainly consists of a variable-speed three-phase driving motor, a pair of test gears, a test gear box, two bearing boxes, two accelerometers, a loading device, and a slave unit. The load on test gears is set by the loading coupling and torsion bar. The coupling ⑤ is loaded by a connecting lever with some weights. Then, the loading coupling is screwed together with the torsion bar ⑥. Therefore, the load is set on test gears. Two accelerometers (type-type NP-2120, Ono Sokki Co., Ltd., Kanagawa, Japan) are set at the center of the upper part of both test gear box and bearing box. They are used to measure the vibration accelerations. A sound level meter (type LA-1210, Ono Sokki Co., Ltd., Kanagawa, Japan) is placed 300 millimeters beside the gearbox to measure the gear noise during the experiment. The measured gear noise is recorded by the data recorder. To extract a periodic signal from the measured data for a detail analysis, a pitch disk with one hole is installed on the gear shaft together with the test driven gear. Then, a photosensor is used to generate the pitch signal of meshing gear pair. The output pitch

signal is recorded by the data recorder (type TM-3100, Ono Sokki Co., Ltd., Kanagawa, Japan). Figure 4.3 shows the measurement mechanism of pitch signal. When the light shines through the hole, the pulse level is high, otherwise the pulse level is low.

The lubrication method was oil bath and turbine oil ISO VG32 was selected as the lubricant. Because the viscosity of lubricants varies with the temperature of lubricants, which will influence the vibration of test gears, it is necessary to stabilize the temperature of lubricants. The T type thermocouples are used to monitor the oil temperature. The fixing position of thermocouples is shown in Fig. 4.4. The temperature of lubricant is kept at 313±3 K using a heater (type sensitively SR-51, YAMATO) and refrigeration pipe. A thermometer placed on the test gear box cover is used to measure the temperature to control the heater. The diagram of refrigeration for test gear box is shown as Fig. 4.5. Figure 4.6 shows the diagram of temperature control of lubricant using thermometer and heater.

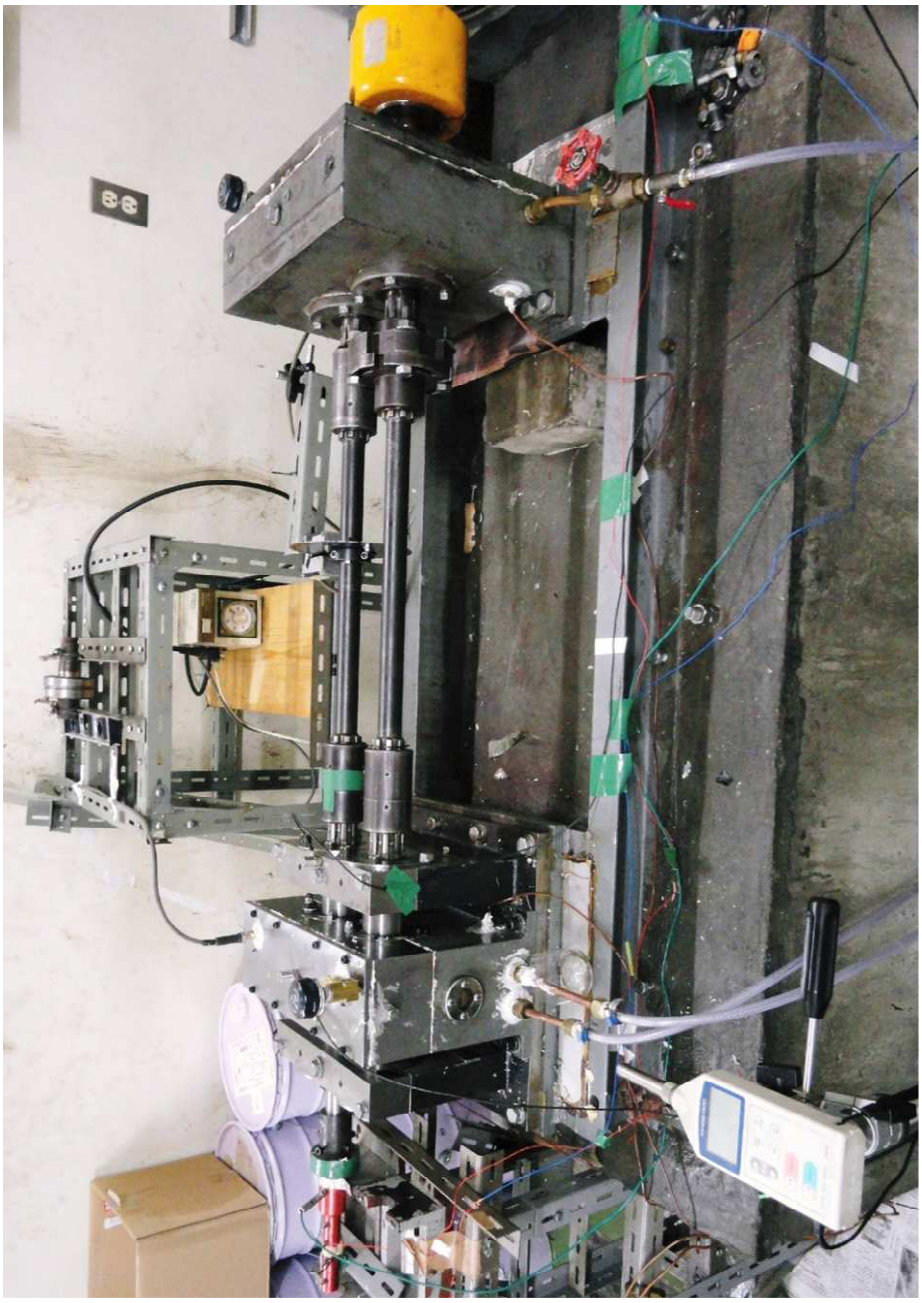

Fig. 4.1 Photo of the power circulating type gear testing machine

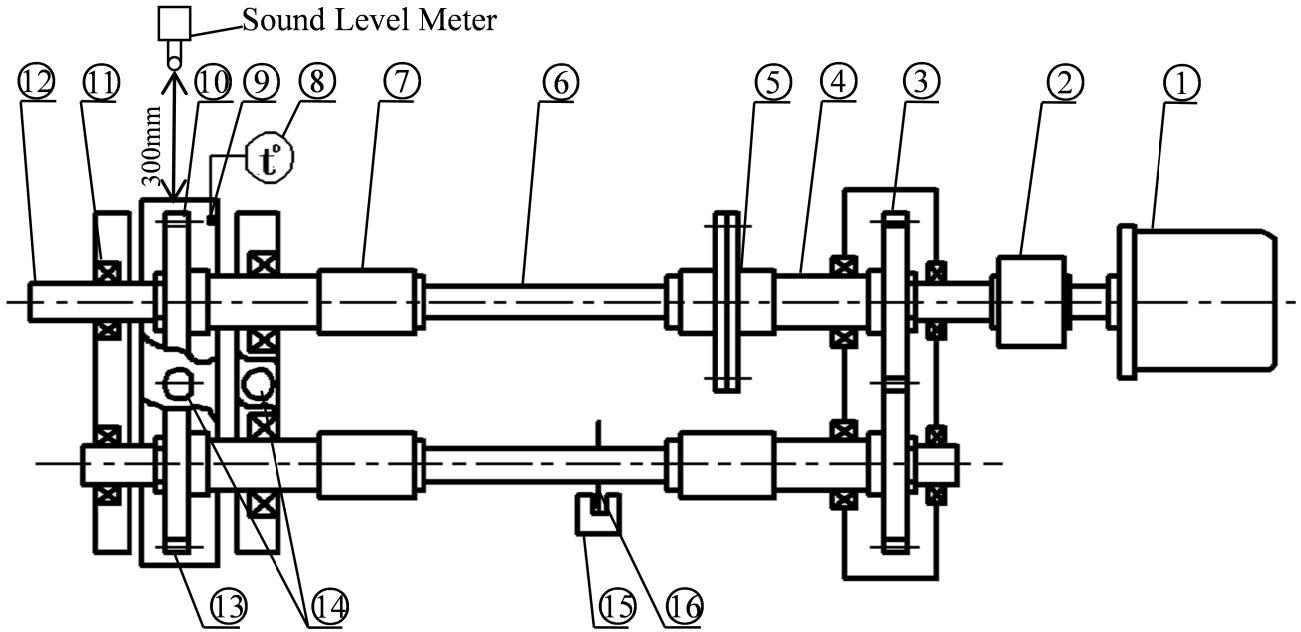

1	Variable speed motor	5	Loading coupling	9	Thermocouple	13	Test gear (Driven)
2	Chain coupling	6	Torsion bar	10	Test gear (Driving)	14	Accelerometer
3	Slave unit	7	Muff coupling	11	Ball bearing	15	Photo sensor
4	Gear shaft	8	Thermometer	12	Gear shaft	16	Index disk

Fig. 4.2 The scheme of the power circulating type gear testing machine

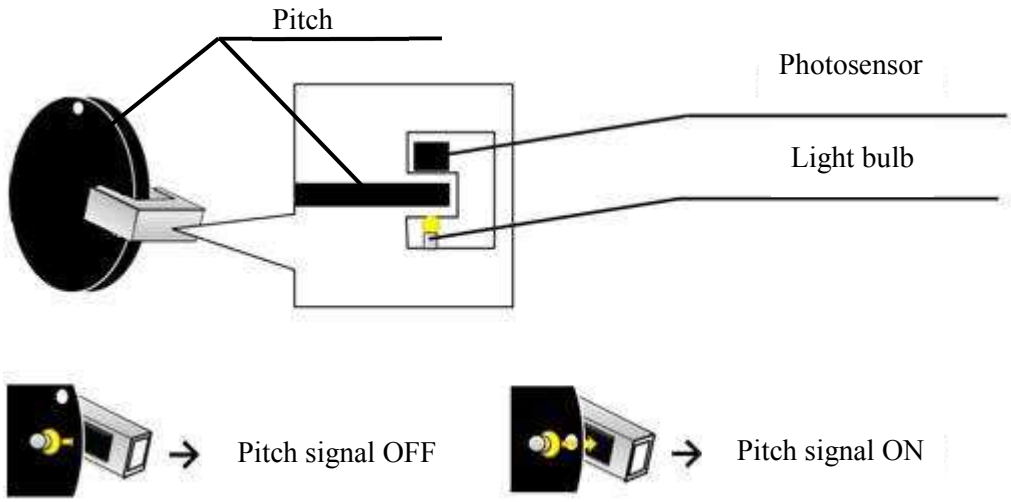

Fig. 4.3 The measurement mechanism of pitch signal

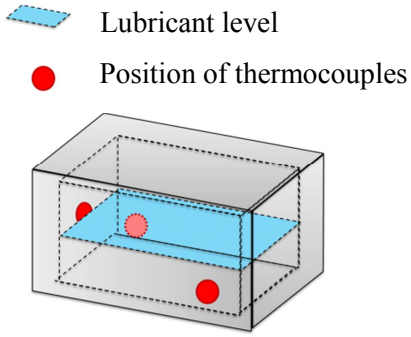

Fig. 4.4 Fixing position of thermocouples

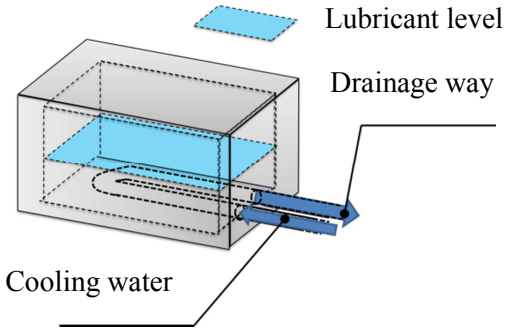

Fig. 4.5 The diagram of refrigeration in test gear box

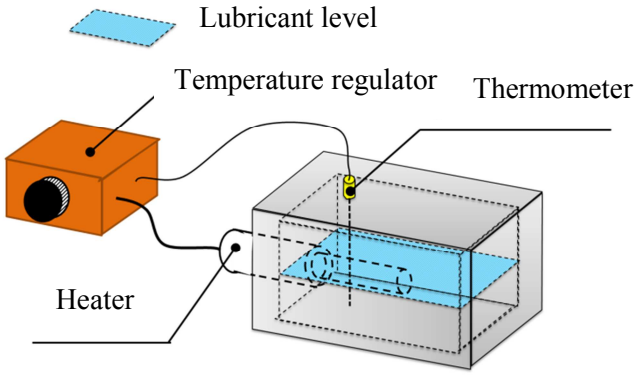

Fig. 4.6 The diagram of temperature control of lubricant using thermometer and heater

4.2.1 Measurement of Vibration Acceleration

The vibration accelerations on gear box and bearing box are measured by accelerometers (type- type NP-2120, Ono Sokki Co., Ltd., Kanagawa, Japan). Figure 4.7 shows the fixing positions of accelerometers on test gear box and bearing box. Two accelerometers are installed at the center of the cover of both test gear box and bearing box. Figure 4.8 shows the block diagram of measurement of vibration acceleration, gear noise and pitch signal. The obtained signals measured by accelerometers are inputted into the charge amplifier (type CH-1200, Ono Sokki Co., Ltd., Kanagawa, Japan). The amplified signals are recorded by the data recorder. Meanwhile, the noise signal and pitch signal are recorded by the data recorder synchronously.

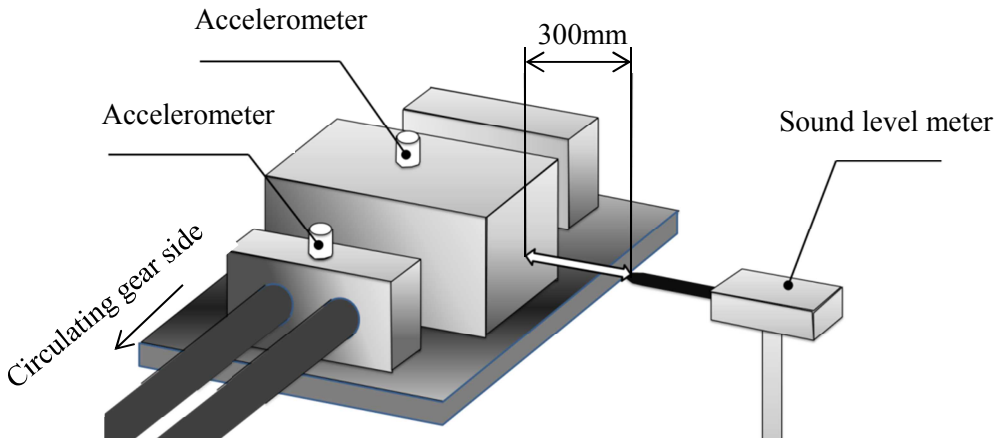

Fig. 4.7 The fixing positions of accelerometers on test gear box and bearing box

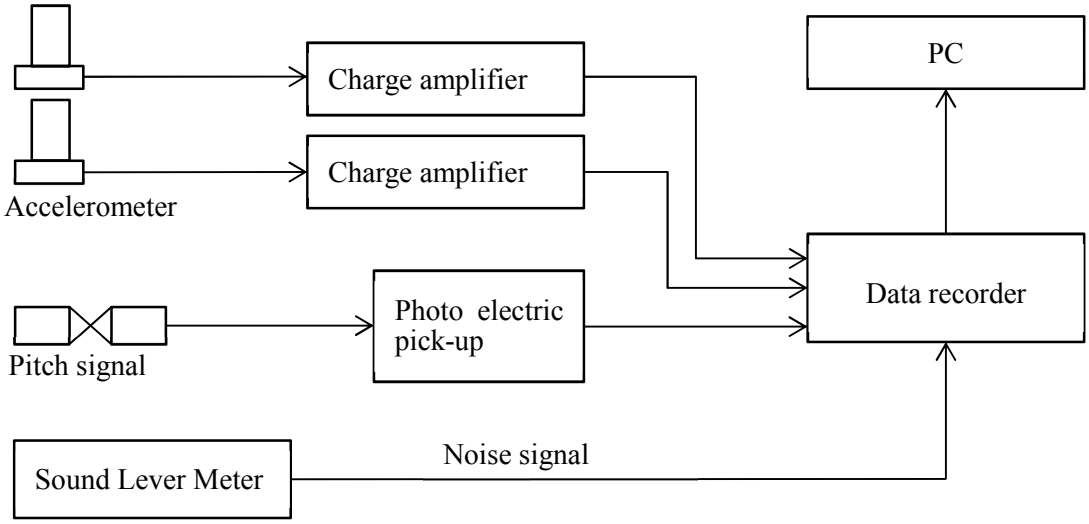

Fig. 4.8 The block diagram of measurement of vibration acceleration, noise signal and pitch signal

4.3 Test Gears

4.3.1 Specifications of Test Gear

Three kinds of gears, namely normal gear, spot damaged gear and pitted gear, were tested. Especially, the gear with a drilled spot damage on one of its teeth surface is called spot damaged gear I, with two drilled spots damage is called spot damaged gear II and with three drilled spots damage is called spot damaged gear III. Their dimensions are shown in Table 4.1. Figure 4.9 shows the diagram of test gears. The test gears are the involute spur gears whose module is 4mm, number of teeth is 29, and pressure angle is 20^{o}. They are made of thermal refining steel JIS S45C, the gear surface finishing is hobbing, and the accuracy is JIS B1702 Grade 4.

The damaged area is measured by the method of Suzuki's Universal Micro Printing. According to this method, the tooth surface is copied and is amplified about 10 times by the projector. Then, the damaged part is traced and is recorded by the computer. Finally, the damaged area is calculated by using some software for area measurement. The average damaged area ratio is defined as a rate of the whole failure area of test gears to the entire meshing area of the two meshing gears. While the maximum damaged area ratio is defined as a rate of the maximal damaged area of a gear tooth to the entire area of the two meshing teeth.

Figure 4.10 shows the tooth surface of test gears. Figure 4.10 (a) shows the normal gear with no failure on tooth surface. The spot damaged gear I shown in Fig. 4.10 (b) has a drilled spot damage with diameter 2 mm around the pitch line on the No. 1 tooth surface, whose average damaged area ratio is 0.1% and the maximum damaged area ratio of a tooth is 2.8%. Figure 4.10 (c) shows the tooth surface of spot damaged gear II with two drilled spots damage around the pitch line on its No.1 tooth surface. Its average damages area ratio is 0.15% and the maximum damaged area of a tooth is 4.44%. Figure 4.10 (d) shows the tooth surface of spot damaged gear III with three drilled spots damage around the pitch line on its No. 16 tooth surface. Its average damages area ratio is 0.23% and the maximum damaged area of a tooth is 6.53%. The tooth surfaces of pitted gear are shown in Figure 4.10 (e). Because the damaged teeth of pitted gear is large, the tooth surface of No. 5, No. 20 and No. 26 teeth are selected to represent the surface of pitted gear. The damaged area ratio of every gear tooth changes from 0% to 24.6%, and the average damaged area ratio of the whole gear is 2.5%. In this experiment, the spot damage is artificially created by drilling, while the pitted gear failure is generated naturally in service.

Table 4.1 Dimensions of test gears

Tooth profile		Involute
Module	m [mm]	4
Number of teeth	z_1/z_2	29/29
Pressure angle	α_0 [deg]	20
Addendum	h_a [mm]	4
Dedendum	h_d [mm]	5
Pitch circle diameter	d [mm]	116
Tip circle diameter	d_a [mm]	124
Face width	b [mm]	10
Contact ratio	ε	1.65
Material		JIS S45C Thermal refining steel
Surface finishing		Hobbing

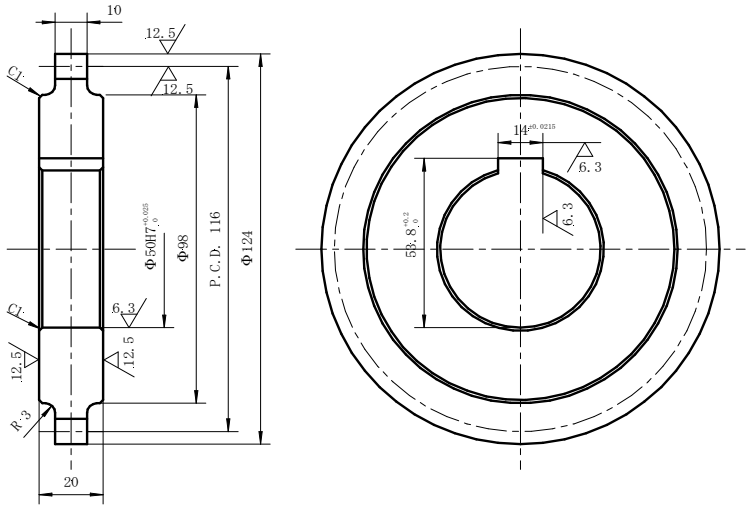

Fig. 4.9 The diagram of test gears

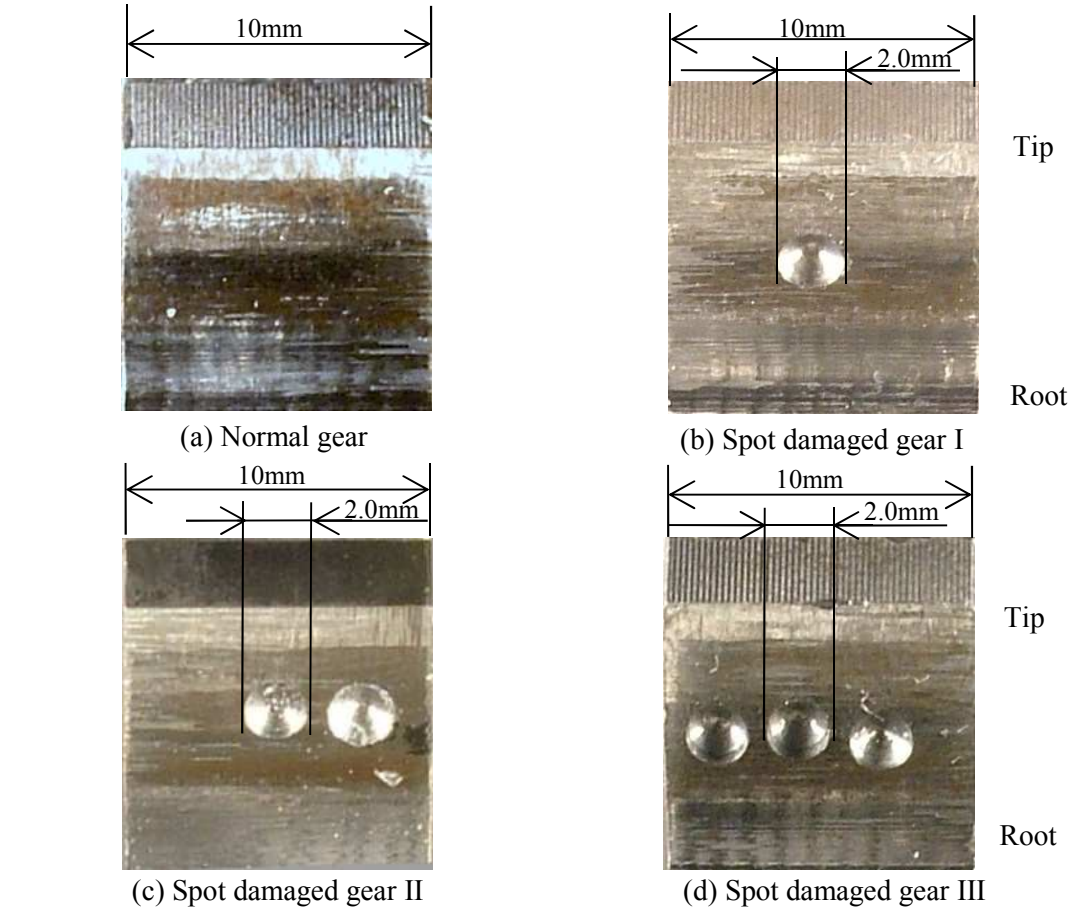

(a) Normal gear (b) Spot damaged gear I

(c) Spot damaged gear II (d) Spot damaged gear III

(e) Pitted gear

Fig. 4.10 Photographs of tooth surface of test gears

4.3.2 Tooth Profile Error

Figure 4.11 shows the tooth profile error of test gears. The spot damage is all drilled on the pitch line of test gear surface. The tooth profile error of spot damaged gear I is adopted to present the tooth profile error of the spot damaged gear. The teeth of driving gear shown in Fig. 4.11 (b) and 4.11 (c) have spot damage and pitted failure respectively. All test gears were manufactured with the same lot, such as the same material, the same process, the same cutting machine and so on. The difference of tooth profile error on driven tooth between the normal gear and spot damaged gear is not obvious. The tooth profile error of driving tooth of spot damaged gear is large. The tooth profile error of pitted gear is larger than that of the other gears. Because the pitting failure is generated naturally in service, the tooth profile error will become larger with the deterioration of tooth surface after a long working time.

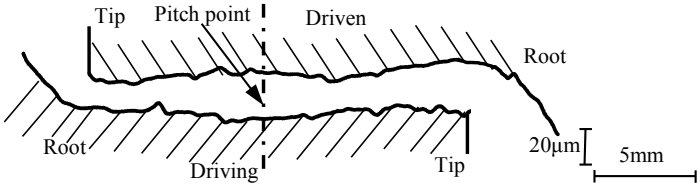

(a) Normal gear

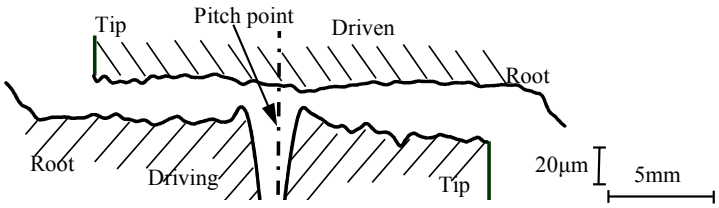

(b) Spot damaged gear

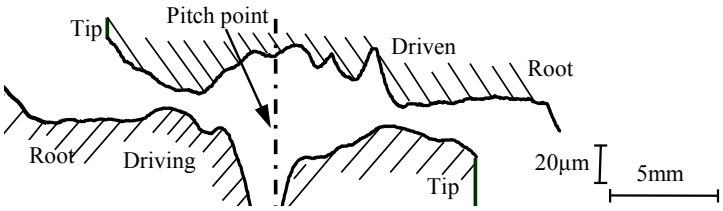

(c) Pitted gear

Fig. 4.11 Tooth profile error of test gears

4.4 Experimental Conditions

Test gears were driven by the motor with speed from 1200 rpm to 3000 rpm by increments of 600 rpm. A number of tests are repeatedly carried out under different loading torques of 40 N-m and 70 N-m with the same speed respectively. The temperature of lubricant is kept at about 60℃±3℃ to reduce the influence of lubricant viscosity in the vibration of test gears. The vibration accelerations on gear box and bearing box, the sound level signal and the pitch signal are measured during the experiment. The sampling frequency is 20 kHz and test time is 2s.

4.5 Experimental Results and Discussions

Analyzing the vibration accelerations of gear box or bearing box is one of the most effective methods to detect the gear damage. The vibration accelerations on gear box and bearing box, sound level signal and pitch signal are obtained during the damage contrast test. However, due to unsteady gear rotation, lubrication situation, tooth stiffness variations, and other reasons, the collected vibration signal is usually non-stationary, and the failure symptoms are not obvious especially in the early stage of gear failure. Hence, how to emphasize the failure characteristics of the measured signals and extract failure features from collected data is crucial for gear failure diagnosis. To address this, the residual signal is obtained from the raw signal in this paper because of its much less sensitive to the altering experimental conditions and more obvious representations of failure signatures. Because the noise contained in residual signal is relatively large, the method of discrete wavelet transform is employed to reduce noise from the residual signal and the coefficients of discrete wavelet transform are reconstructed as the processed signal as analytical data for the following study. In the following sections, the experimental results are presented and analyzed.

4.5.1 Vibration Accelerations on Gearbox and Bearing box and Sound Level Signal

Figures 4.12~4.21 separately show the vibration accelerations on gear box and bearing box of test gears measured under conditions of applied torque T=40, 70N-m and rotation speeds n= 1200, 1800, 2400 and 3000rpm. The waveform corresponds to one wheel revolution. The abscissa axis shows gear tooth number and the ordinate axis represents the vibration acceleration.

As shown in Figs. 4.12 and 4.13, the vibration accelerations of normal gear are nearly stable and there are no abnormal large amplitudes in the waveform. In Figs. 4.14 and 4.15, the vibration accelerations on bearing box change slightly. However, the waveform on gear box is always

fluctuating over the whole period. The spot damaged gear I has a spot damage on its No.1 tooth surface. Some larger amplitude occur around No.1 tooth in the waveform on gear box in Figs. 4.14 (c) and (c), Figs. 4.15 (a) ~ (c). In spot damaged gear II, the 2 spots damage is drilled on the tooth surface of No. 1 tooth. In Figs. 4.16 and 4.17, although the vibration accelerations on gear box fluctuate, it is still difficult to detect gear damage only based on the original waveform. Figures 4.18 and 4.19 present the vibration accelerations of spot damaged gear III which has 3 drilled spots damage on its No. 16 tooth surface. As shown in the two figures, the larger amplitudes almost appear around No. 16 tooth in all of the vibration accelerations on gear box. Besides, in Figs 4.19 (c) and (d), the waveform on bearing box also appears the indication of damage. Most of the vibration accelerations on bearing box changes slightly. Figs 4.20 and 4.21 represent the vibration accelerations of pitted gear. The short-time larger amplitude appears around No. 7 tooth both in waveforms on gear box and bearing box. It indicates that the pitting damage on No. 7 tooth surface is more serious.

As found in these figures, the vibration acceleration on gear box is a little larger than that on bearing box. The waveform on bearing box is more stable than that on gear box. Comparing with the vibration accelerations on gear box, it is more difficult to detect gear damage based on the vibration accelerations on bearing box whether the failure is slight or serious. This can be considered as: the gear box and bearing box are respectively installed on the same baseplate through the screw connection. The vibration of test gears will generate the vibration of bearings through the gear shaft between them. Then, the vibration of bearing causes the vibration of bearing box and the vibration of baseplate. Then, the vibration of gear box is resulted from the vibration of baseplate. The accelerometers are set at the center of the gear box cover and the upper part of bearing box. The thickness of the upper part of bearing box is larger than the stiffness of gear box cover. The stiffness of the upper part of bearing box is larger than that of gear box cover. Moreover, the width of gear box cover is larger than that of bearing box. Therefore, the vibration of gear box cover is stronger than that of the upper part of bearing box. In addition, along with the increase of rotation speeds the vibration accelerations become larger and the indication of damage also becomes more and more obvious, such as Figs. 4.18~4.21. The vibration accelerations acquired under T=70N-m is a little stronger than that acquired under T=40N-m. Generally, the vibration acceleration gradually increases in the order of normal gear, spot damaged gear, and pitted gear. The reason for this is that the large vibration acceleration is mainly generated by the tooth profile error which becomes larger along with the increase of the damaged area. Since the amplitudes of waveform are large and fluctuate strongly when the pitting area is large, the gear condition of severe failure can be diagnosed roughly according to the measured waveform, such as pitted gear. However, it is difficult to detect the early gear damage from the original signals, such as spot

damaged gear I and II.

The noise is generated by the vibration of gears and other components of the machine. Moreover, the noise changes with the variation of gear conditions. However, the sound level signal is easily affected by the vibration of the other parts of the testing machine or the disturbance from the environment. Therefore, it makes more difficult for operators to measure and analyze the sound level signal. Figure 4.22 presents the sound level signal in one rotation of test gears acquired under conditions of n=1800rpm, T=40N-m and 70N-m respectively. The abscissa axis shows the gear tooth number and the ordinate axis represents the sound pressure. The sound level signal of normal gear and spot damaged gear is nearly stable, and the transient abnormal amplitude can't be found in these signals. The sound pressure of pitted gear is larger than that of the other gears. However, it is still difficult to diagnose gear damage only based on the original sound level signal.

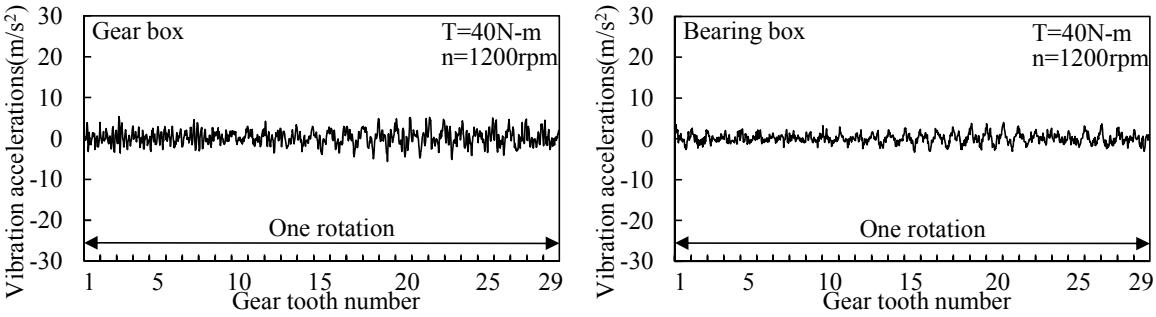

(a) Vibration accelerations on gear box and bearing box under n=1200rpm

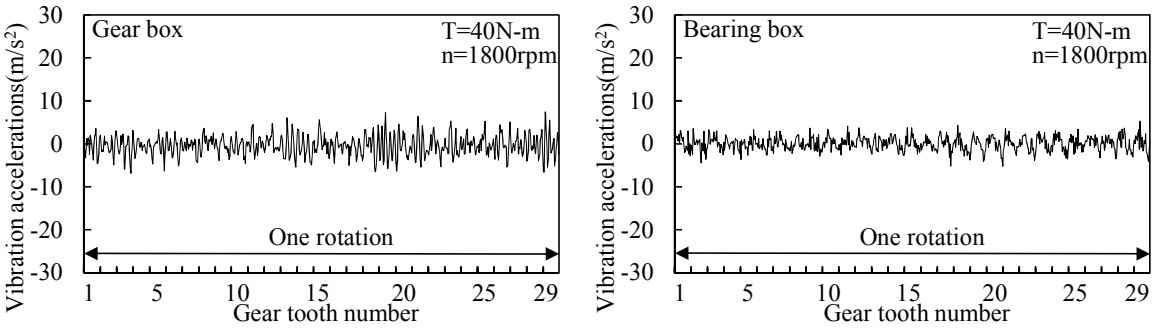

(b) Vibration accelerations on gear box and bearing box under n=1800rpm

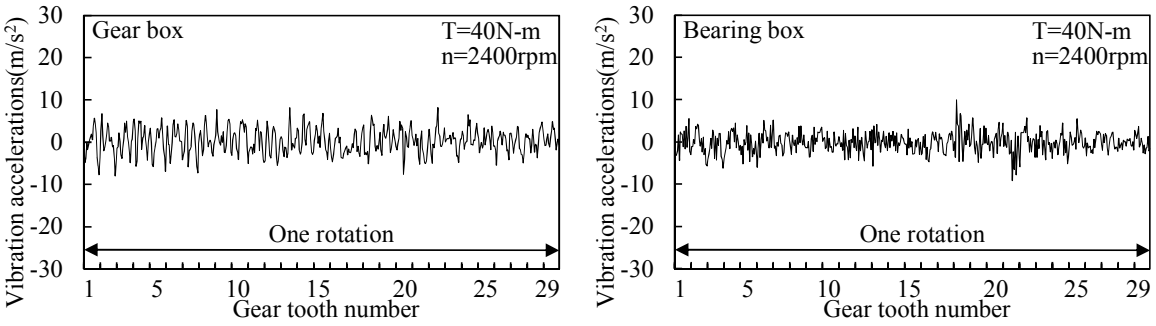

(c) Vibration accelerations on gear box and bearing box under n=2400rpm

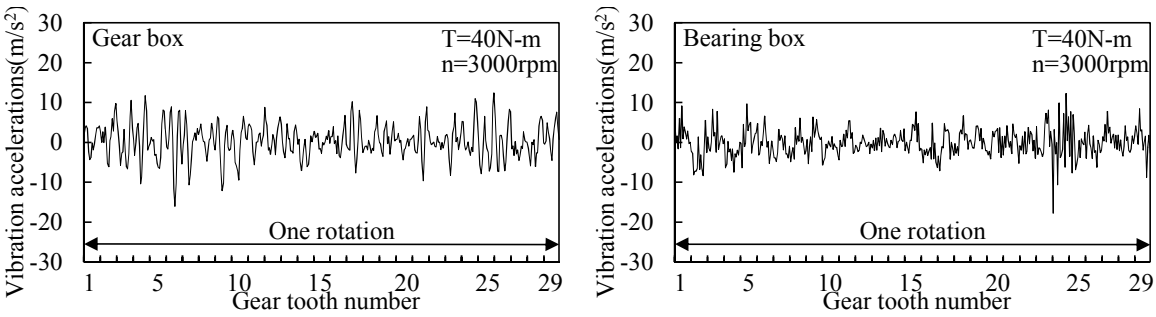

(d) Vibration accelerations on gear box and bearing box under n=3000rpm

Fig. 4.12 Vibration accelerations of normal gear under load T=40N-m

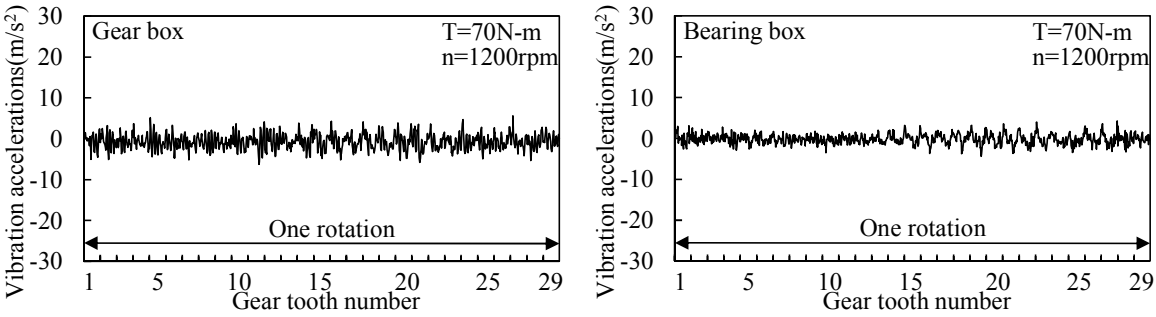

(a) Vibration accelerations on gear box and bearing box under n=1200rpm

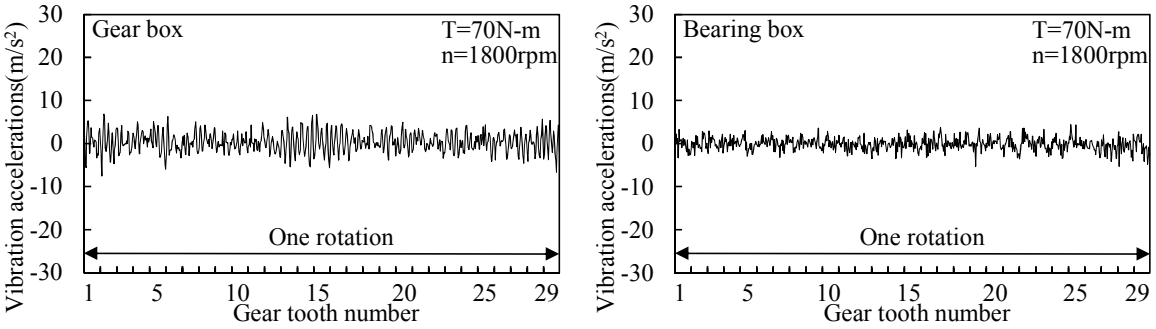

(b) Vibration accelerations on gear box and bearing box under n=1800rpm

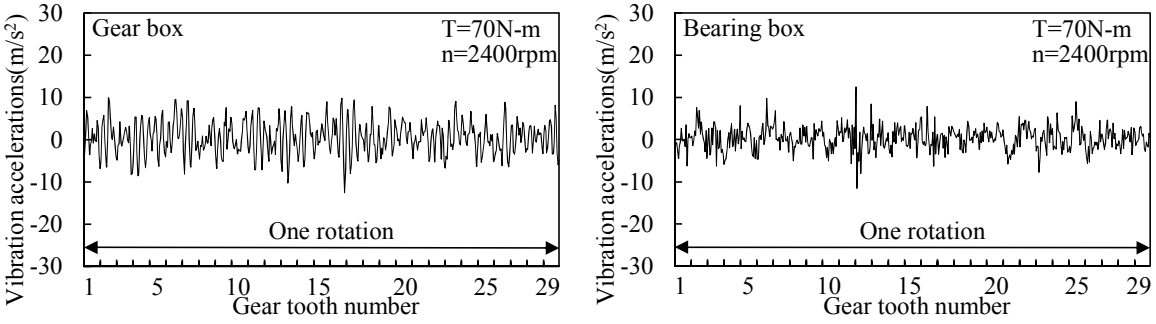

(c) Vibration accelerations on gear box and bearing box under n=2400rpm

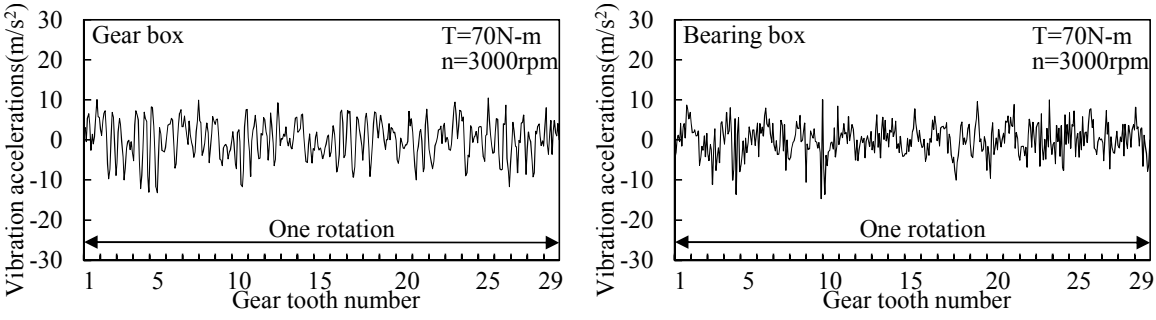

(d) Vibration accelerations on gear box and bearing box under n=3000rpm

Fig. 4.13 Vibration accelerations of normal gear under load T=70N-m

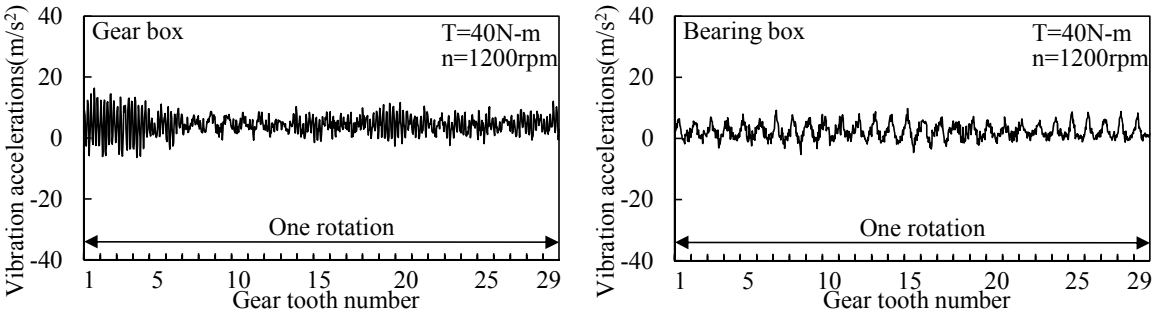

(a) Vibration accelerations on gear box and bearing box under n=1200rpm

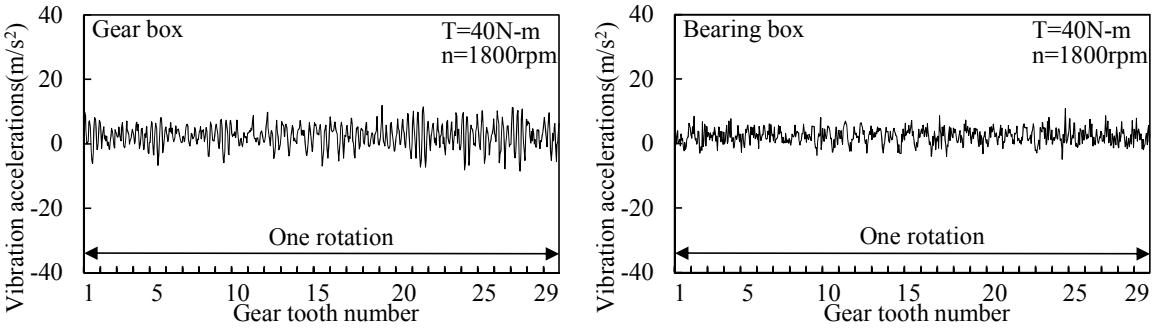

(b) Vibration accelerations on gear box and bearing box under n=1800rpm

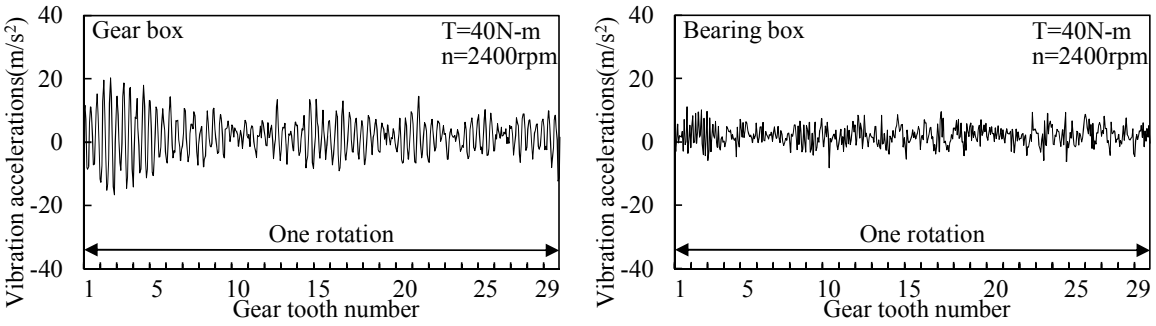

(c) Vibration accelerations on gear box and bearing box under n=2400rpm

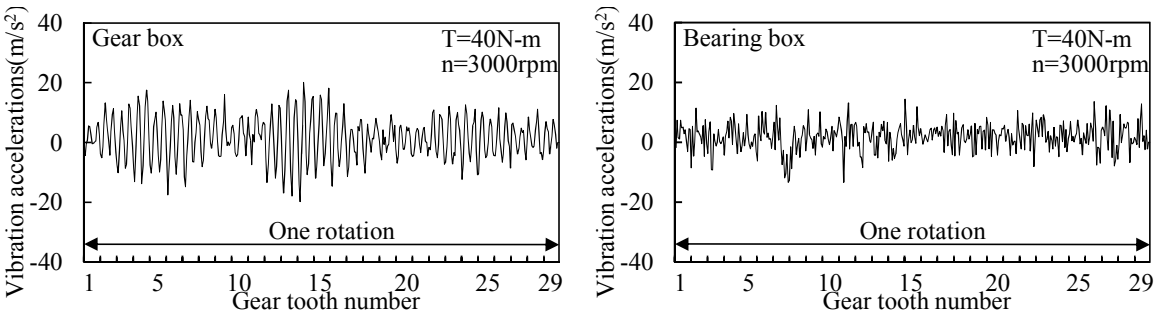

(d) Vibration accelerations on gear box and bearing box under n=3000rpm

Fig. 4.14 Vibration accelerations of spot damaged gear I under load T=40N-m

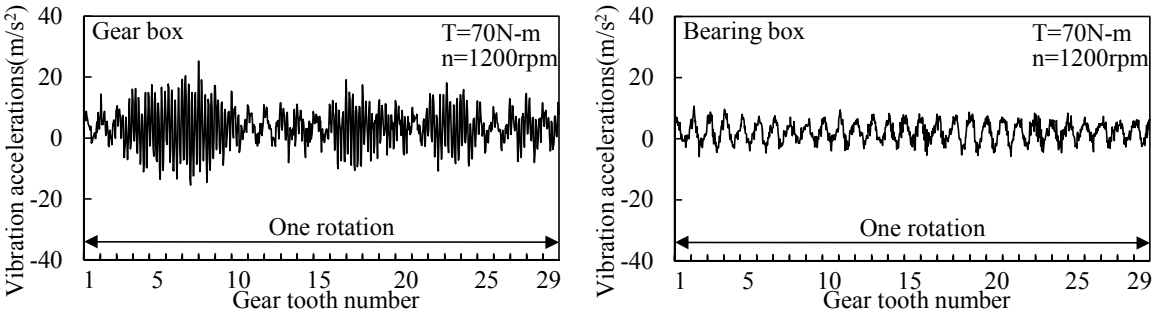

(a) Vibration accelerations on gear box and bearing box under n=1200rpm

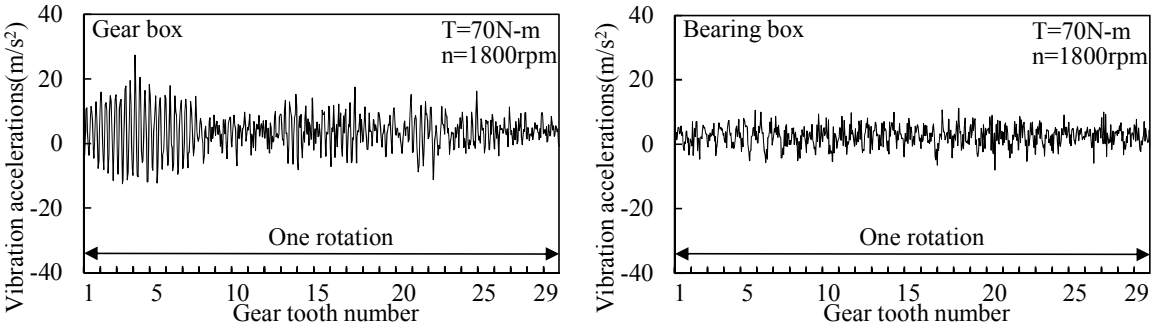

(b) Vibration accelerations on gear box and bearing box under n=1800rpm

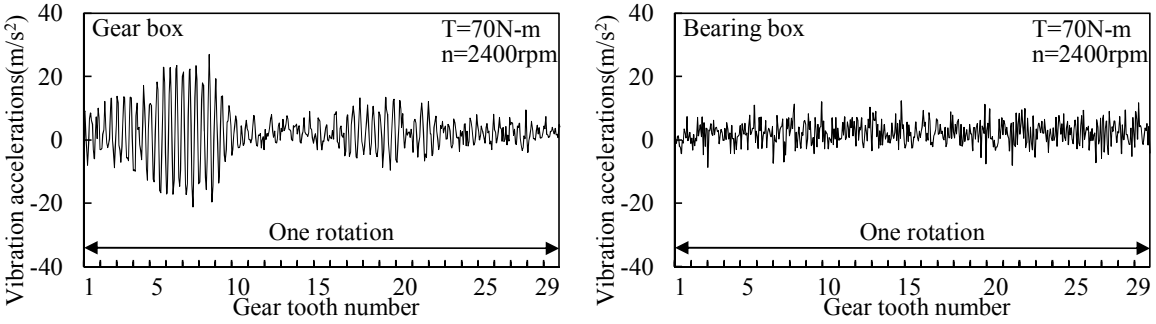

(c) Vibration accelerations on gear box and bearing box under n=2400rpm

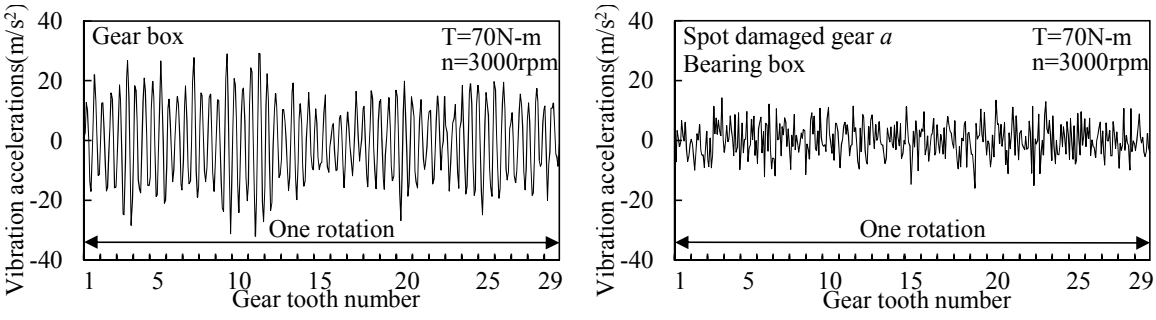

(d) Vibration accelerations on gear box and bearing box under n=3000rpm

Fig. 4.15 Vibration accelerations of spot damaged gear I under load T=70N-m

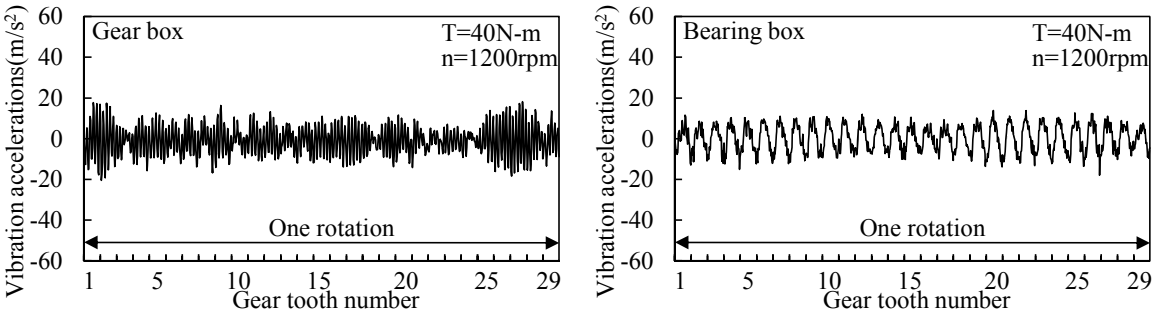

(a) Vibration accelerations on gear box and bearing box under n=1200rpm

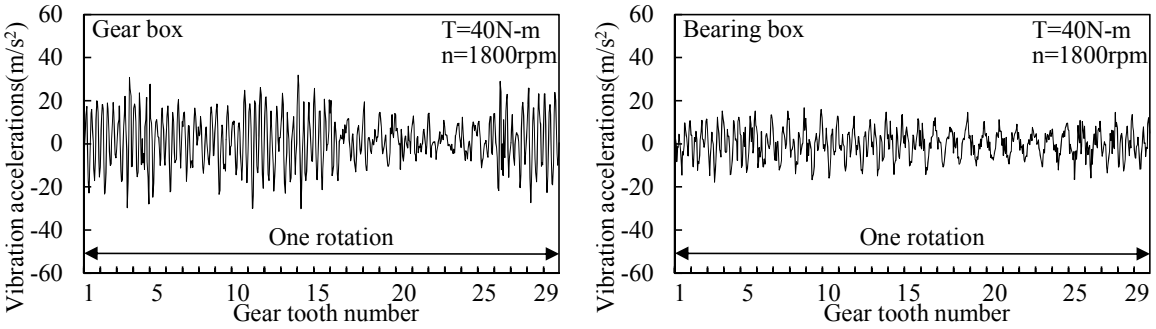

(b) Vibration accelerations on gear box and bearing box under n=1800rpm

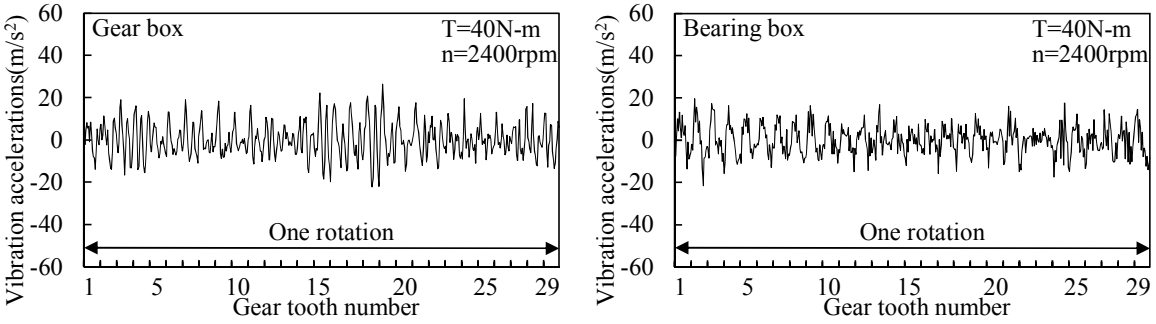

(c) Vibration accelerations on gear box and bearing box under n=2400rpm

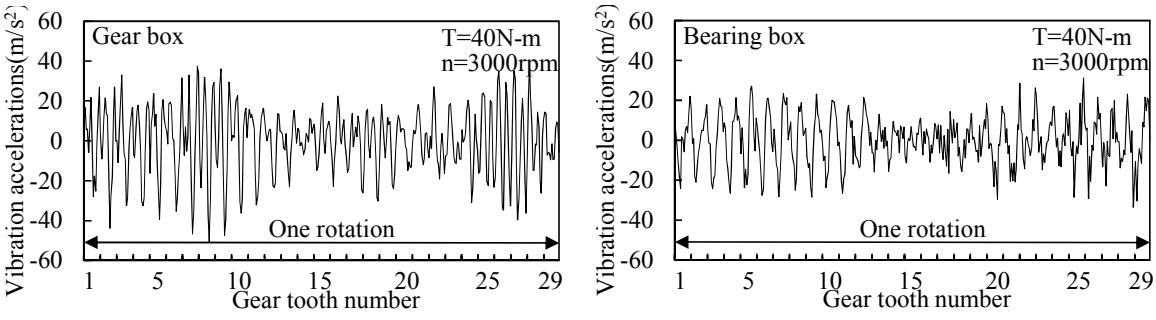

(d) Vibration accelerations on gear box and bearing box under n=3000rpm

Fig. 4.16 Vibration accelerations of spot damaged gear II under load T=40N-m

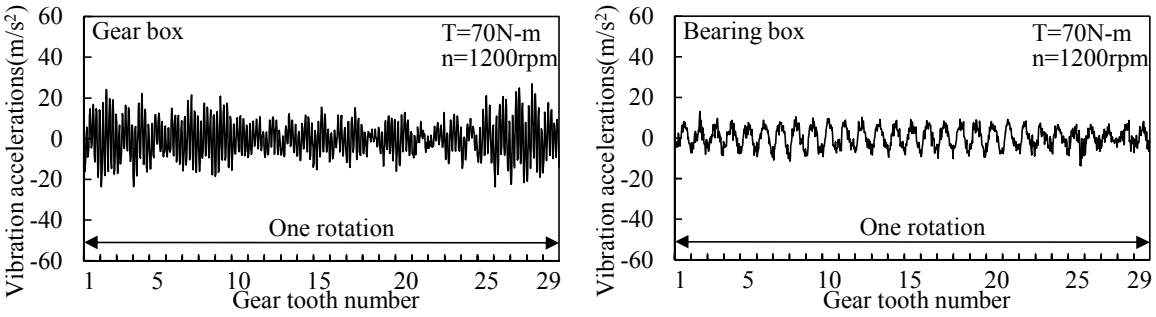

(a) Vibration accelerations on gear box and bearing box under *n*=1200rpm

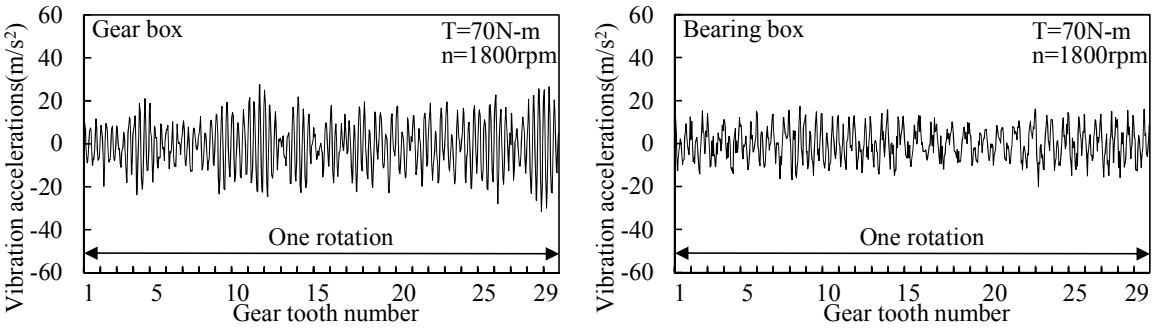

(b) Vibration accelerations on gear box and bearing box under *n*=1800rpm

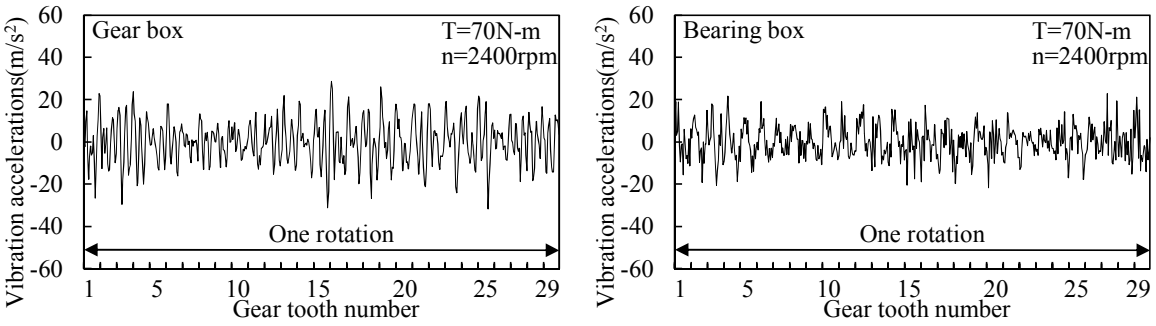

(c) Vibration accelerations on gear box and bearing box under *n*=2400rpm

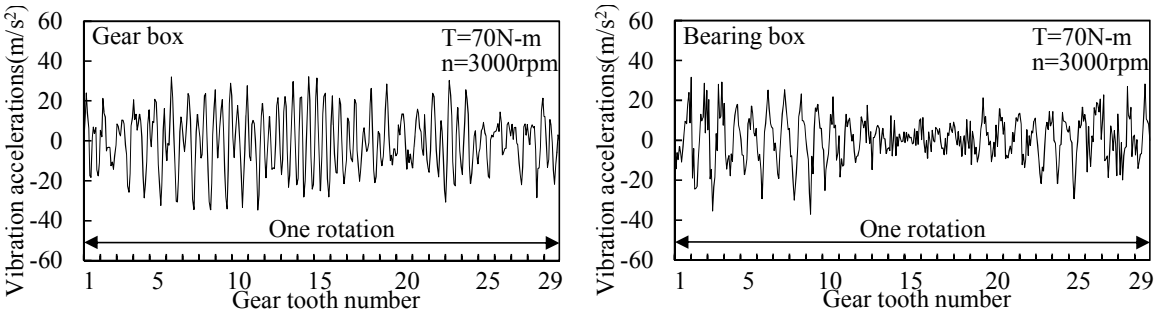

(d) Vibration accelerations on gear box and bearing box under *n*=3000rpm

Fig. 4.17 Vibration accelerations of spot damaged gear II under load *T*=70N-m

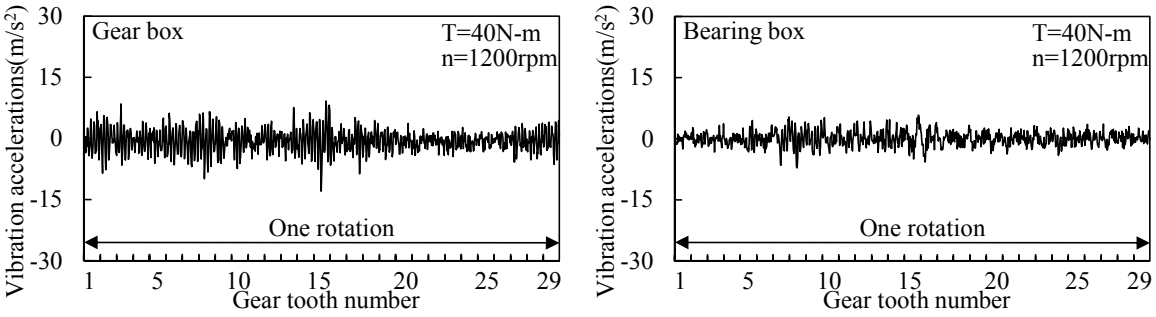

(a) Vibration accelerations on gear box and bearing box under n=1200rpm

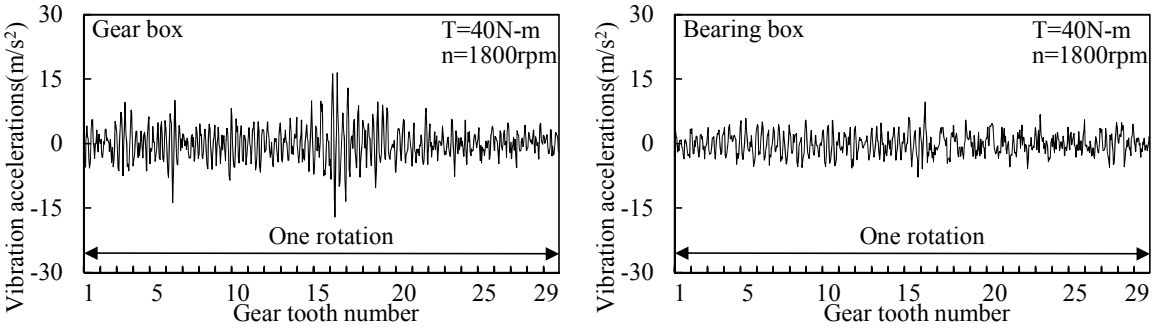

(b) Vibration accelerations on gear box and bearing box under n=1800rpm

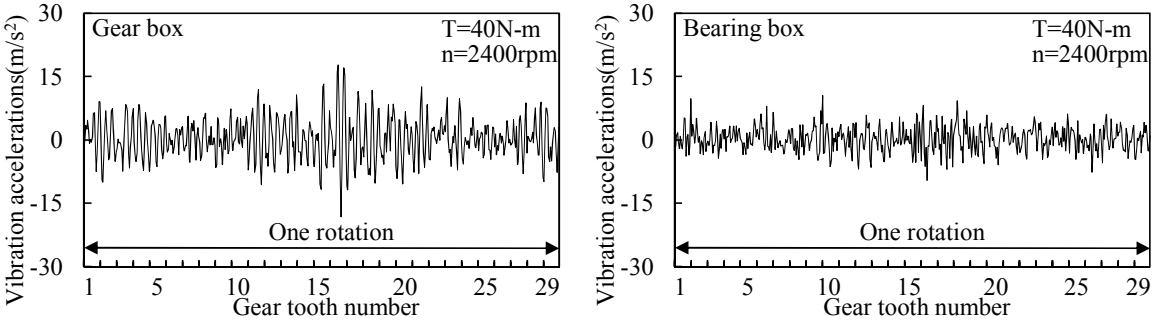

(c) Vibration accelerations on gear box and bearing box under n=2400rpm

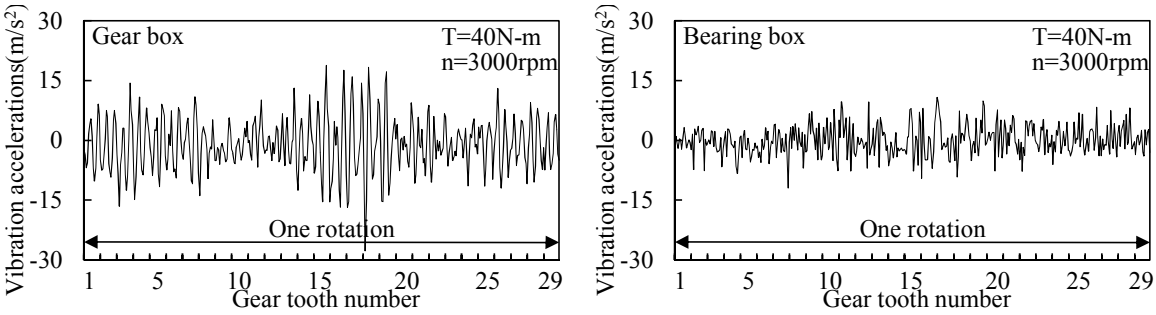

(d) Vibration accelerations on gear box and bearing box under n=3000rpm

Fig. 4.18 Vibration accelerations of spot damaged gear III under load T=40N-m

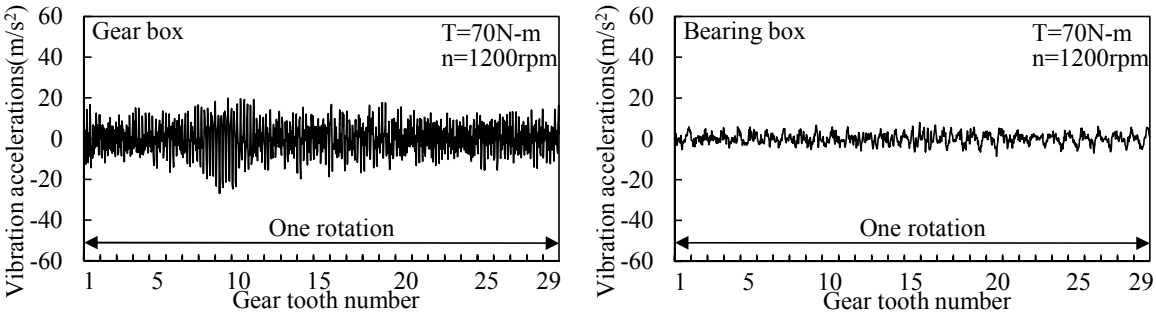

(a) Vibration accelerations on gear box and bearing box under *n*=1200rpm

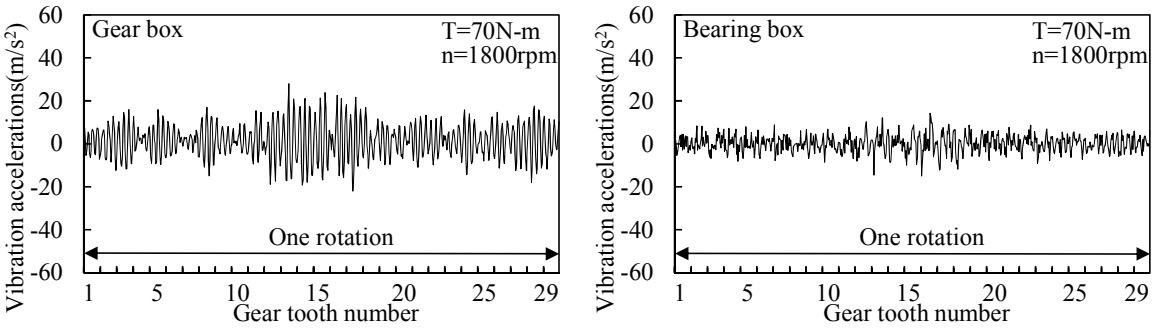

(b) Vibration accelerations on gear box and bearing box under *n*=1800rpm

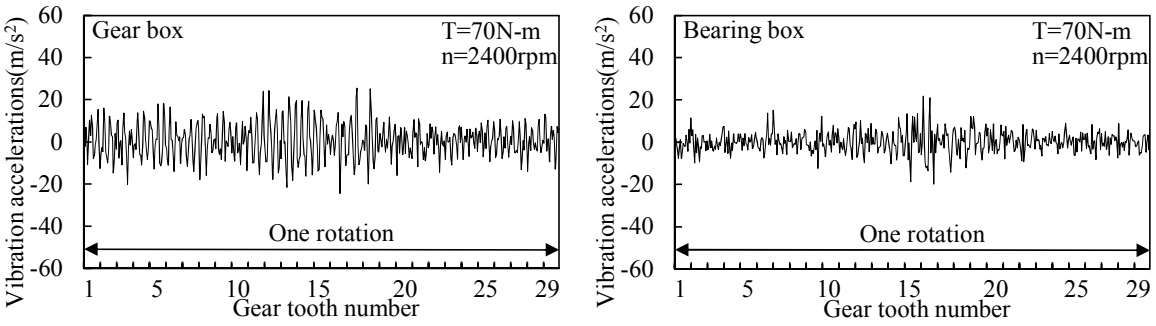

(c) Vibration accelerations on gear box and bearing box under *n*=2400rpm

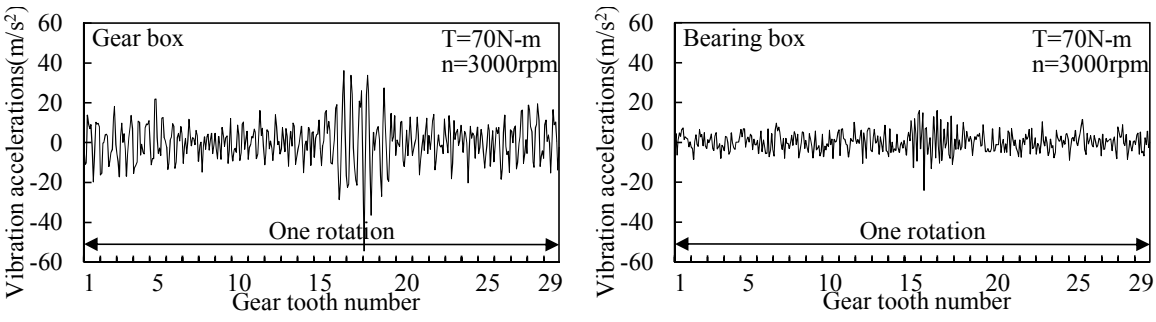

(d) Vibration accelerations on gear box and bearing box under *n*=3000rpm

Fig. 4.19 Vibration accelerations of spot damaged gear III under load *T*=70N-m

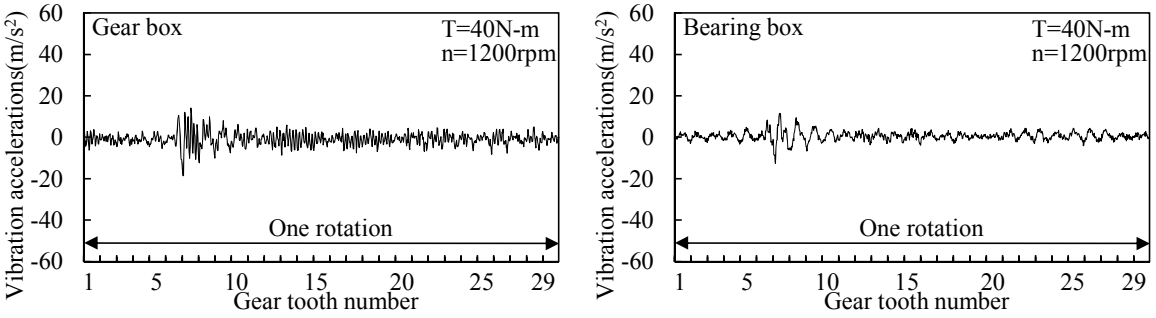

(a) Vibration accelerations on gear box and bearing box under n=1200rpm

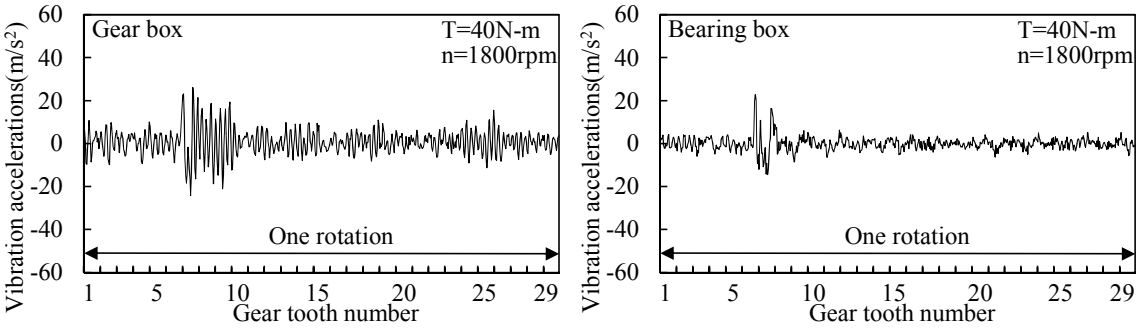

(b) Vibration accelerations on gear box and bearing box under n=1800rpm

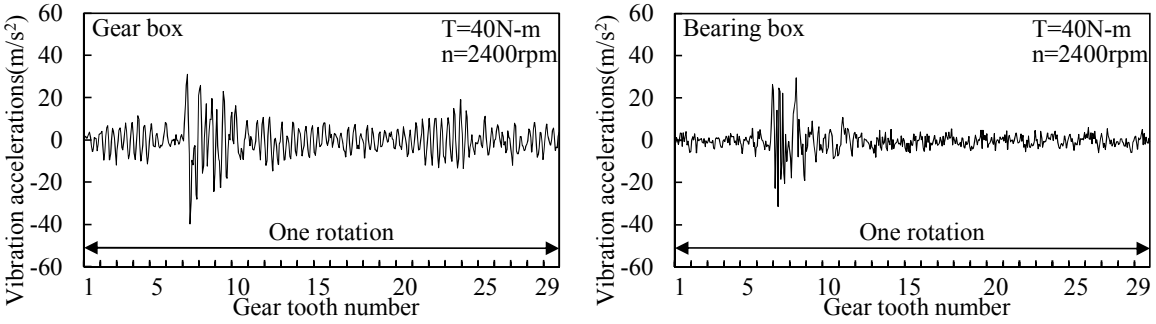

(c) Vibration accelerations on gear box and bearing box under n=2400rpm

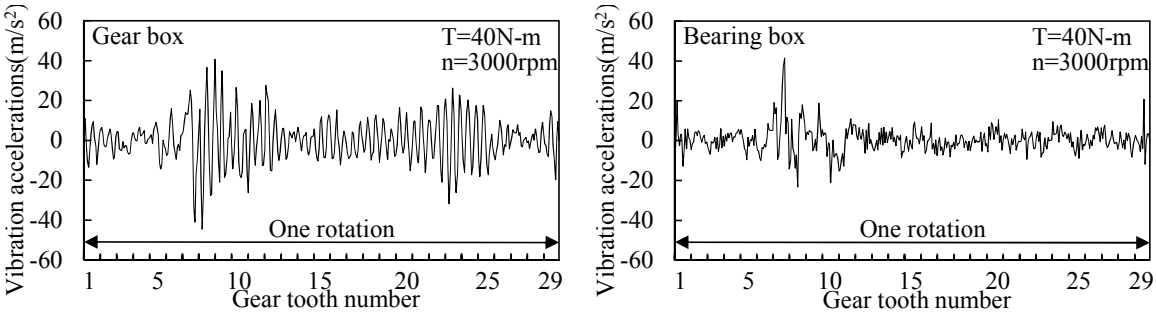

(d) Vibration accelerations on gear box and bearing box under n=3000rpm

Fig. 4.20 Vibration accelerations of pitted gear under load T=40N-m

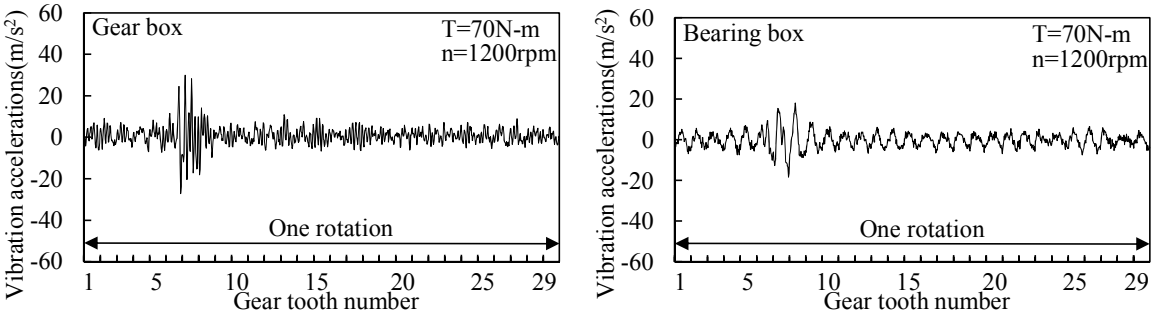

(a) Vibration accelerations on gear box and bearing box under *n*=1200rpm

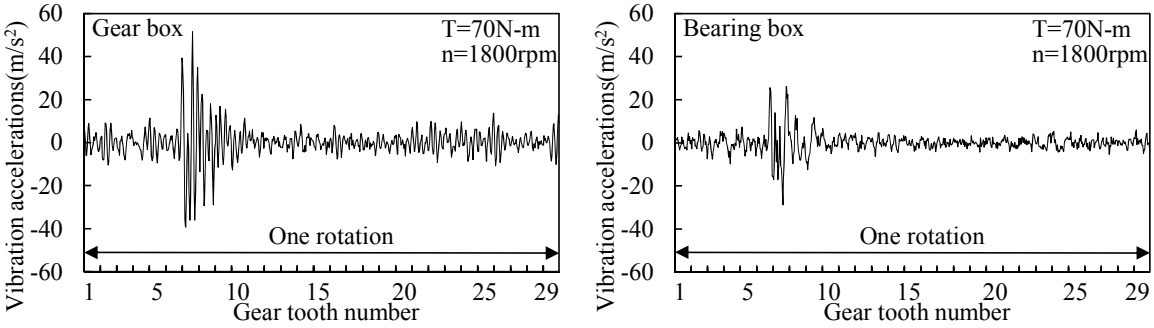

(b) Vibration accelerations on gear box and bearing box under *n*=1800rpm

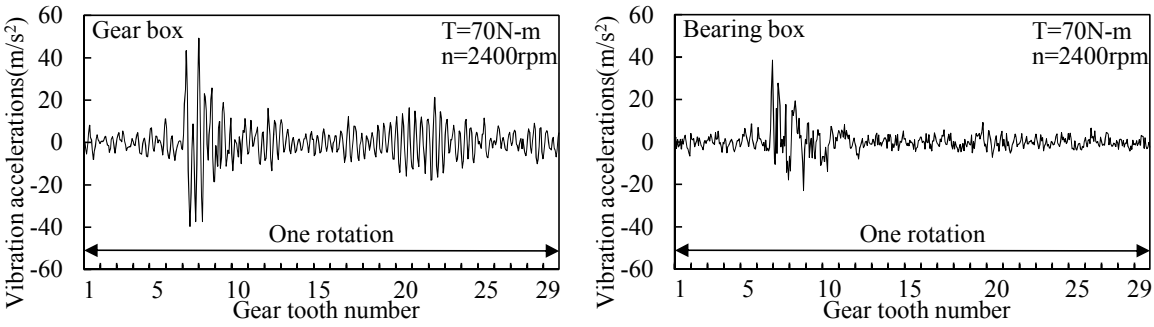

(c) Vibration accelerations on gear box and bearing box under *n*=2400rpm

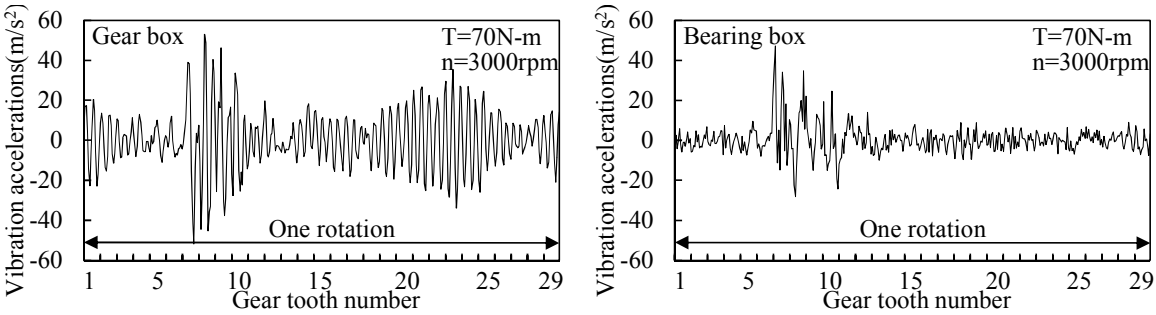

(d) Vibration accelerations on gear box and bearing box under *n*=3000rpm

Fig. 4.21 Vibration accelerations of pitted gear under load *T*=70N-m

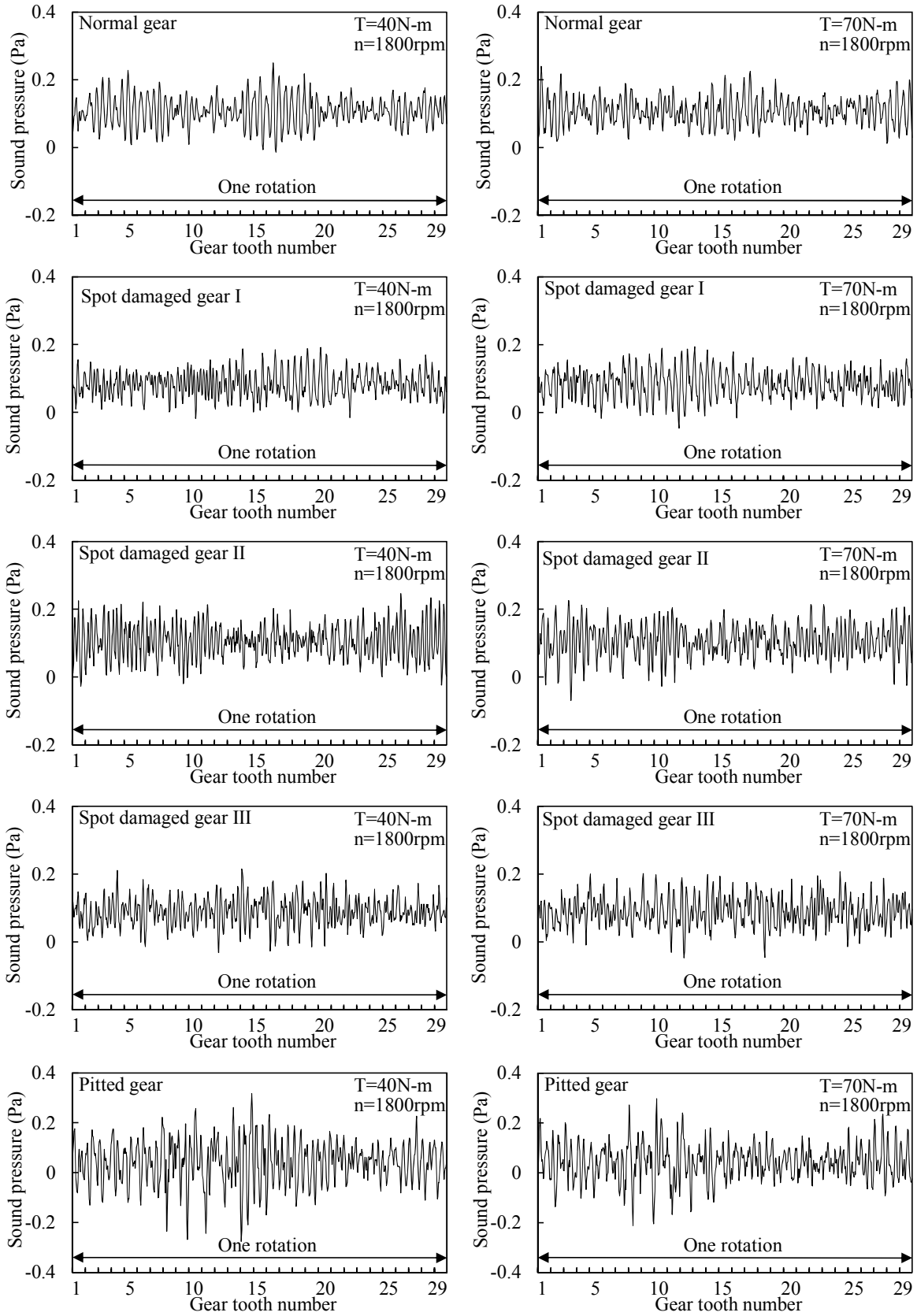

Fig. 4.22 Sound level signal under *T*=40N-m and 70N-m, *n*=1800rpm

4.5.2 Frequency Analysis of Vibration Accelerations

In frequency domain, the spectrum is always varying with the gear conditions. The meshing frequency and its harmonics, together with sidebands show respective characteristics of various gear conditions. The meshing frequency and its harmonics are the main components of the vibration signal. In case of a localized fault on tooth surface, the amplitude and phase modulation of the meshing frequency can be visible in frequency spectrum of the vibration signal. In the other words, sidebands will appear around the meshing frequency and its harmonics, the spacing of sidebands corresponds to the rotational frequency of the shaft carrying the defective gear [5, 84]. Therefore, fault features can be detected by analyzing the frequency spectrum of vibration signal. The signals acquired from accelerometer mounted on gear box are often inevitably contaminated by the interference signal, which is caused by vibrations from shafts, bearings, and other components on the testing machine. In addition, the signals are also polluted with the white noise which is generated by the accelerometer or the environmental electromagnetic disturbances. Except for the signal of interest, the other unnecessary signal components are considered as noise in this study. The noise is usually random and unstable, whose variation would be reflected in the frequency spectrum, especially in the high frequency bands.

I adopt the frequency spectrum of vibration accelerations on gear box under T=70N-m and n=1800rpm to representatively illustrate the characteristics of gear damage in frequency domain, which is shown in Fig. 4.23. Figures on the left depict the holistic spectrum of the signal, while figures on the right presents the details of meshing frequency and its sidebands. With the experimental conditions of gear rotation speed n=1800rpm and the number of teeth 29, the rotational frequency and the meshing frequency are 30Hz and 870Hz respectively. The natural frequency of system is about 3000Hz, and the analytical frequency is 10 kHz in Fast Fourier Transform.

From the spectrum of vibration signal for normal gear, it can be seen that the spectrum for normal gear is mainly dominated by the meshing frequency, two harmonic components and the natural frequency. High-order harmonics hardly appear in the spectrum, and the amplitudes of high frequencies are quite small, which shows the noise contained in the measured signal is weak. Moreover, the sidebands around the meshing frequency are narrow and weak, which indicates that there is no damage on the gear tooth surface.

In the spectrum of vibration signal for spot damaged gear I, the natural frequency, and the 2nd and 3rd harmonics become more significant and dominating and the amplitude of meshing frequency becomes smaller. Moreover, the modulation sideband around the meshing frequency with the frequency interval of rotational frequency becomes large, but it is still not obvious. This is

because the damaged area is small, which is incapable of strongly impacting the vibration of gears. Therefore, the modulation phenomenon is not clear.

In the spectrum of vibration signal for spot damaged gear II, the 3rd and 4th harmonics and natural frequency becomes more significant and dominating. In addition, the amplitude of the modulation sideband around the meshing frequency is large. In the spectrum of vibration signal for spot damaged gear III, the harmonics and sidebands become larger and wider. The modulation phenomenon is clearly observed from the spectrums for spot damaged gear II and III.

As shown in the spectrum of pitted gear, the natural frequency and harmonics appear with significant amplitude and the amplitude of meshing frequency is relatively weaker. Especially, the 3rd harmonic and natural frequency account for a considerable proportion in the spectrum. In addition, the sidebands around the meshing frequency are wide and strong, which shows the gear condition is abnormal.

Comparing the spectrums for normal gear, spot damaged gear and pitted gear, it is found that the amplitudes of harmonics and the natural frequency become larger with the increase of damaged area. Similarly, the sidebands also become stronger and broader. This is because the tooth profile error caused by gear damage intensifies the vibration when the failure tooth meshing, which can generate larger modulation of amplitude and phase in frequency spectrum. Consequently, the frequency spectrum can represent particular characteristics of various gear conditions, and representative failure features can be extracted from the spectrum.

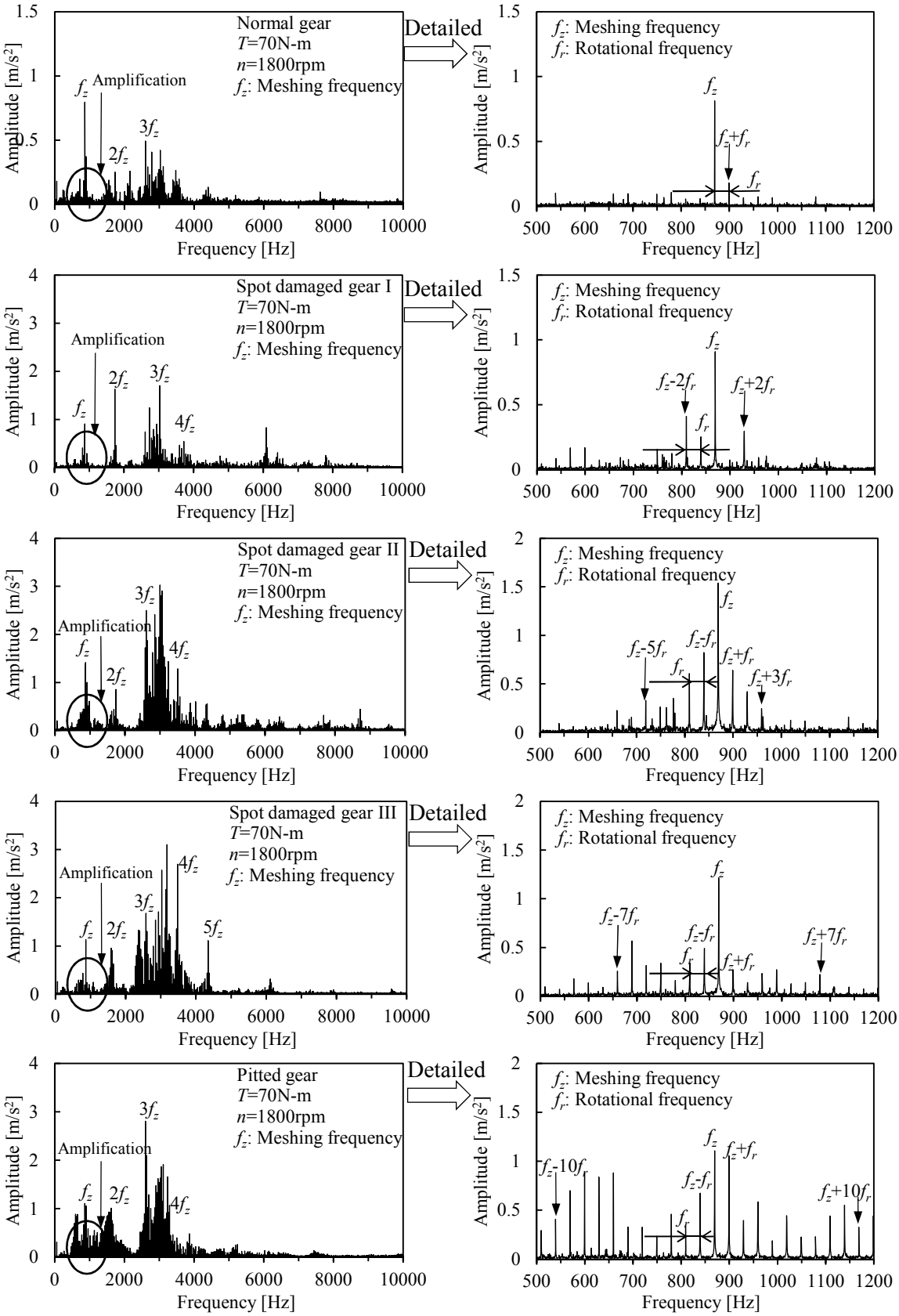

Fig. 4.23 Frequency spectrum of the vibration acceleration under T=70N-m, n=1800rpm

4.5.3 Residual Signal

Residual signal as a useful signal preprocessing method has been proved to be much less sensitive to the altering experimental conditions and more obvious representations of failure signatures in many literatures. Boulahbal, Golnaraghi and Ismail [85] used both the amplitude and phase maps of the wavelet to assess the condition of a gear. They found that the amplitude wavelet map of the residual vibration signal offers a better indicator of the presence of faults than the map of the actual signal. Dalpiaz, Rivola and Rubini [18] compared the results of wavelet transform using the raw signal, time synchronously averaged signal and residual signal of gear motion. The results show that the sensitivity of the wavelet transform of residual signal to cracks is quite satisfactory. Wang, et al. [41] compared the results of waveforms and statistical parameters using time synchronously averaging signals and residual signals under different torque levels and different gear states. The results show that the residual signal and its statistics are less sensitive to the torque level and the fault impulse in residual signal is more obvious.

In this study, the residual signal is obtained from the original signal as the data for the following analysis. The original signal of gear motion can be expressed as follows:

$$S(t)=\sum_{m=1}^{M}A_m\left(1+a_m(t)\right)\cos\left(2\pi f_m t+\phi_m+b_m(t)\right)+d(t)+n(t) \tag{4.1}$$

Where, $S(t)$ is the raw signal, M is the order of harmonics, f_m is the frequency of harmonics, which is the meshing frequency when m=1, A_m and $\emptyset_m$ are the amplitude and phase of f_m respectively, $a_m(t)$ is the amplitude modulation function and $b_m(t)$ is the phase modulation function, $d(t)$ is the resonance signal caused by the natural frequency of system, finally, $n(t)$ is the noise signal.

Most energy of the raw signal mainly concentrates around the meshing frequency and its harmonics. It is hard to distinguish the signal generated by the gear damage from the raw signal, especially in the early stage of failure occurrences. The residual signal can be acquired by removing the fundamental and harmonics of the meshing frequency and resonance signal from FFT spectrum of the raw signals and then reconstructing the remaining signal in the time domain [41]. The relationship between the raw signal and residual signal is shown as follows:

$$S_r(t)=S(t)-g(t)=S(t)-\left(\sum_{m=1}^{M}A_m\cos\left(2\pi f_m t+\phi_m\right)+d(t)\right) \tag{4.2}$$

Where, $S_r(t)$ is the residual signal, $S(t)$is the raw signal and $g(t)$ is the general signal which is constructed by the carrier signal and resonance signal. Since most energy in the healthy

state of the target gear is concentrated at the meshing frequency and its harmonics, the residual signal will be much less sensitive to the alternating experimental conditions than the original signal.

I just present the residual signals on gear box and bearing box under conditions of load T=40N-m, 70N-m and rotation speed n=1800rpm. The residual signals corresponding to one wheel revolution are shown in Figs. 4.24 and 4.25. As shown in these figures, the residual signal of the normal gear is still stable. Comparing with the original signal, the fluctuation of the amplitude seems to be strengthened in the residual signal of spot damaged gear. Especially in the residual signal of spot damaged gear III in Fig. 4.25, the amplitude around No. 16 tooth seems larger in the waveform on bearing box. The evident of fault impulse for spot damage is a little more obvious in residual signals on gear box. However, it is still hard to detect gear faults from the residual signal on bearing box. There is no evident indication in the residual signal for spot damaged gear II. Although the residual signal can strengthen the characteristics of gear damage to some extent, it is still hard to diagnose the early gear faults only based on the residual signal. Additionally, the amplitude value of the residual signal is smaller than that of the raw signal. The reason for this is considered as the harmonics and resonance signal is eliminated from the raw signal and the energy of the residual signal becomes smaller.

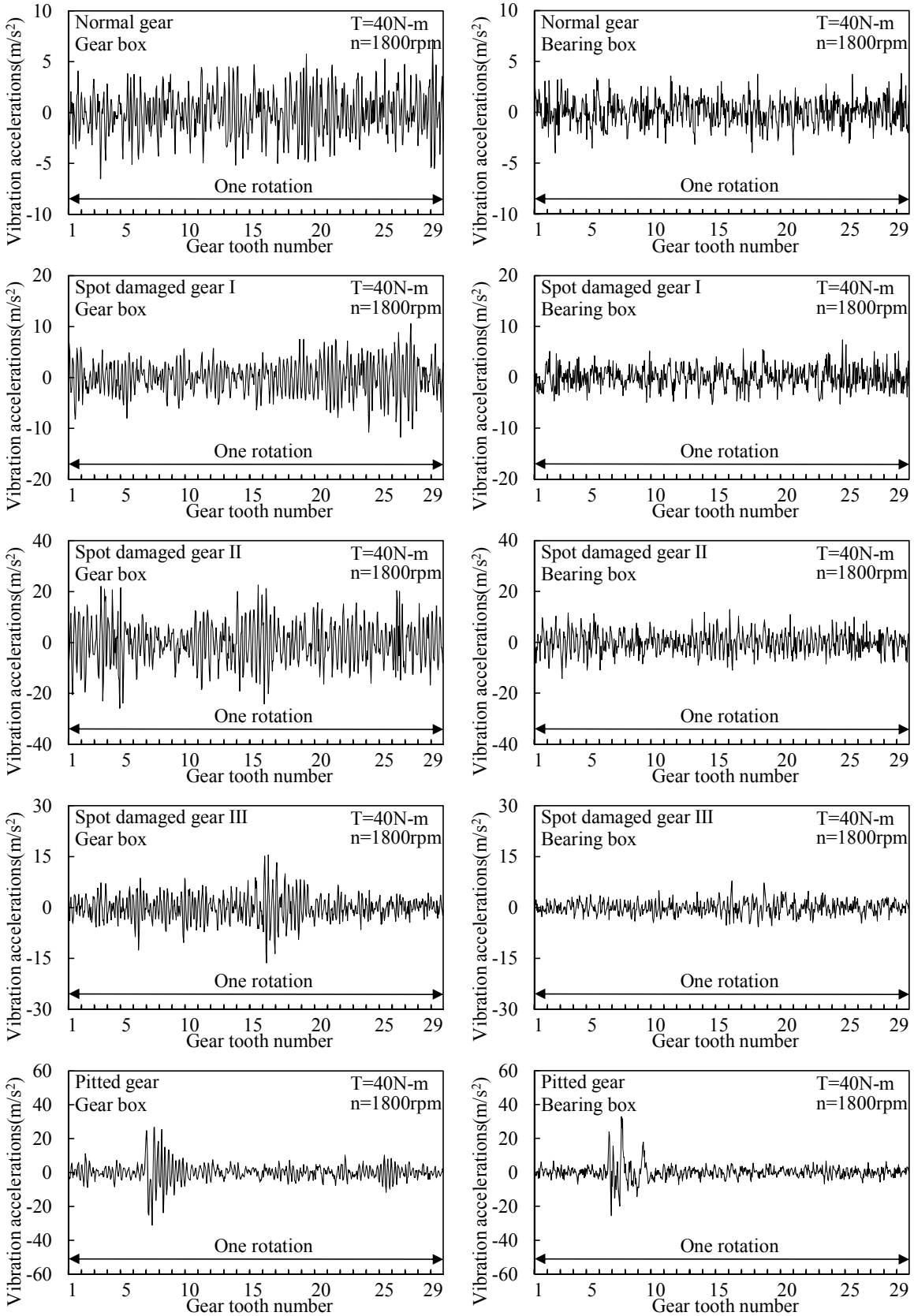

Fig. 4.24 Residual signals of vibration accelerations under T=40N-m and n=1800rpm

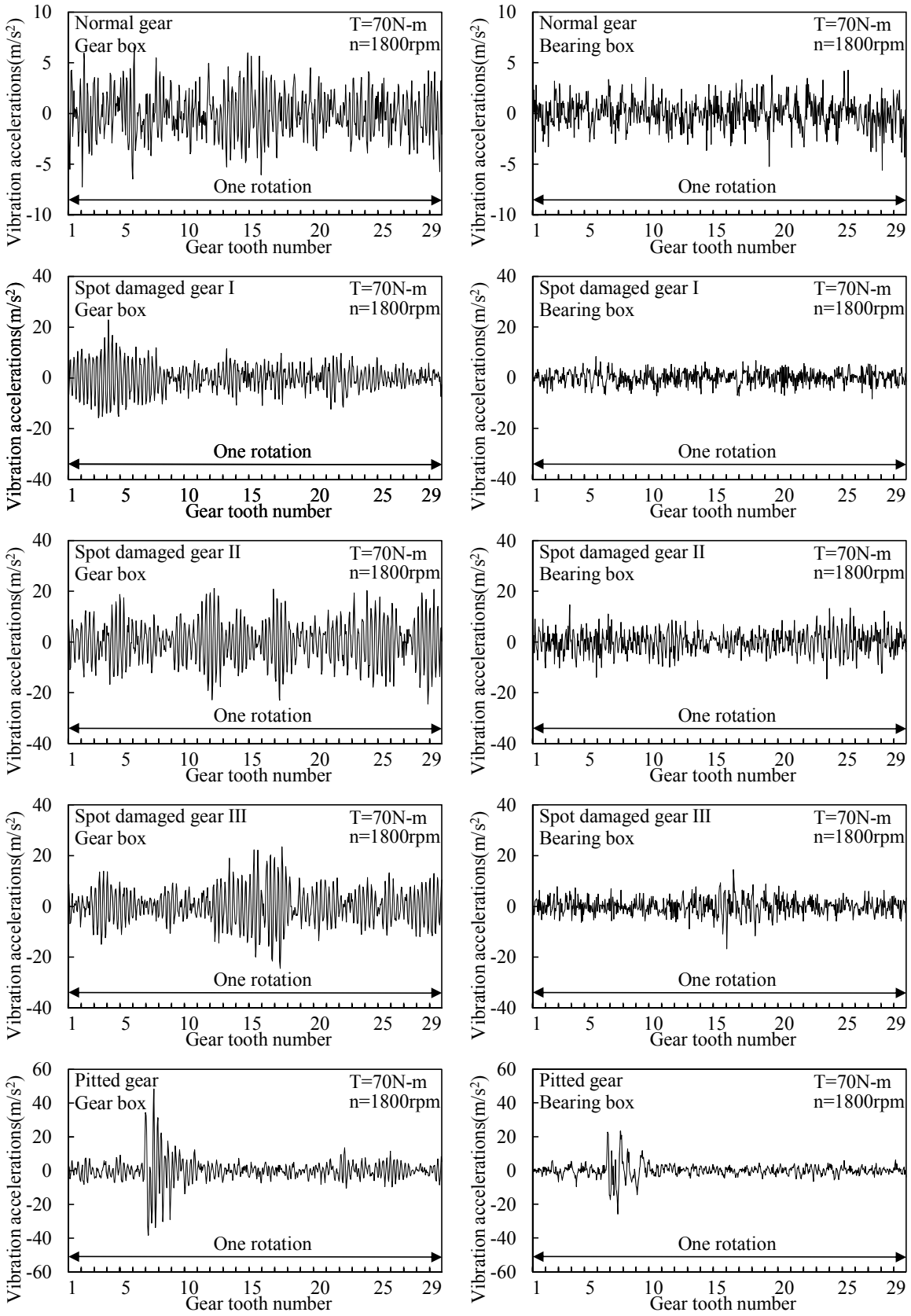

Fig. 4.25 Residual signals of vibration accelerations under T=70N-m and n=1800rpm

4.5.4 Processed Signal Acquired Using Discrete Wavelet Transform

Wavelet analysis has been the favorite analytical tool of gear damage detection in time-frequency domain and used to extract the failure signatures from the measured signal in many studies [51, 86]. Because the noise contained in the residual signal is relatively large and affects the diagnosis of gear damage, it is necessary to eliminate the noise from the residual signal. In this study, discrete wavelet transform with Daubechies 4 wavelet was employed to reduce the noise from the residual signal. After that, the coefficients of discrete wavelet transform with noise filtered are reconstructed as analytical data, called processed signal, for extracting characteristic parameters in the following study.

Unlike the Fourier transform, in which a signal is decomposed in to a sinusoid function basis, the wavelet transform uses a more general basis to decompose the signal into a series of resolutions in a single time-scale display. Because the wavelet transform uses a series of sizes of windows to compare with all sections of the signal, it is possible to display the symptoms of damage all simultaneously. According to the algorithm of wavelet transform, the original signal $x(t)$ can be decomposed into a family of functions which are the translation and dilation of a unique-valued function $\psi(t)$. The wavelet transform is defined as the following equation [50]:

$$WT_x(s,\tau) = \int_{-\infty}^{\infty} x(t) s^{-1/2} \psi(s^{-1}(t-\tau)) \mathrm{d}_t \tag{4.3}$$

Where, s is a scaling factor which produces dilation, τ is the time or some other spatial coordinate, and $\psi(t)$ is called a wavelet. The corresponding wavelet family is generated by translation of the wavelet in the time domain and dilation in the scale domain. The wavelet family is defined as[50]:

$$\psi_{s,\tau}(t) = s^{-1/2}\psi\big(s^{-1}(t-\tau)\big) \quad (\tau, s \in R^2) \tag{4.4}$$

Where, R denotes the set of real numbers. Any function $x(t)$ in R^2 can be characterized by its decomposition of the wavelet family of equation (4.4). A wavelet transform can be interpreted as a decomposition of a signal into a set of frequency channels.

Make, $s = s_0^j, \tau = n\tau_0 s_0^j$, the discrete wavelet family is defined as:

$$\psi_{j,n}(t) = {s_0}^{-j/2}\psi\big(s_0^{-j}t - n\tau_0\big) \quad (j, n \in Z^2) \tag{4.5}$$

Where, Z denotes the set of integers. The discrete wavelet transform is defined as [50]:

$$WT_x(j,n) = \int_{-\infty}^{\infty} x(t) {s_0}^{-j/2} \psi\big(s_0^{-j}t - n\tau_0\big)\, \mathrm{d}_t \tag{4.6}$$

For discrete wavelet transform, the reconstruction of signal $x(t)$ can be acquired by[50]:

$$x(t) = \sum_{j \in Z} \sum_{n \in Z} WT_x(j,n) s_0^{-j/2} \psi\left(s_0^{-j} t - n\tau_0\right) \tag{4.7}$$

Because of the orthogonality of wavelets, the orthogonal wavelets such as the well-known Daubechies wavelet series can offer faster algorithms and no redundancy in the decomposition. The translation results of time-frequency functions can also more correctly reflect the properties of the signal. Therefore, the Daubechies 4 wavelet is selected in this study. The residual signal is decomposed into a compact wavelet series by discrete wavelet transform. Then, the processed signal is acquired by reconstructing the coefficients of wavelets.

Sqtwolog, heursure, rigrsure and minimax are the common methods to reduce the noise in wavelet transform. In this paper, I try to select the best denoising method from these approaches based on Signal to Noise Ratio (SNR). SNR is defined as a ratio of the power of analytical signal to the power of the noise, which is calculated as follows [54].

$$\lambda = 10 \log_{10}(P_s / P_N) \tag{4.8}$$

$$P_s = \frac{1}{N} \sum_{n=1}^{N} S_r(n)^2 \tag{4.9}$$

$$P_N = \frac{1}{N} \sum_{n=1}^{N} \left[S_r(n) - S_p(n) \right]^2 \tag{4.10}$$

Where, P_s is the energy of residual signal, P_N is the energy of noise, N is the sampling number of residual signal, $S_r(n)$ is the residual signal and $S_p(n)$ is the processed signal with noise filtered by discrete wavelet transform.

It is known that the smaller the SNR, the better the effect of denoising is. In this paper, the SNR acquired by the method of sqtwolog, heursure, rigrsure and minimaxi are 13.3995, 53.0335, 53.0335 and 19.1002 respectively, which indicates that the best denoising method is sqtwolog. However, the sampling number is very large in this paper, which can substantially increase the threshold value of sqtwolog so as to eliminate useful data from the signal. Moreover, the SNR calculated with the method of heursure and rigrsure is too small to effectively reduce the noise. Therefore, the method of minimaxi was selected to reduce the noise in wavelet transform.

Figure 4.26 depicts the processed signals in one rotation under conditions of T=70N-m and n=1800rpm. As shown in this figure, the amplitude of the processed signal is smaller than that of the residual signal. However, the waveform of the processed signal is much smoother. This is

because some noise is reduced from the residual signal, the energy of the signal become weaker. In the processed signal of normal gear, the waveform on gear box and bearing box is stable over the period. For spot damaged gear I, the amplitude of the signal before No. 5 tooth is much larger than that of the other parts. It can be considered that some damage may exist between No.1~5 teeth of the test gear. The abnormal indication can't be found from the processed signal on bearing box. For spot damaged gear II, although the processed signals on gear box fluctuates irregularly, it is still impossible to detect gear damage based on the indications. For spot damaged gear III, the amplitudes around No. 16 tooth is obviously large in the processed signals on both gear box and bearing box. Especially, the indication of gear damage is strengthened in the processed signal of bearing box. For the pitted gear, the difference of amplitude value becomes larger. The fault indication is more significant in the processed signal. In the processed signals of spot damaged gear I, III and pitted gear, the amplitude value of normal teeth is reduced more than that of the damaged tooth, which enlarges the difference of the waveform. Therefore, the fault features are more clearly visualized in processed signals. It is investigated that the method of discrete wavelet transform can contribute to strengthen the characteristics of damage.

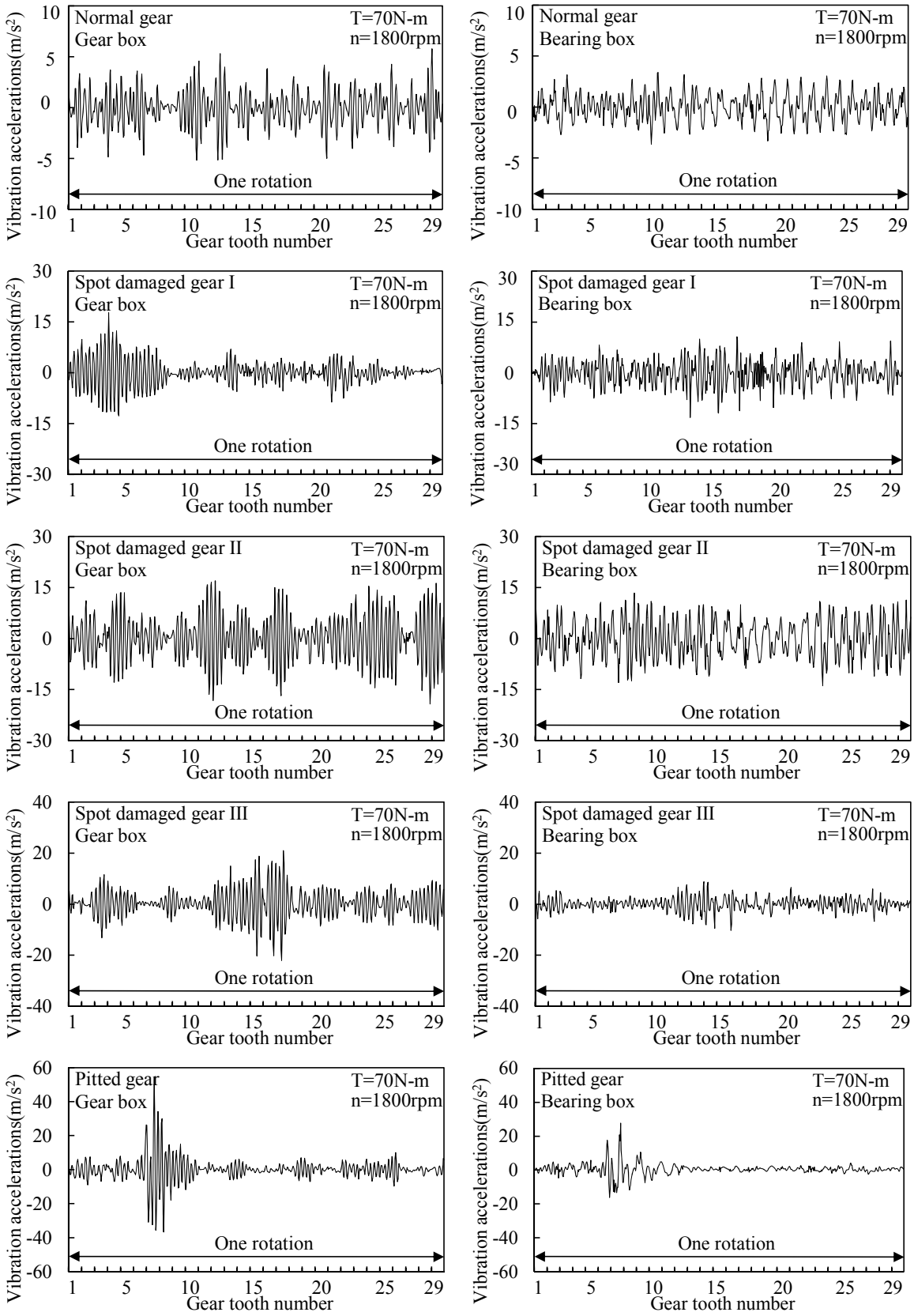

Fig. 4.26 Processed signals of vibration accelerations under *T*=70N-m and *n*=1800rpm

4.6 Summary

In this chapter, the damage contrast test is performed. The vibration accelerations on gear box and bearing box and the sound level signal are presented and discussed. The original vibration accelerations are analyzed using Fast Fourier Transform and discrete wavelet transform. The frequency spectrum, residual signal and processed signal are obtained from the vibration accelerations.

The following conclusions can be drawn from the present work.

1. The large damage on tooth surface will cause transient larger amplitude in the original vibration signals, based on which the abnormal gear condition can be diagnosed. However, the abnormal amplitude is invisible when the damaged area is small. Therefore, the slight gear damage would not be detected based on the original waveform. The vibration accelerations acquired under T=70N-m is a little stronger than that acquired under T=40N-m. In addition, along with the increase of rotation speeds the vibration accelerations become larger and the indication of damage also becomes more and more obvious in the original signal. The influence of varying loads on the vibration accelerations is weaker than the influence of varying gear rotation speed on the vibration accelerations.

2. In the frequency spectrum of various gear conditions, the amplitudes of high-order harmonics and the natural frequency become larger with the increase of damaged area. Moreover, the sidebands also become stronger and broader. The frequency spectrum can represent particular characteristics of different gear conditions. Representative failure features can be extracted from the spectrum.

3. Comparing with the original signal, the method of residual signal can emphasize the abnormal amplitude generated by the gear damage. The evidence of fault impulse is a little more obvious in residual signals on gear box. Although the residual signal can strengthen the failure features of gear damage to some extent, it is still hard to diagnose the early gear faults only based on the residual signal.

4. The noise can be effectively reduced from the residual signal by employing the method of discrete wavelet transform. The processed signal is acquired with reconstructing the coefficients of discrete wavelet transform. In the processed signals of spot damaged gear and pitted gear, the difference of amplitude value is enlarged. Therefore, the fault indications are more clearly visualized in processed signals. It is confirmed that the method of discrete wavelet transform can contribute to strengthen the characteristics of gear damage.

5 Cyclic Fatigue Test

5.1 Introduction

In order to investigate the generation and progression of gear failures and confirm the validity of the proposed method, cyclic fatigue test was implemented on the power circulating type gear testing machine. The experimental apparatus is the power circulating type gear testing machine, as same as the experimental set-up introduced in chapter 4. The vibration accelerations on gear box and bearing box, gear noise and pitch signal are measured during the fatigue test. Then the vibration accelerations are analyzed by Fast Fourier Transform, by which the frequency spectrum and residual signal are obtained. In order to emphasize the failure features shown in the residual signal, the technique of discrete wavelet transform is employed to reduce noise from the residual signal. Then, the processed signal is acquired by reconstructing the coefficients of discrete wavelet transform.

This chapter introduces the cyclic fatigue test. The original vibration accelerations and sound level signal are presented. The algorithm of residual signal and discrete wavelet transform is also introduced. Then, the residual signal, processed signal and frequency spectrum are represented.

5.2 Test Gears

Two involute spur gears are used as test gears, whose module is 4 mm, number of teeth is 29, and pressure angle is 20°. They are made of thermal refining steel JIS S45C, the gear surface finishing is hobbing, and the accuracy is JIS B1702 Grade 4. Their dimensions are shown in Table 5.1. Figure 5.1 shows the diagram of test gears.

Table 5.1 Dimensions of test gears

Module	m [mm]	4
Number of teeth	z_1/z_2	29/29
Pressure angle	α_0 [deg]	20
Addendum	h_a [mm]	4
Dedendum	h_d [mm]	5
Pitch circle diameter	d [mm]	116
Tip circle diameter	d_a [mm]	124
Face width	b [mm]	10
Contact ratio	ε	1.65
Material		JIS S45C Thermal refining steel
Surface finishing		Hobbing

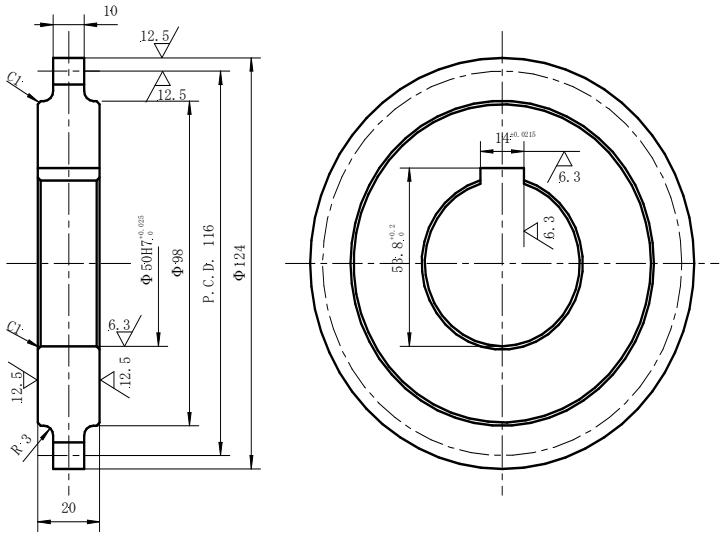

Fig. 5.1 The diagram of test gears

Table 5.2 Experimental conditions of the cyclic fatigue test

Torque	T [N-m]	70
Rotation speed	n [rpm]	1800
Cycles	N	0, 5×10^4, 1×10^5, 2×10^5, 5×10^5, 1×10^6, 2×10^6, 3×10^6, 5×10^6, 7×10^6, 1×10^7

5.3 Experimental Conditions

Table 5.2 presents the experimental conditions of cyclic fatigue test, test gears were continuously driven until 1×10^7 cycles with the rotation speed n =1800rpm and load torque 70 N-m. During the fatigue test, the vibration accelerations of gear box and bearing box, gear noise and pitch signal are measured at cycles N = 0, 5×10^4, 1×10^5, 2×10^5, 5×10^5, 1×10^6, 2×10^6, 3×10^6, 5×10^6, 7×10^6 and 1×10^7 respectively to investigate the progression of pitting failure. Meanwhile, the photo of tooth surface, gear tooth profile error and pitting area ratio are also taken and measured. The sampling frequency is 20 kHz, and the sampling time is 2 seconds.

5.4 Experimental Results and Discussions

5.4.1 Photographs of Tooth Surface

Figures 5.2 and 5.3 represent the photographs of tooth surfaces of test driving gear and test driven gear respectively. The width of gear teeth is 10mm, and the dashed line represents the tracing line for measuring tooth profile error of test gears. The photographs are taken at various cycles N, which illustrate the occurrence and progressing of the pitting damage. At N=0, there is only tool marks on the gear tooth surface. The roughness of tooth surface becomes smaller with the increase of cycles N. However, damage also gradually generates and becomes larger as the driving time passes. For test driving gear, the initial pitting begins to occur on the root of tooth surface at N=2×10^6. While for test driven gear, the pitting begins to generate on tooth surface at N=5×10^6. The pitting damage more early generates on the tooth surface of driving gear. Moreover, the pitting damage on driving gear is severer than that on driven gear. Additionally, the pitting damage of both driving gear and driven gear initially appear on the root of tooth surface, and the damaged area becomes larger with the increase of cycles N.

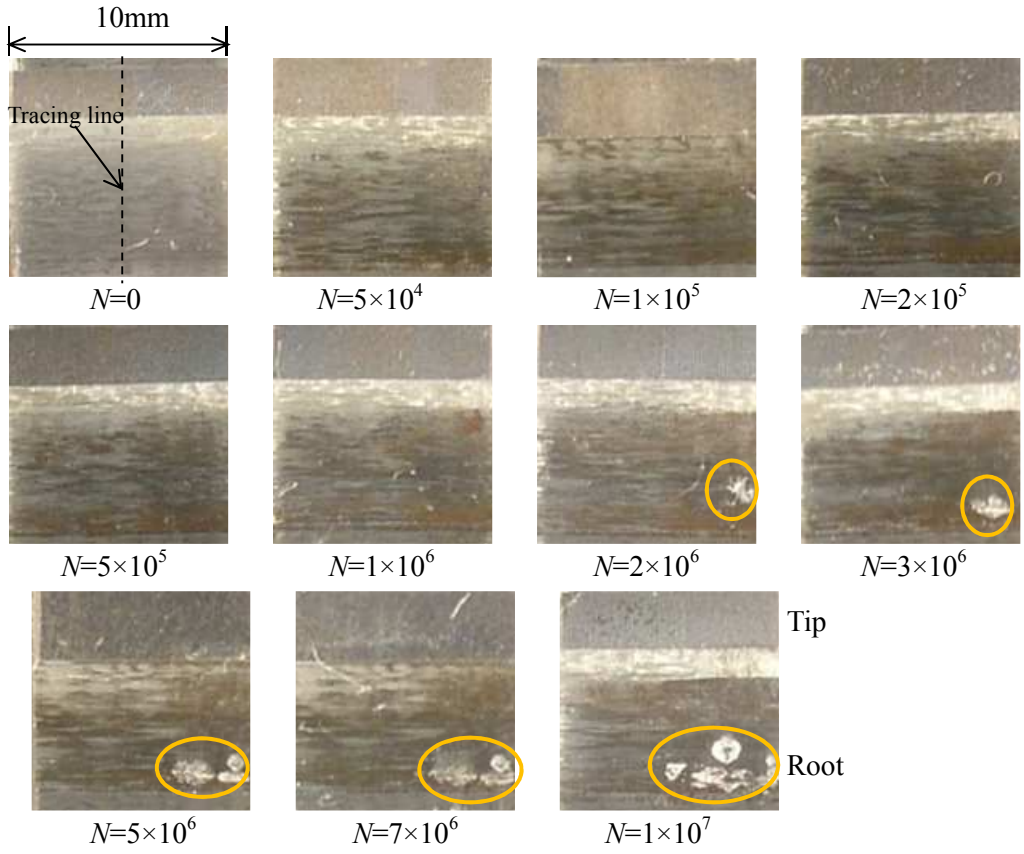

Fig. 5.2 Photographs of tooth surface of test driving gear

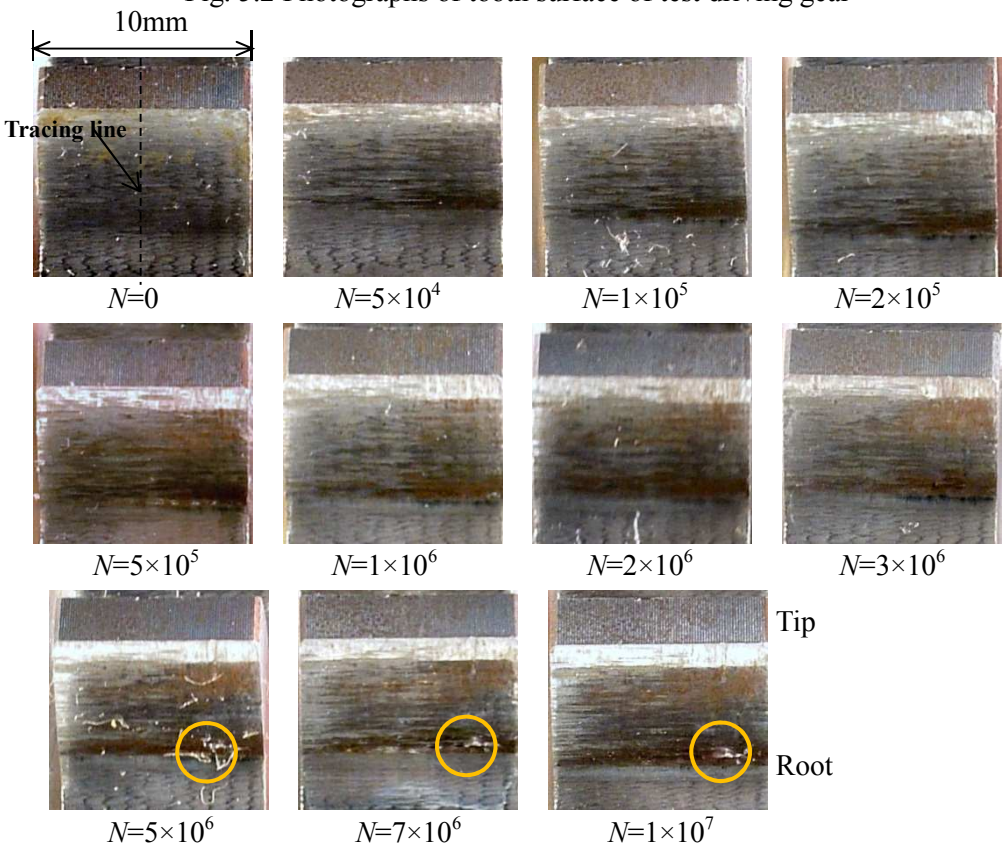

Fig. 5.3 Photographs of tooth surface of test driven gear

5.4.2 Pitting Area Ratio of Test Gears

The damaged area ratio is defined as a rate of the whole pitting area of a gear tooth to the entire meshing area. It can be measured by the method of Suzuki's Universal Micro Printing.

Figure 5.4 shows the pitting area ratio of test gears. As shown in this figure, the pitting failure begins to occur on tooth surface of driving gear since N=2×10^6. The average pitting area ratio is 4% and the maximal pitting area ratio of one tooth reaches 7.4%. For test driven gear, the pitting failure begins to occur on tooth surface of driving gear since N=5×10^6. The average pitting area ratio is about 2%. Obviously, the pitting area of driving gear is larger than that of the driven gear. Additionally, the pitting area becomes larger with the increase of cycles N. Especially after N=3×10^6, the pitting area increases significantly and almost every tooth has pitting failure after N=7×10^6.

According to the average pitting area ratio of test gear, I separate the gear condition into three types, called normal, slight failure and severe failure. When the average pitting area ratio is 0, the gear condition is normal. If the average pitting area ratio is between 0 and 2%, the gear condition is defined as slight failure. The gear condition is severe failure while the pitting area ratio is greater than 2%. Therefore, the condition of driving gear is normal at cycles N=0～1×10^6, is slight failure at N=2×10^6～3×10^6 and is severe failure at N=5×10^6～1×10^7. Similarly, the condition of driven gear is normal at cycles N=0～3×10^6 and is slight failure at N=5×10^6～1×10^7.

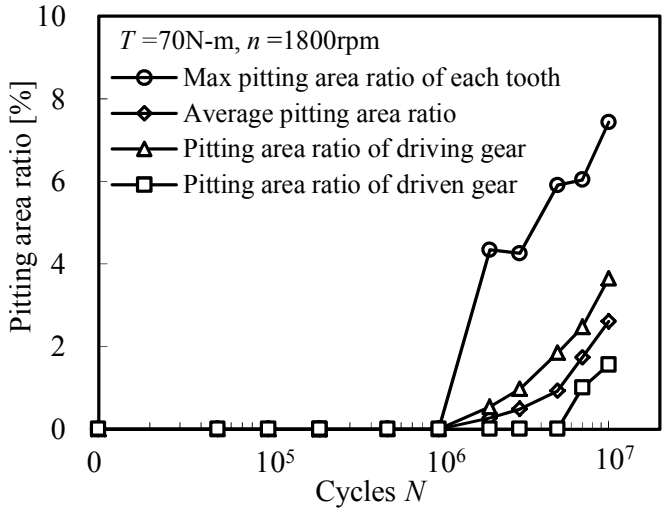

Fig. 5.4 Pitting area ratio of test gears

5.4.3 Tooth Profile Error of Test Gears

The tooth profile error of test driving gear and test driven gear is acquired by measuring the tooth profile along the center line of tooth width. Figure 5.5 shows the change in tooth profile error of test driving gear and driven gear. From the tooth profile error of driving gear, it can be seen that comparing with the other parts of gear tooth, the wear of tooth root is larger and enlarges with the increase of cycles N. While for the driven gear, the wear of tooth tip is severer than that of the other parts. This is because the tooth tip of driven gear is meshing around the tooth root of driving gear when the two gears begin to mesh. The impact generated by the initial meshing on the two parts is stronger which can exacerbate the wear. The wear begins to occur on the pitch point of driving gear after cycles $N=1\times10^6$, while the wear appear on the pitch point of driven gear after $N=3\times10^6$. For the involute gear, the wear of pitch point is little due to the small sliding speed, and the wear of tooth tip or root is continuously generated because of larger sliding speed of these parts. However, accompany with the increase of wear of the other parts, the pitch point becomes higher and the contact stress of this point also becomes larger. Therefore, the wear of pitch point also becomes larger with the increase of cycles. The wear of the whole tooth would be generated after some cycles. Consequently, the tooth profile error becomes larger with the increase of driving time.

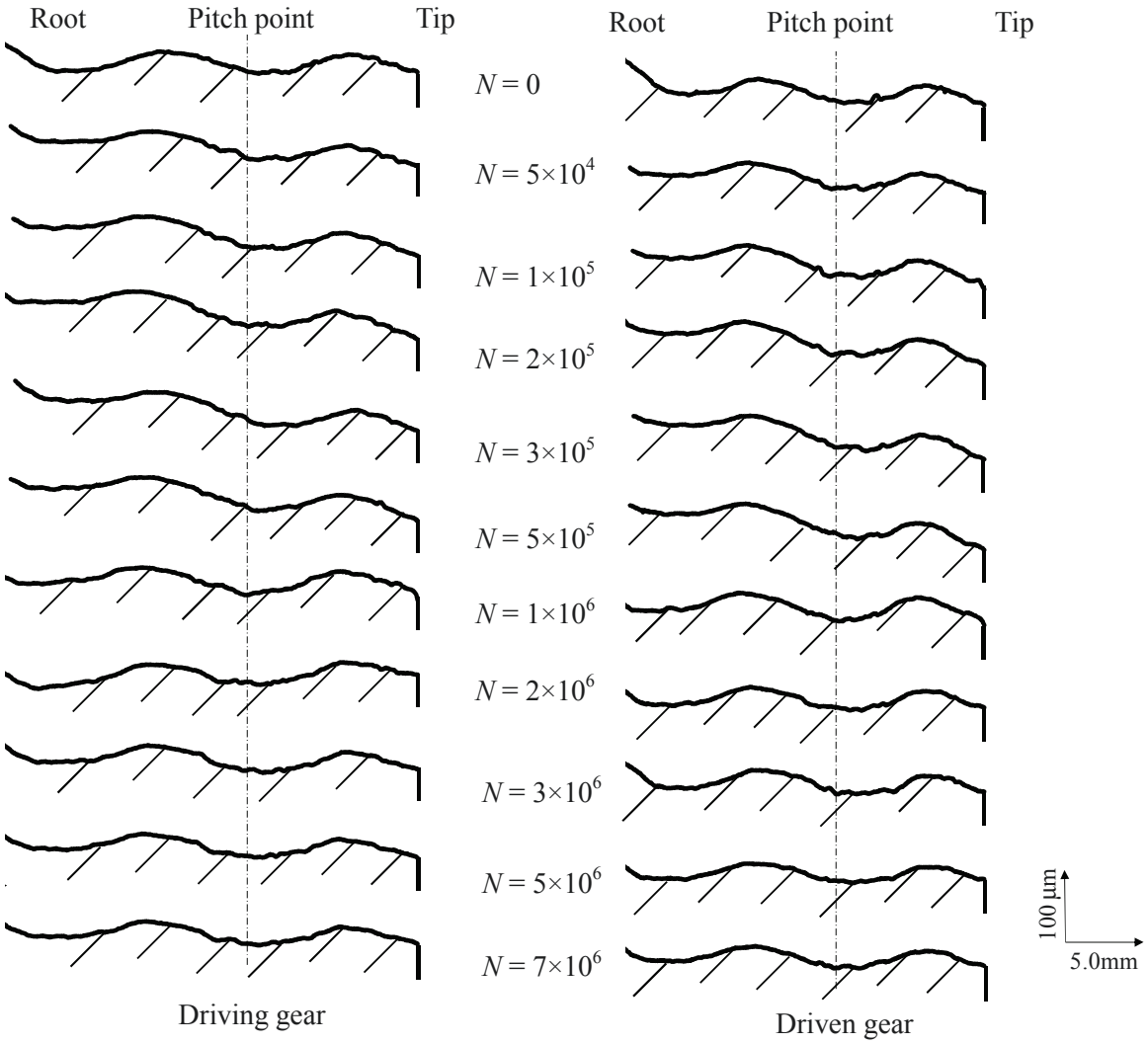

Fig. 5.5 Change in tooth profile error of test gears

5.4.4 Vibration Accelerations on Gearbox and Bearing box and Sound Level Signal

The vibration and noise produced by the working test gears is one of the important factors that directly cause the vibration of gear box. Therefore, analyzing the vibration accelerations of gear box is one of the most effective methods to detect the gear damage.

Figure 5.6 shows the vibration accelerations on test gear box in one rotation, which is measured under conditions of applied torque T=70N-m and rotation speed n=1800rpm. The abscissa axis shows gear tooth number and the ordinate axis represents the vibration acceleration. The histogram shows the pitting area of each tooth. As shown in Fig. 5.6, the waveform changes

slightly from cycles N=0 to N=3×10^6. After N=5×10^6, the vibration accelerations and its fluctuations increase rapidly as the increase of cycles N and pitting area. The abnormal large amplitude transiently appear at the neighborhood of number 9 tooth in the waveform of N=5×10^6 and N=7×10^6. Also, the pitting area of number 9 tooth is the largest in the whole gear teeth. Additionally, comparing with the normal teeth which have no failure on tooth surface, the vibration accelerations of the failure teeth are a little larger and manifest an increasing tendency with the growth of pitting area. The reason is that the tooth profile error becomes larger with the increase of pitting area, which will cause stronger vibration when meshing with the failure teeth. Since the amplitudes of waveform are large and fluctuate strongly when the pitting area is large, the gear condition for severe failure can be diagnosed roughly according to the measured waveform, such as graphs of N=7×10^6 and N=1×10^7 shown in Fig. 5.6. However, it is difficult to discriminate the gear condition of slight failure from normal condition when the pitting area is small at N=2×10^6 and N=3×10^6. Therefore, it is necessary to extract some representative features from the acquired data to diagnose the early gear damage.

The vibration of test gears can affect the vibration of its adjacent bearing box through the gear shaft between them. Therefore, the abnormal of gears can be reflected from the vibration accelerations of bearing box. Figure 5.7 shows the vibration accelerations on bearing box in one rotation measured under conditions of applied torque T=70N-m and rotation speed n=1800rpm. The abscissa axis shows gear tooth number and the ordinate axis represents the vibration acceleration. The histogram shows the pitting area of each tooth. As shown in this figure, the amplitude of vibration accelerations at N= 0 and 2×10^5 is very large. However, there is no damage on teeth surface at these cycles. This can be considered as the fixation of the testing machine become loose resulting in the stronger vibration of bearing box. The vibration accelerations for normal gear condition at cycles N=5×10^4, 1×10^5, 5×10^5 and 1×10^6 change slightly, and there is not any abnormal large amplitude appear on the waveform. For slight failure condition at cycles N=2×10^6 and 3×10^6, there is still not any large fluctuations in the vibration accelerations. Therefore, it is difficult to detect the early gear damage from the original signals at these cycles. The vibration accelerations at cycle N=5×10^6 is very large. However, the abnormal amplitude can't be found in the waveform. The fluctuation of the waveform is a little stronger at cycle N=7×10^6. Conversely, the vibration accelerations at cycle N=1×10^7 are relatively stable. Comparing with the vibration accelerations on gear box, it is more difficult to detect gear damage based on the vibration accelerations on bearing box whether the failure is slight or serious.

The noise would be generated by the test gears when they are operating. Moreover, the noise also changed with the variation of gear conditions. However, the sound level signal is easily affected by the vibration of the other parts of the testing machine or the disturbance from the

environment. Therefore, the measurement and analysis of sound level signal makes more difficult to operators. Figure 5.8 presents the sound level signal in one rotation of test gears during the fatigue test. The abscissa axis shows the gear tooth number and the ordinate axis represents the sound pressure. The histogram corresponds to the pitting area ratio of each tooth. The sound pressure of the signal from cycles N= 0 to 3×10^6 is nearly stable, and the transient abnormal amplitude can't be found in the signal. The sound pressure presented at N= 7×10^6 and 1×10^7 is larger than that at the other cycles. However, it is still difficult to diagnose gear damage only based on the original sound level signal.

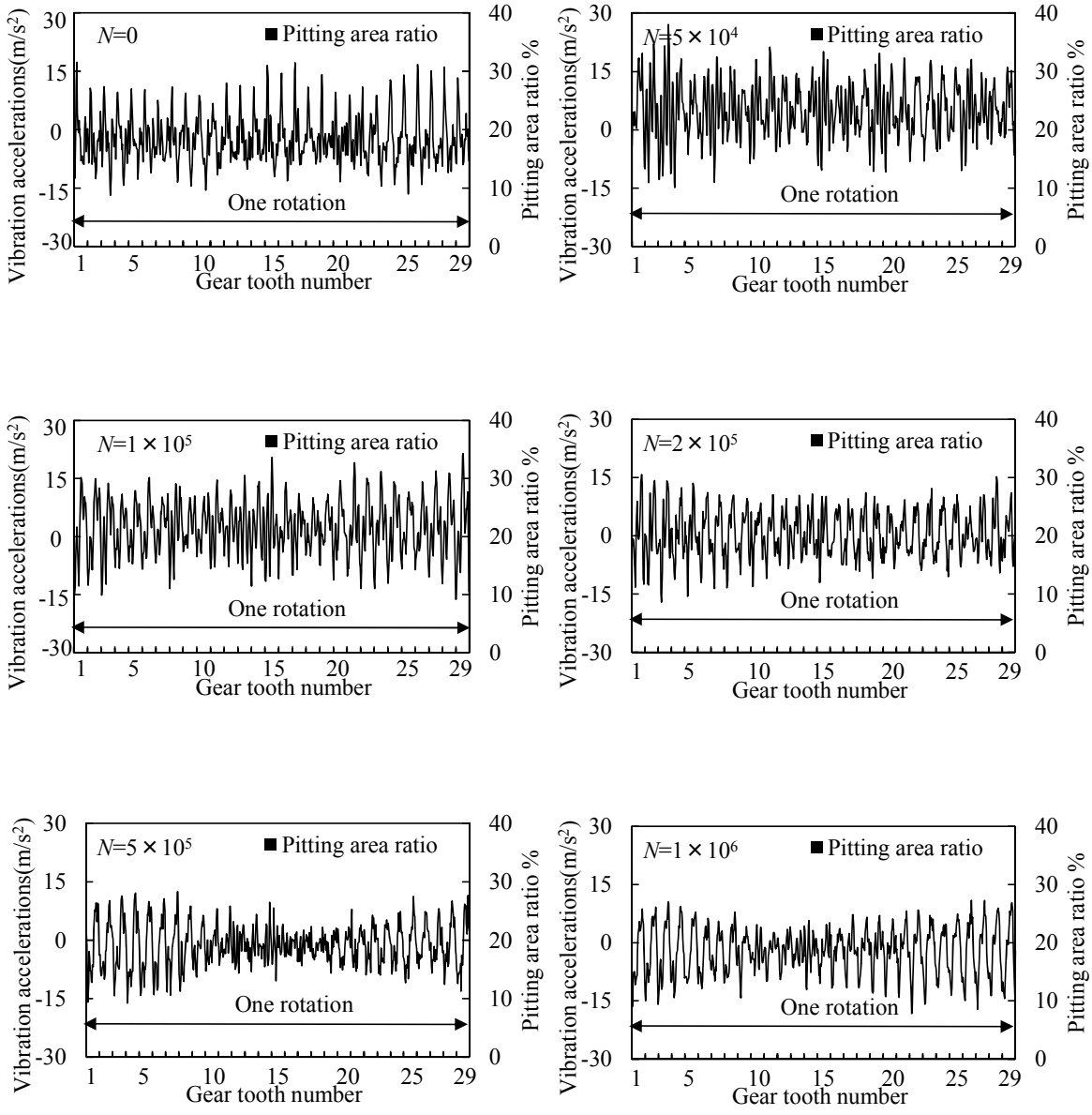

(a) Vibration accelerations on gear box (T=70N-m, n=1800rpm, N=0 ~ 1×10^6)

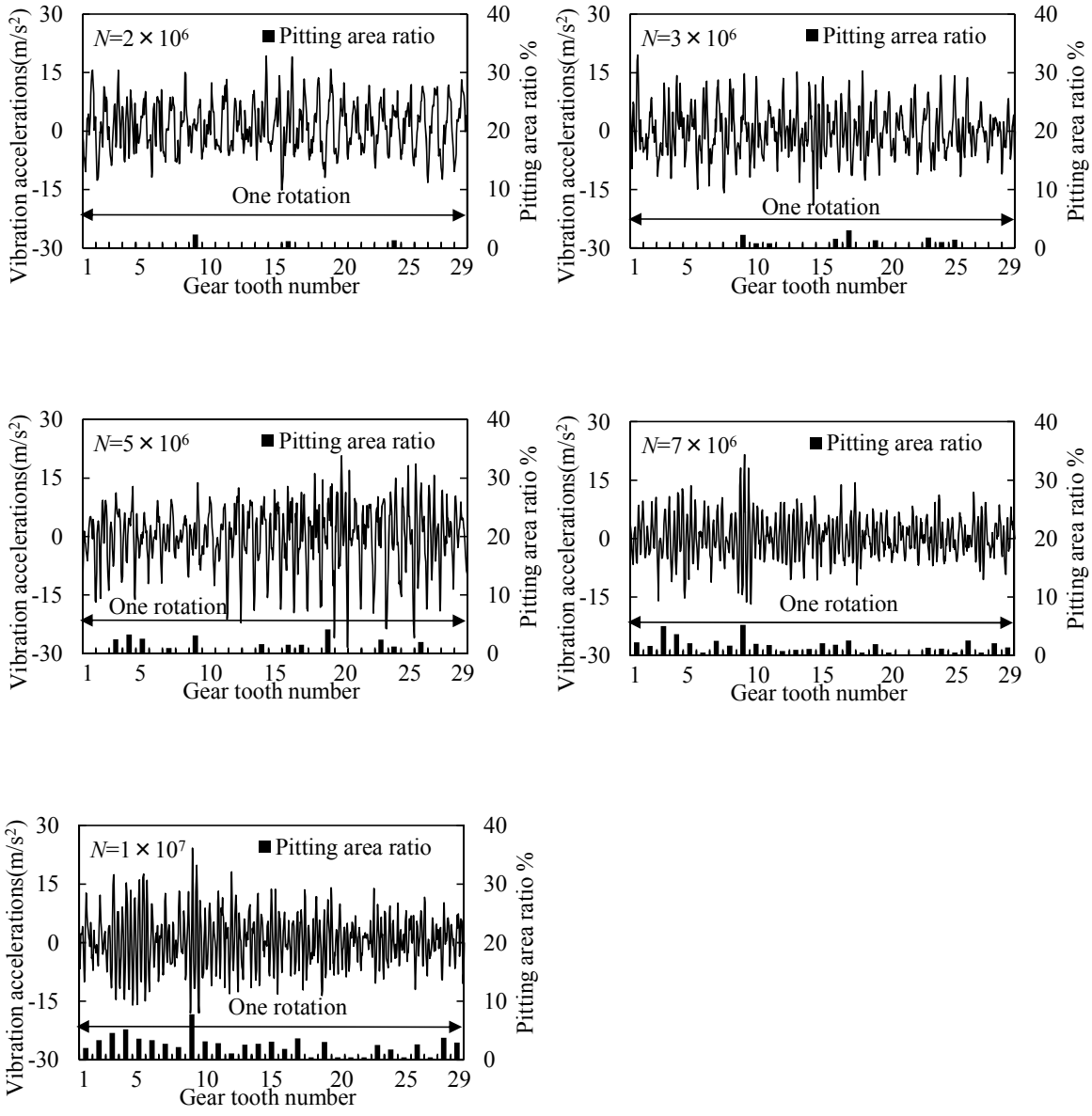

(b) Vibration accelerations on gear box (T=70N-m, n=1800rpm, N=2×10^6 ~ 1×10^7)

Fig. 5.6 Vibration accelerations on gear box in cyclic fatigue test

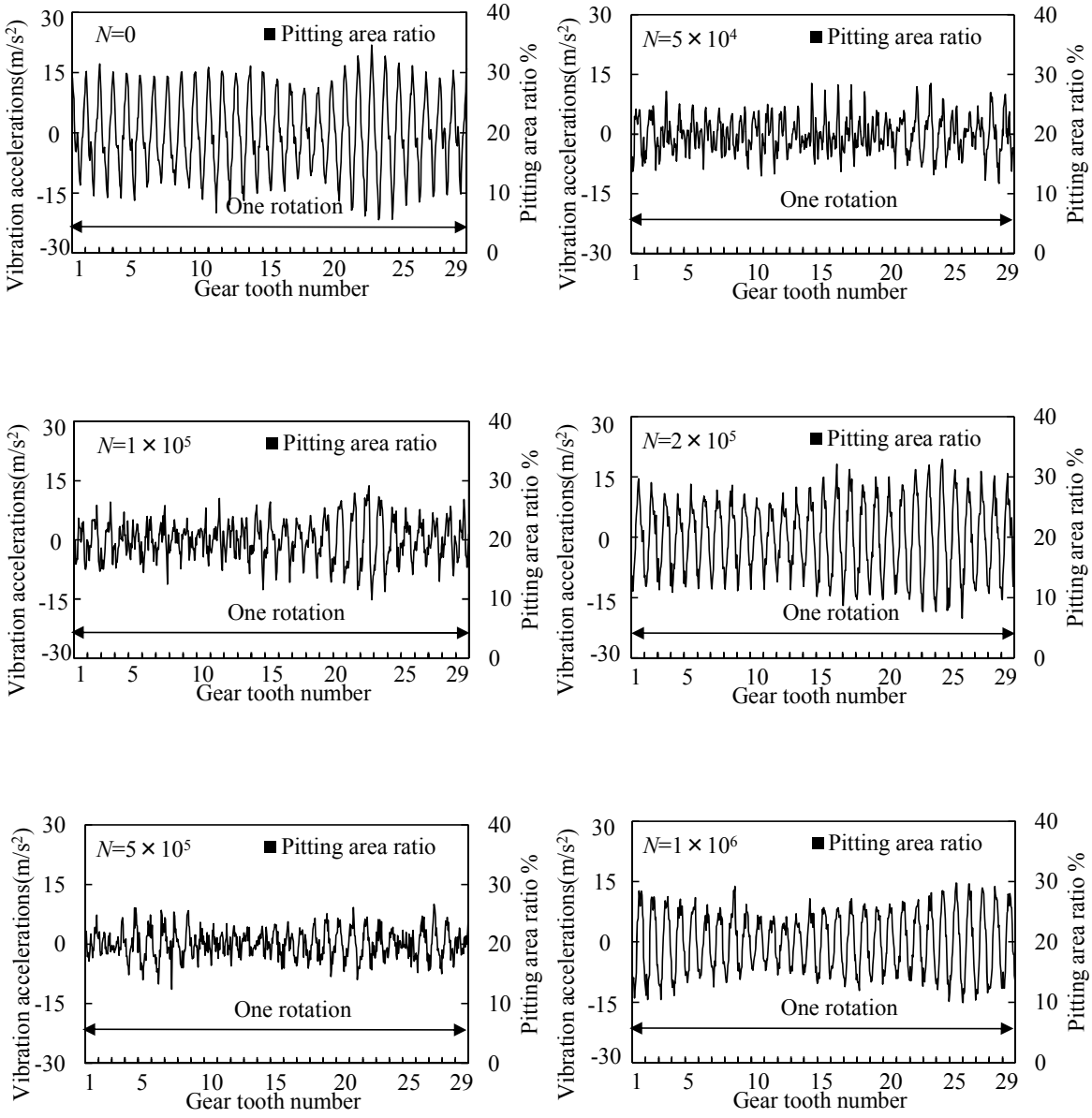

(a) Vibration accelerations on bearing box (T=70N-m, n=1800rpm, N=0 ~ 1×10^6)

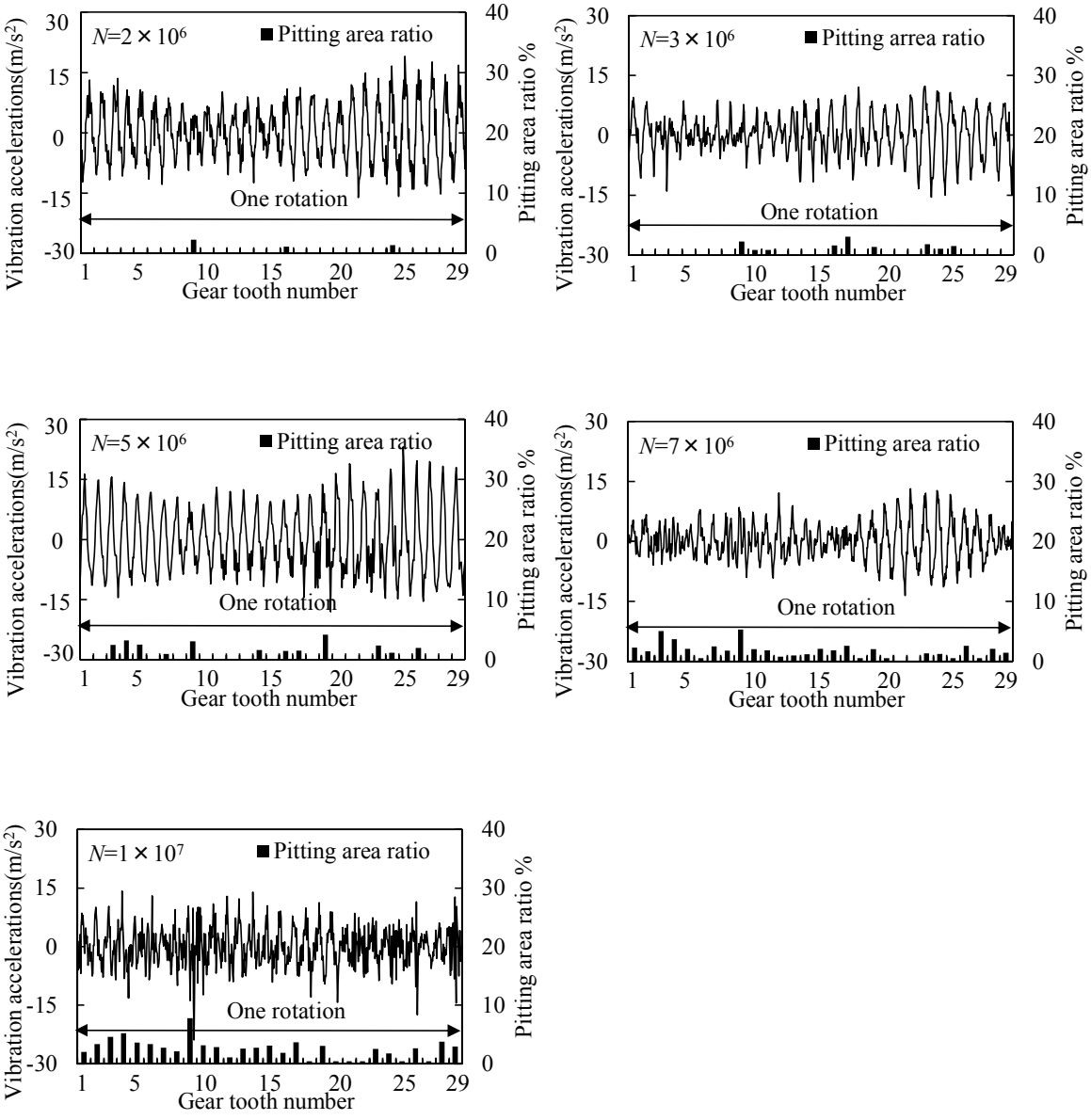

(b) Vibration accelerations on bearing box (T=70N-m, n=1800rpm, N=2×10^6 ~ 1×10^7)

Fig. 5.7 Vibration accelerations on bearing box in cyclic fatigue test

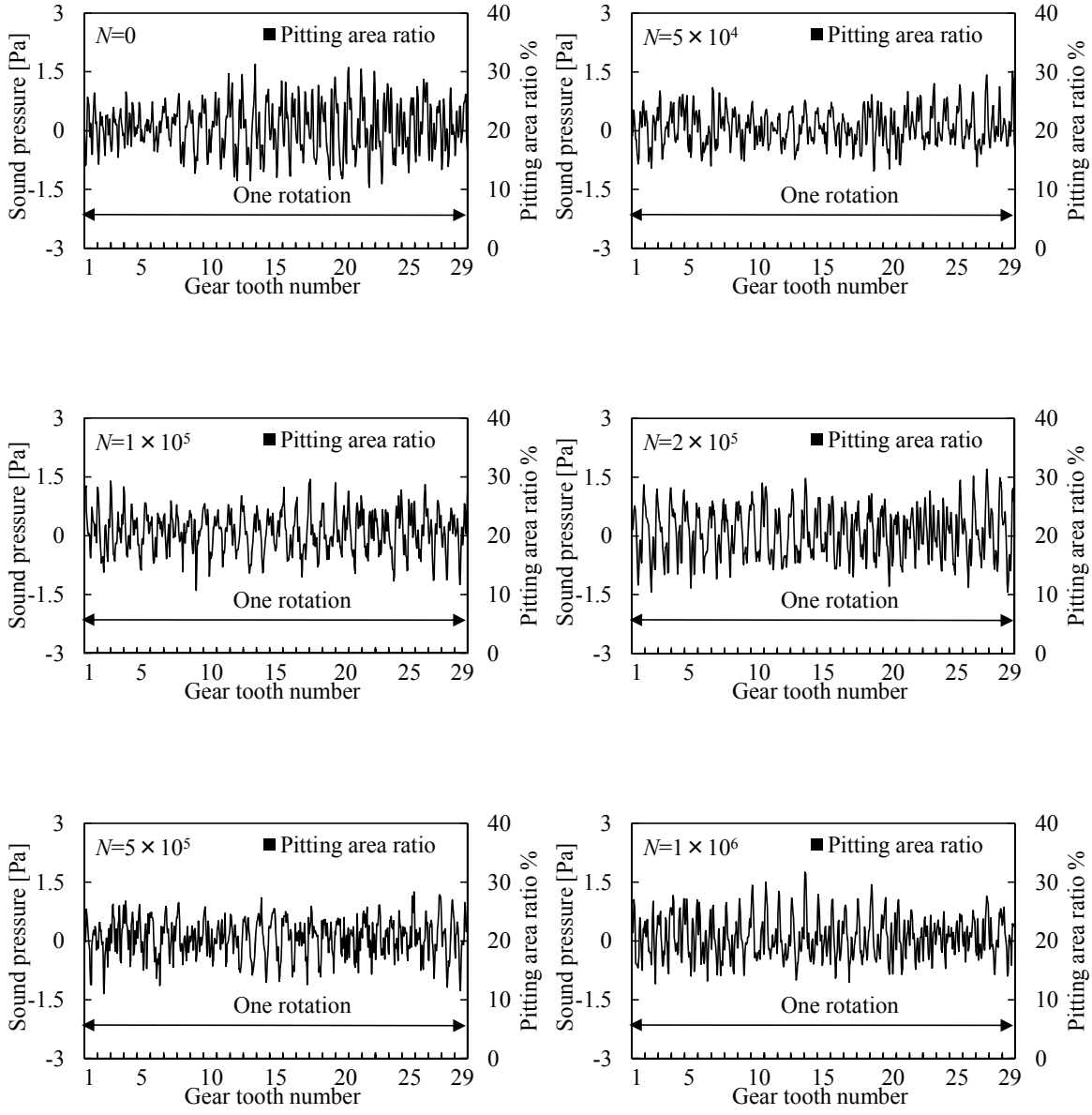

(a) Sound level signal (T=70N-m, n=1800rpm, N=0 ~ 1×10^6)

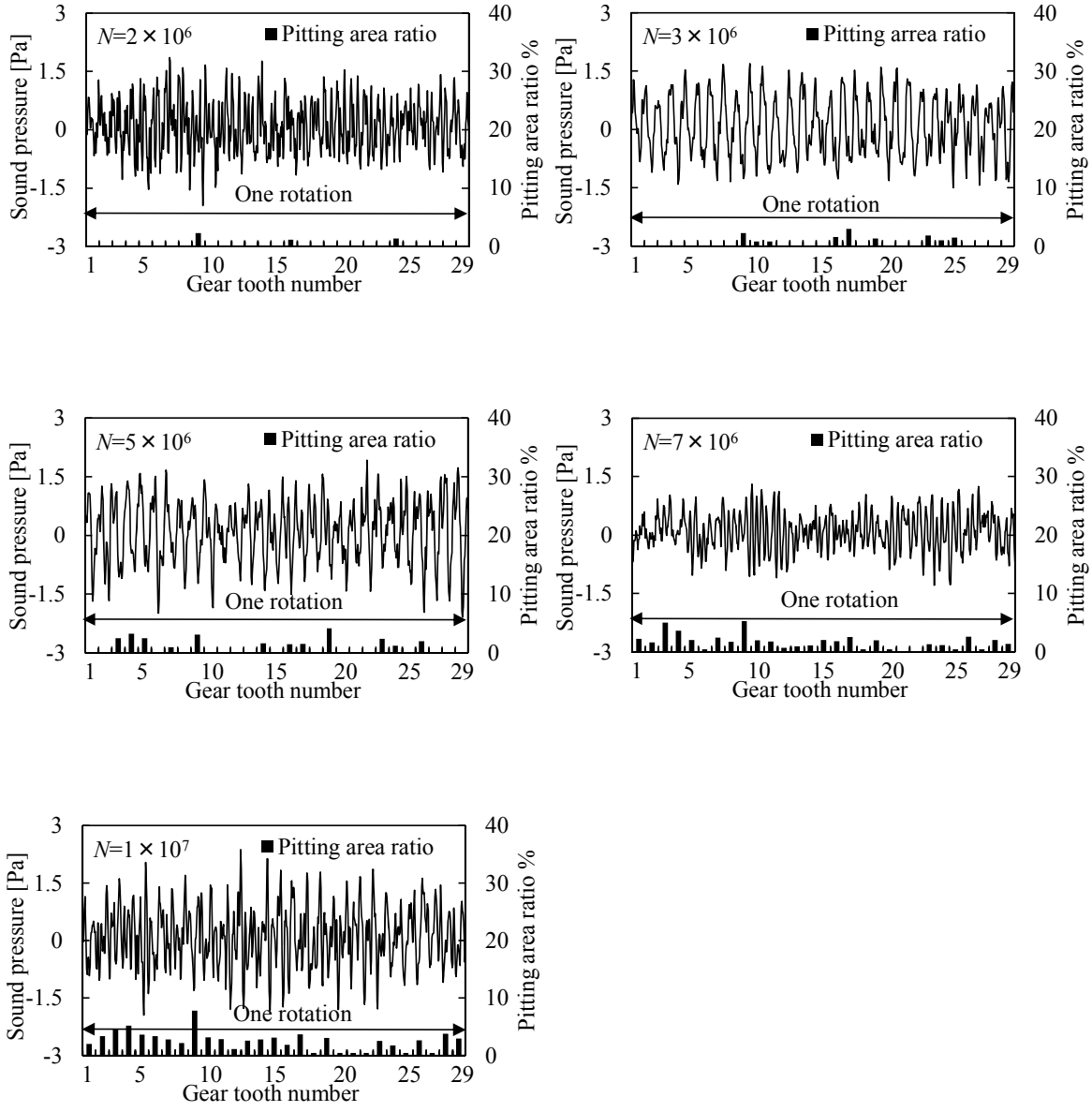

(b) Sound level signal (T=70N-m, n=1800rpm, N=2×10^6 ~ 1×10^7)

Fig. 5.8 Sound level signal acquired in cyclic fatigue test

5.4.5 Frequency Analysis of Vibration Accelerations

In frequency domain, the spectrum is always varying with the gear conditions. The meshing frequency and its harmonics, together with sidebands show respective characteristics of various gear conditions. In case of a localized fault on tooth surface, the amplitude and phase modulation of the meshing frequency can be visible in frequency spectrum of the vibration signal. In the other words, sidebands will appear around the meshing frequency and its harmonics, the spacing of sidebands corresponds to the rotational frequency of the shaft carrying the defective gear. Therefore, fault features can be detected by analyzing the frequency spectrum of vibration signal. With the experimental conditions of gear rotation speed n=1800rpm and the number of teeth 29, the rotational frequency and the meshing frequency are 30Hz and 870Hz respectively. The natural frequency of the system is about 3000Hz, and the analytical frequency is 10 kHz in Fast Fourier Transform. The frequency spectrum of the vibration accelerations has been analyzed and presented in the paper.

The frequency spectrum of vibration accelerations on test gear box is shown in Figure 5.9. Figure 5.9 (a) shows the frequency spectrum of vibration accelerations at cycle 5×10^5 for normal gear condition. It can be seen that the spectrum for normal condition is mainly dominated by the meshing frequency. The amplitude of harmonics is relatively smaller. Moreover, high-order harmonics hardly appear in the spectrum, and the amplitudes of high frequencies are quite small. The sidebands around the meshing frequency are weak and not obvious.

Figure 5.9 (b) depicts the spectrum of vibration accelerations at cycle 3×10^6 for slight failure condition. As shown in this figure, the 3rd harmonic is significant and dominating, while the amplitude of meshing frequency becomes smaller. The amplitude of the modulation sideband around the meshing frequency is large. The modulation phenomenon is clearly observed in the spectrum for slight failure condition.

Figure 5.9 (c) depicts the spectrum of vibration signal at cycle 1×10^7 for severe failure condition. As shown in Fig. 5.9 (c), the harmonics appear with significant amplitude and the amplitude of meshing frequency is relatively weaker. Especially, the 3rd harmonic accounts for a considerable proportion in the spectrum. In addition, the sidebands around the meshing frequency are wide and strong, which shows the gear condition is abnormal.

Comparing the spectrum for normal, slight failure and severe failure condition, it is found that the amplitudes of the harmonics become stronger with the increase of damaged area. Similarly, the amplitude of sidebands becomes stronger and the band width also becomes broader. This is because the tooth profile error caused by gear damage intensifies the vibration when the failure tooth

meshing, which can generate larger modulation in aspect of amplitude and phase in frequency spectrum.

Figure 5.10 presents the frequency spectrum of vibration accelerations on bearing box. The frequency spectrum for normal gear condition, slight failure condition and severe failure condition are shown in Fig. 5.10 (a), Fig. 5.10 (b) and Fig. 5.10 (c) respectively. In these figures, the meshing frequency is uniformly strong and dominating in the spectrum. Moreover, the amplitude of the 3rd harmonic is larger than that of the 2nd harmonic. The amplitude of the sidebands for normal condition is weaker. On the contrary, the amplitude of the sidebands for slight failure condition is the largest. Additionally, the width of sidebands for severe failure condition is the broadest. In general, the difference of the frequency spectrum of bearing box is not obvious among the three conditions.

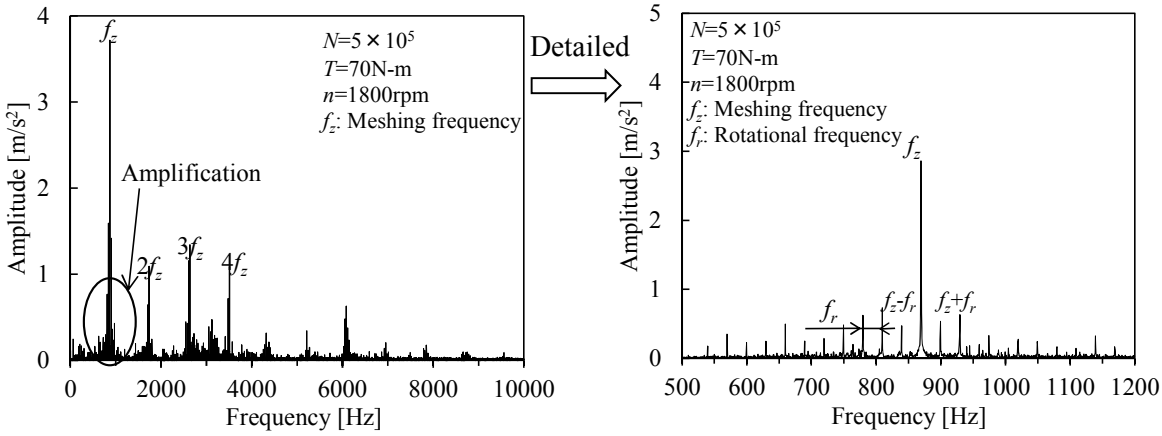

(a) Normal condition

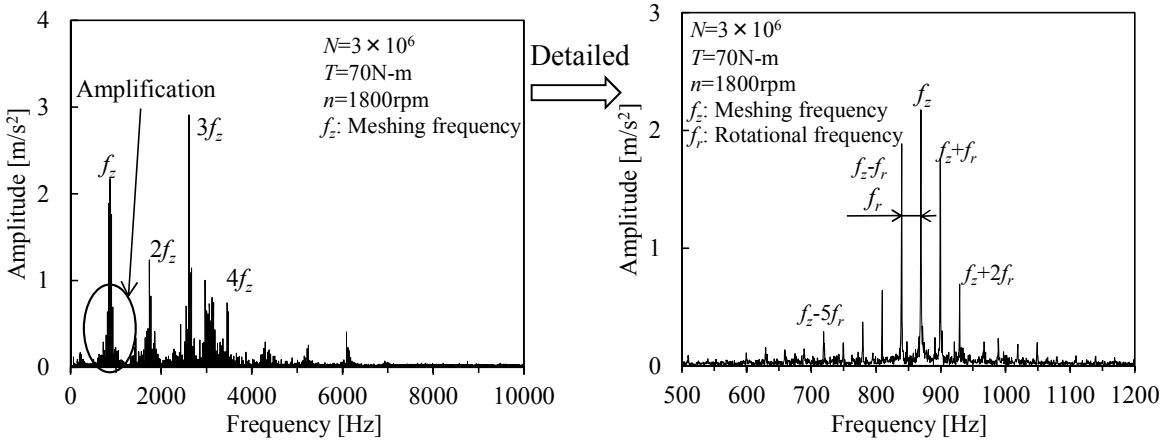

(b) Slight failure condition

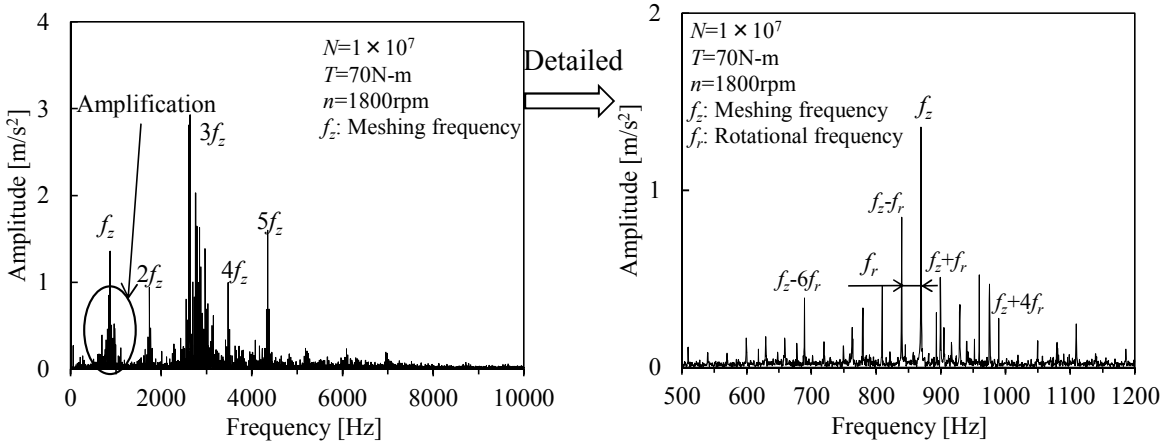

(c) Severe failure condition

Fig. 5.9 Frequency spectrum of the vibration acceleration on gear box in cyclic fatigue test

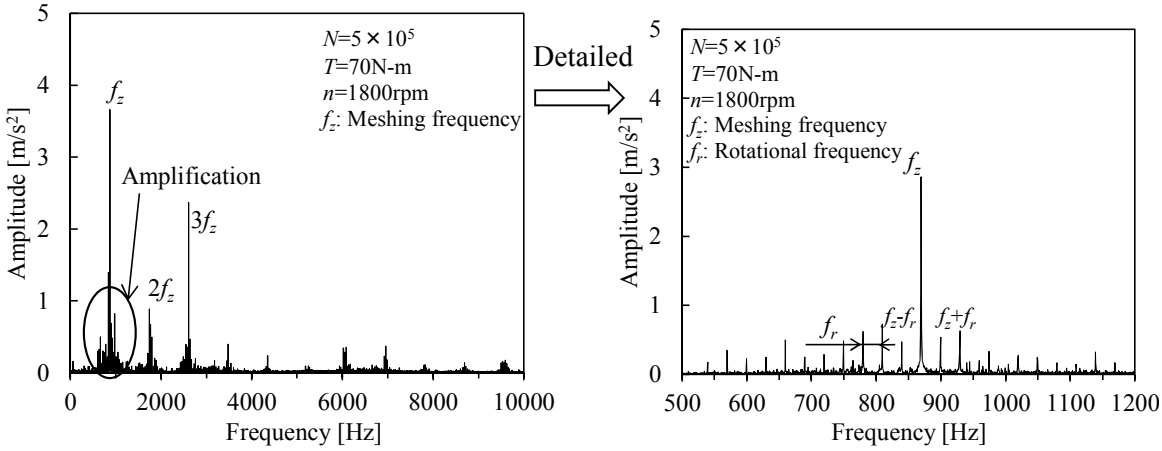

(a) Normal condition

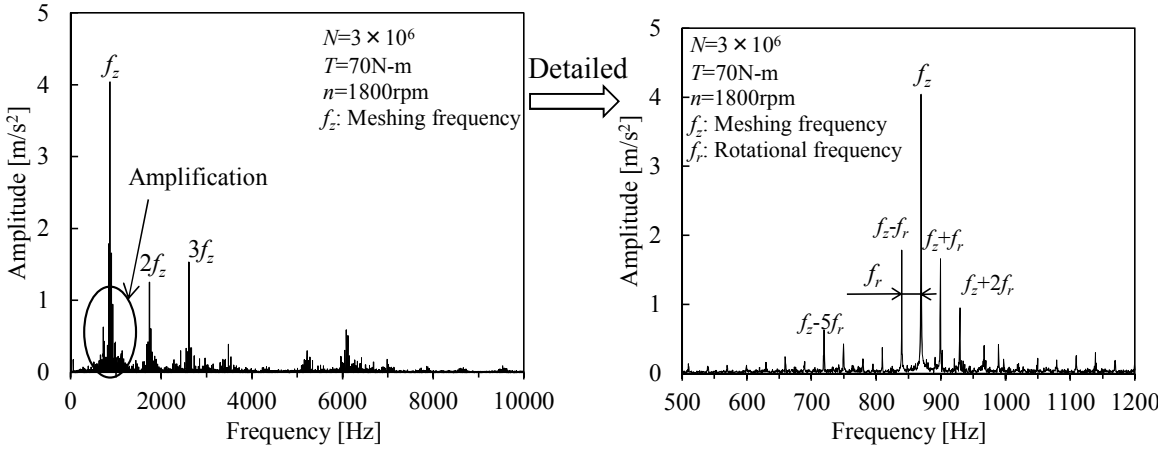

(b) Slight failure condition

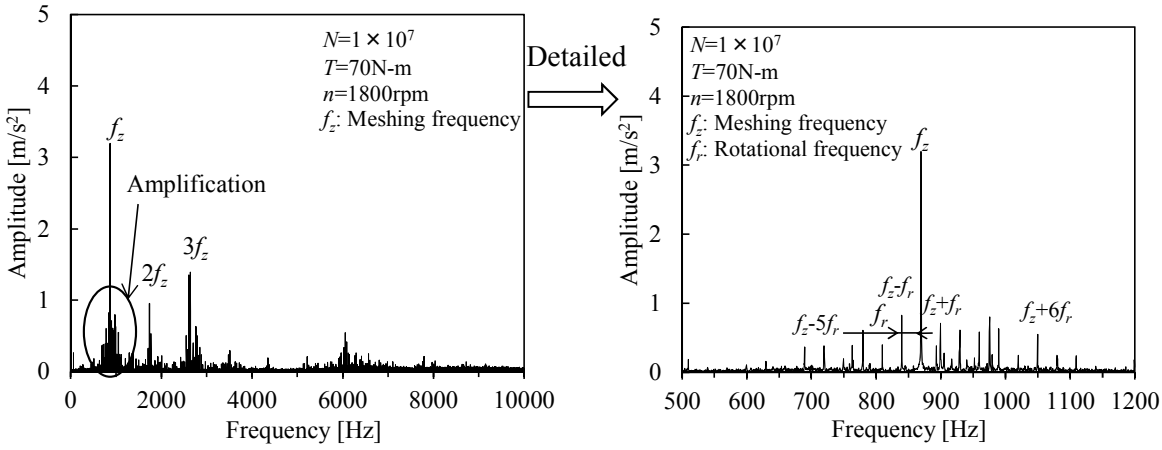

(c) Severe failure condition

Fig. 5.10 Frequency spectrum of the vibration acceleration on bearing box in cyclic fatigue test

5.4.6 Residual Signal

Since the residual signal is much less sensitive to the altering experimental conditions and shows more obvious failure features than the raw signal, it is obtained as the analytical signal in this paper. The residual signal can be acquired by removing the fundamental and harmonics of the meshing frequency and resonance signal from Fast Fourier Transform spectrum of the raw signals and then reconstructing the remaining signal in the time domain [41]. The residual signals on both gear box and bearing box over full gear lifetime are shown in Figs. 5.11 and 5.12. The signals in the plots correspond to one wheel revolution.

The amplitude value of the residual signal is smaller than that of the raw signal. The reason for this is considered as the harmonics and resonance signal is eliminated from the raw signal and the energy of the residual signal becomes smaller. Additionally, we can also observe that the amplitude value and waveform of residual signal is more stable than that of the raw signal for normal condition (see Figs. 5.6 (a) and 5.11 (a), Figs. 5.7 (a) and 5.12 (a)). The observation agrees with the description that the influence of experimental conditions is weaker in residual signal than in the raw signal.

In Fig. 5.11 (b), the residual signals at N=5×10^6 and 7×10^6 appear evident fault impulse. In residual signal at N=1×10^7, there are several greater fault impulses, revealing that several teeth have been broken. In addition, the larger the pitting area the larger the amplitude value is. Comparing with Figs. 5.6 (b) and 5.11 (b), the evident of fault impulse for severe failure is more obvious in residual signals at N=5×10^6 ~ 1×10^7. However, it is hard to detect gear faults from either the raw signal or the residual signal on bearing box in Figs. 5.7 (b) and 5.12 (b).

There is no evident indication both in the residual signal on gear box or bearing box when the damage is small, such as residual signals at N=2×10^6 and 3×10^6 in Figs. 5.11 (b) and 5.12 (b). Therefore, although the residual signal can strengthen the characteristics of gear damage to some extent, it is still hard to diagnose the early gear faults only through the waveform of residual signal.

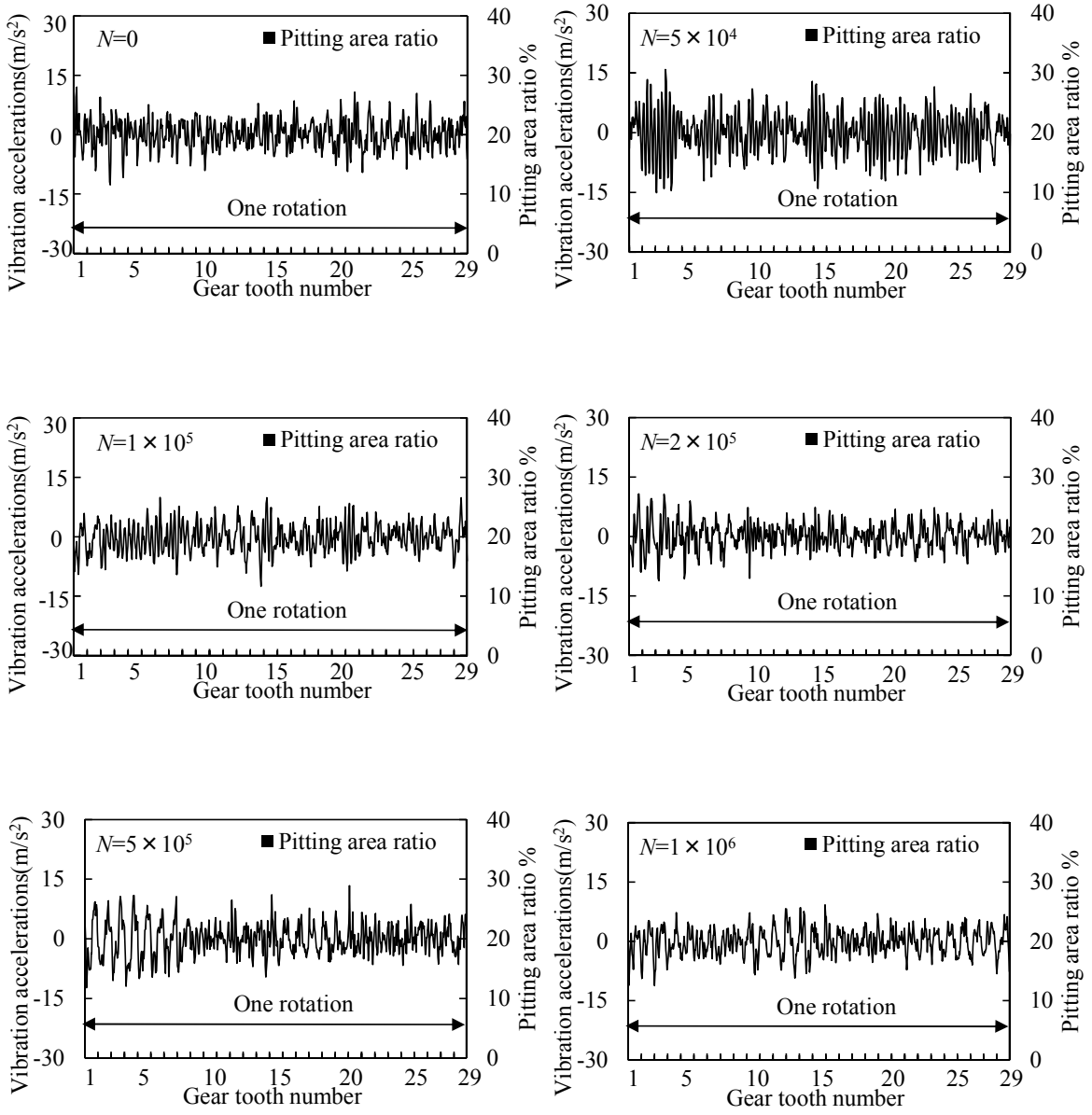

(a) Residual signal on gear box (T=70N-m, n=1800rpm, N=0 ~ 1×10^6)

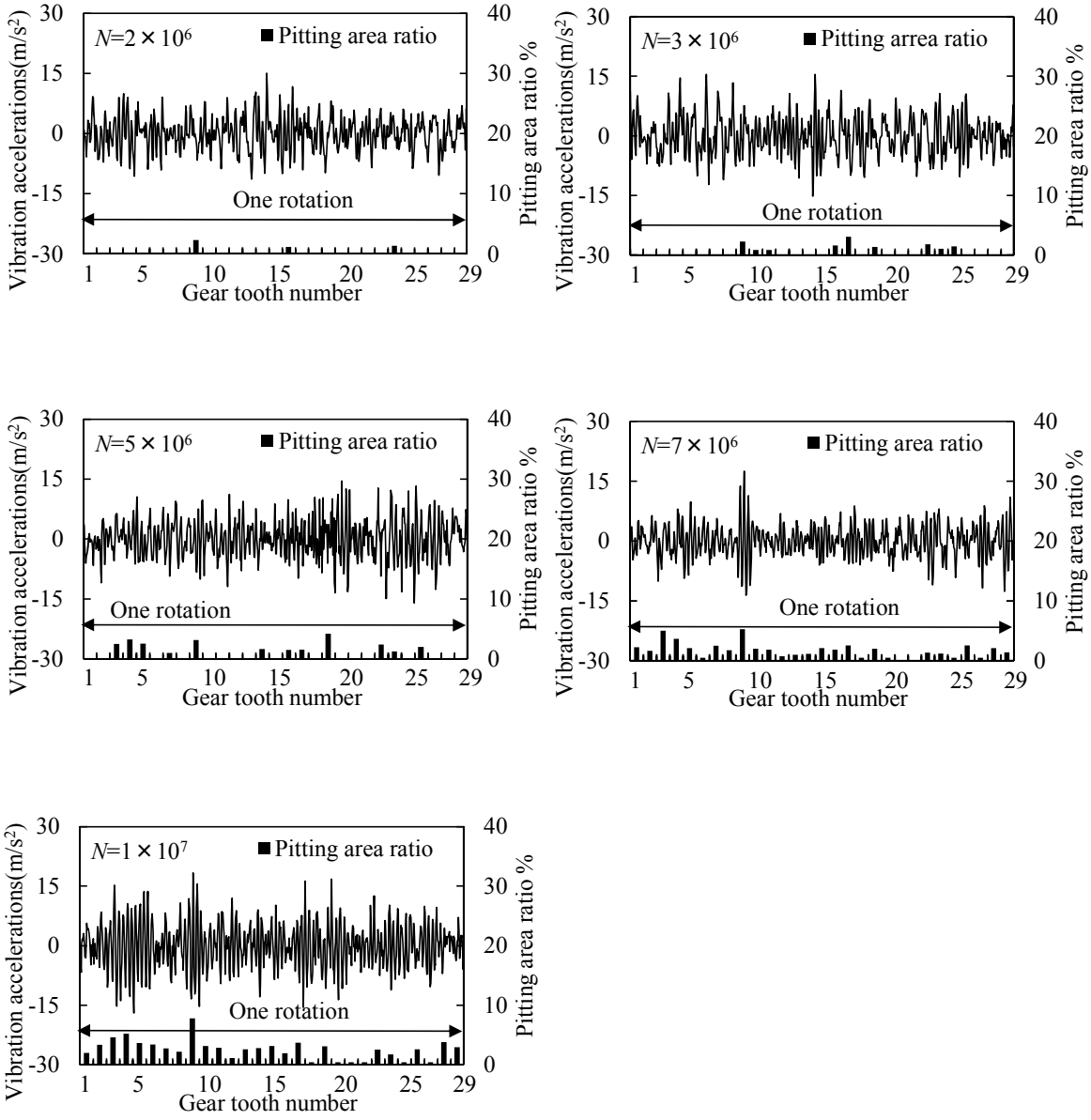

(b) Residual signal on gear box (T=70N-m, n=1800rpm, N=2×10^6 ~ 1×10^7)

Fig. 5.11 Residual signal on gear box in cyclic fatigue test

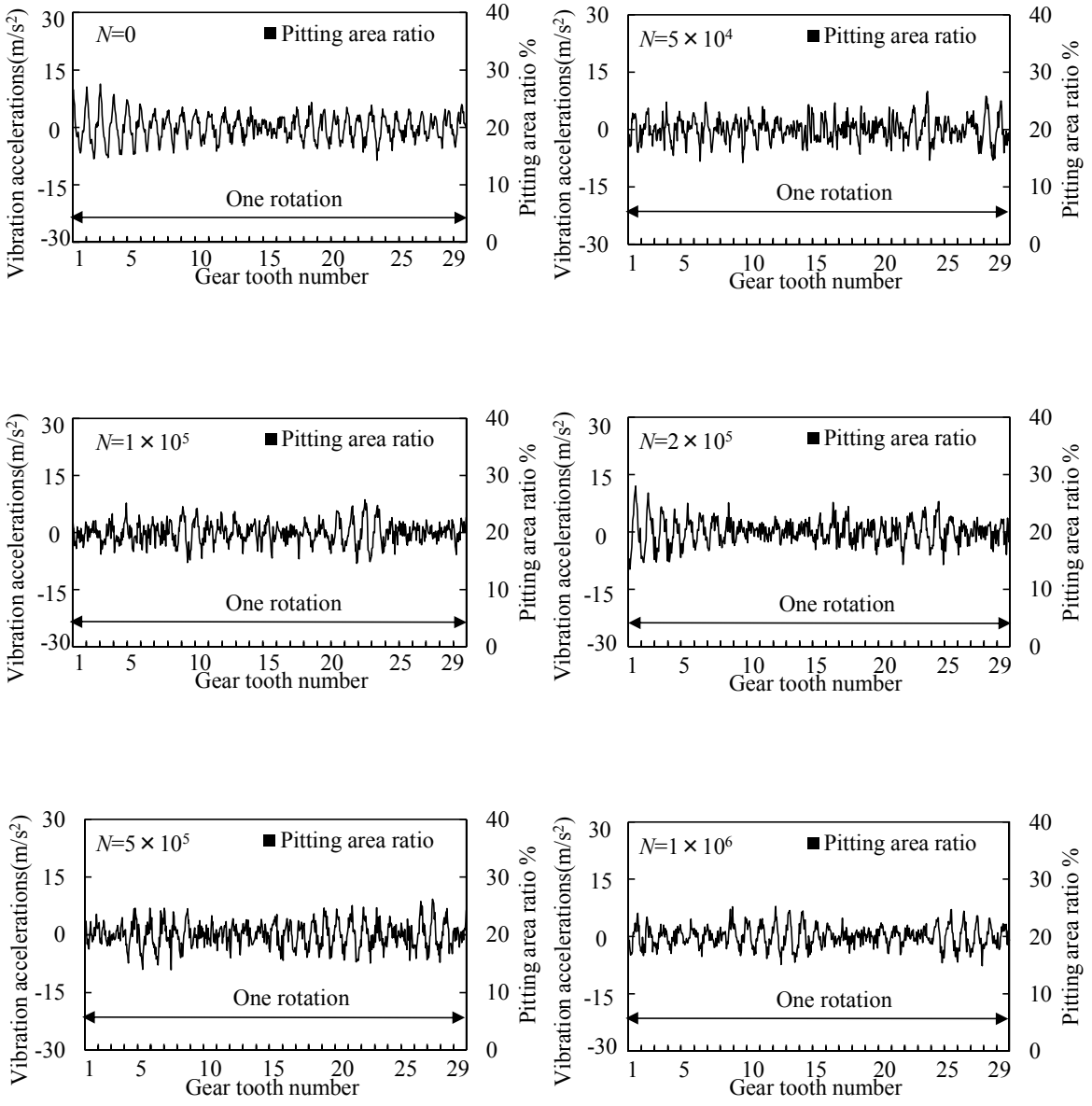

(a) Residual signal on bearing box (T=70N-m, n=1800rpm, N=0 ~ 1×10^6)

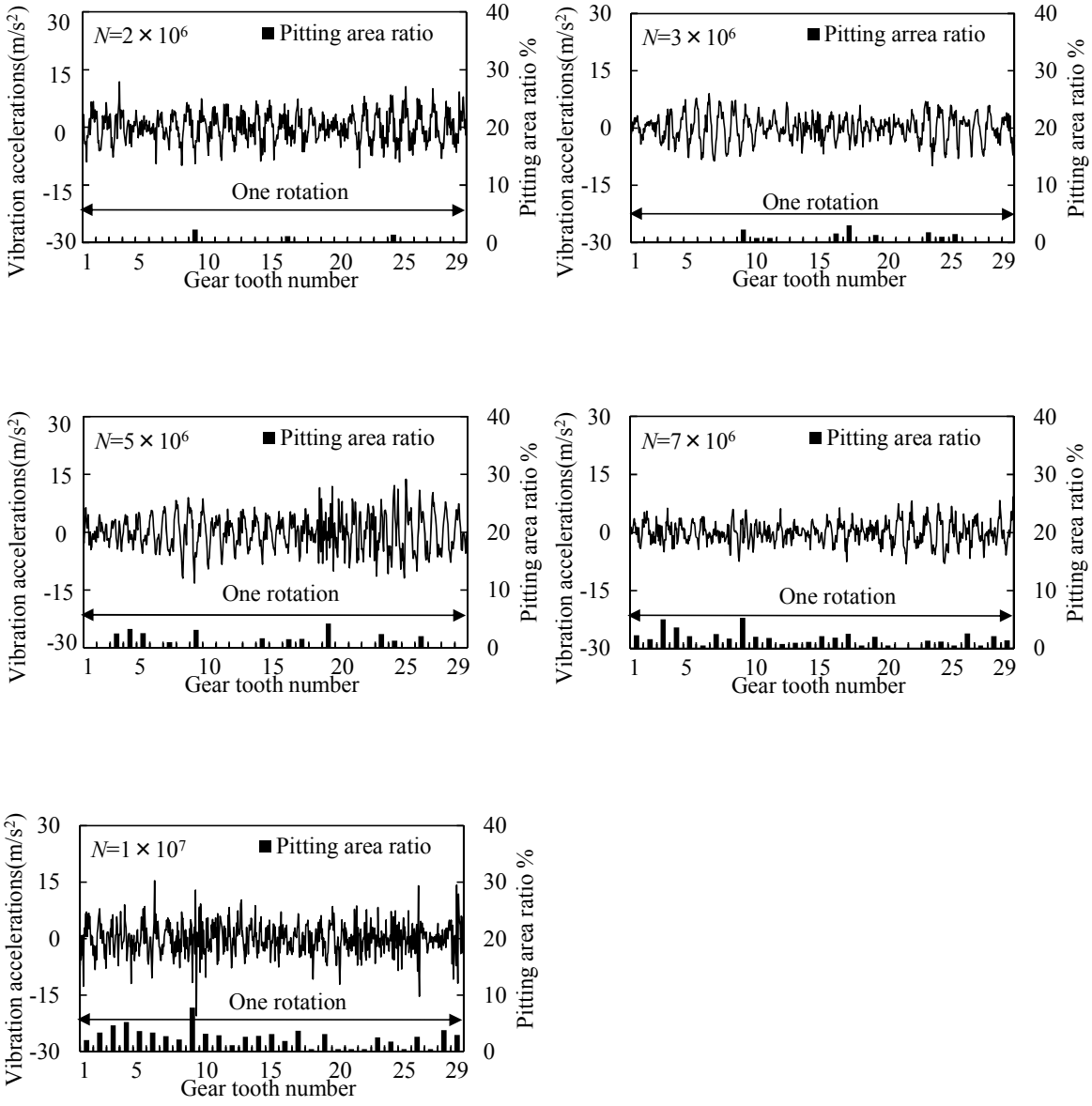

(b) Residual signal on bearing box (T=70N-m, n=1800rpm, N=2×10^6 ~ 1×10^7)

Fig. 5.12 Residual signal on bearing box in cyclic fatigue test

5.4.7 Processed Signal acquired Using Discrete Wavelet Transform

The signals acquired from accelerometers mounted on gear box or bearing box are often inevitably contaminated by the interference signal, which is generated by the vibrations from shafts, bearings, and other components on the testing machine. In addition, the signals are also polluted with the white noise which is generated by the accelerometer or the environmental electromagnetic disturbances. Except for the signal of interest, the other unnecessary signal components are considered as noise in this study. The noise is usually random and unstable, whose variation would be reflected in the frequency spectrum, especially in the high frequency bands. In this study, I adopt discrete wavelet transform with Daubechies 4 wavelet to reduce the noise from residual signal. The noise is reduced by the denoising method of minimaxi. After that, the coefficients of discrete wavelet transform with noise filtered are reconstructed as processed signal for the following analysis.

Figs. 5.13 and 5.14 respectively depict the processed signal on gear box and bearing box obtained using discrete wavelet transform. The waveform corresponds to one wheel revolution over the full lifetime of test gear.

In these figures, the burrs of waveform are weaker in the processed signal. Therefore, the waveform of processed signal is much smoother than that of the residual signal. Moreover, the amplitude value of the processed signal is weaker than that of the residual signal. This is because part of the noise is reduced from the residual signal and the energy of the processed signal is weakened.

For normal condition of test gear at N=0 ~ 1×10^6, almost all the waveform of processed signal is stable in Figs. 5.13 (a) and 5.14 (a). The processed signal of bearing box is more regular than that of gear box. Moreover, the meshing frequency can be clearly observed through the processed signals. It indicates that there is no abnormal on tooth surface. However, the processed signals on gear box at N=5×10^5 and 1×10^6 in Fig. 5.13(a), and on bearing box at N=1×10^5 and 5×10^5 in Fig. 5.14(a) are irregular. It may be caused by the error of operation when measuring. For slight failure condition of test gear at N=2×10^6 and 3×10^6, the amplitude value of number 15 tooth seems a little larger in processed signal in Fig. 5.13 (b). However, the early damage indication is not obvious. For severe failure condition of test gear at N=5×10^6 ~ 1×10^7, the fault features are more clearly visualized in processed signals in Fig. 5.13 (b). In addition, the difference of amplitude value among different pitting areas becomes large. In Fig. 5.14 (b), the amplitude value of No. 9 tooth is larger than that of the others, which corresponds the largest pitting area on No. 9 tooth. Among original signal, residual signal and processed signal of bearing box, the indication of damage can be only observed through the processed signal.

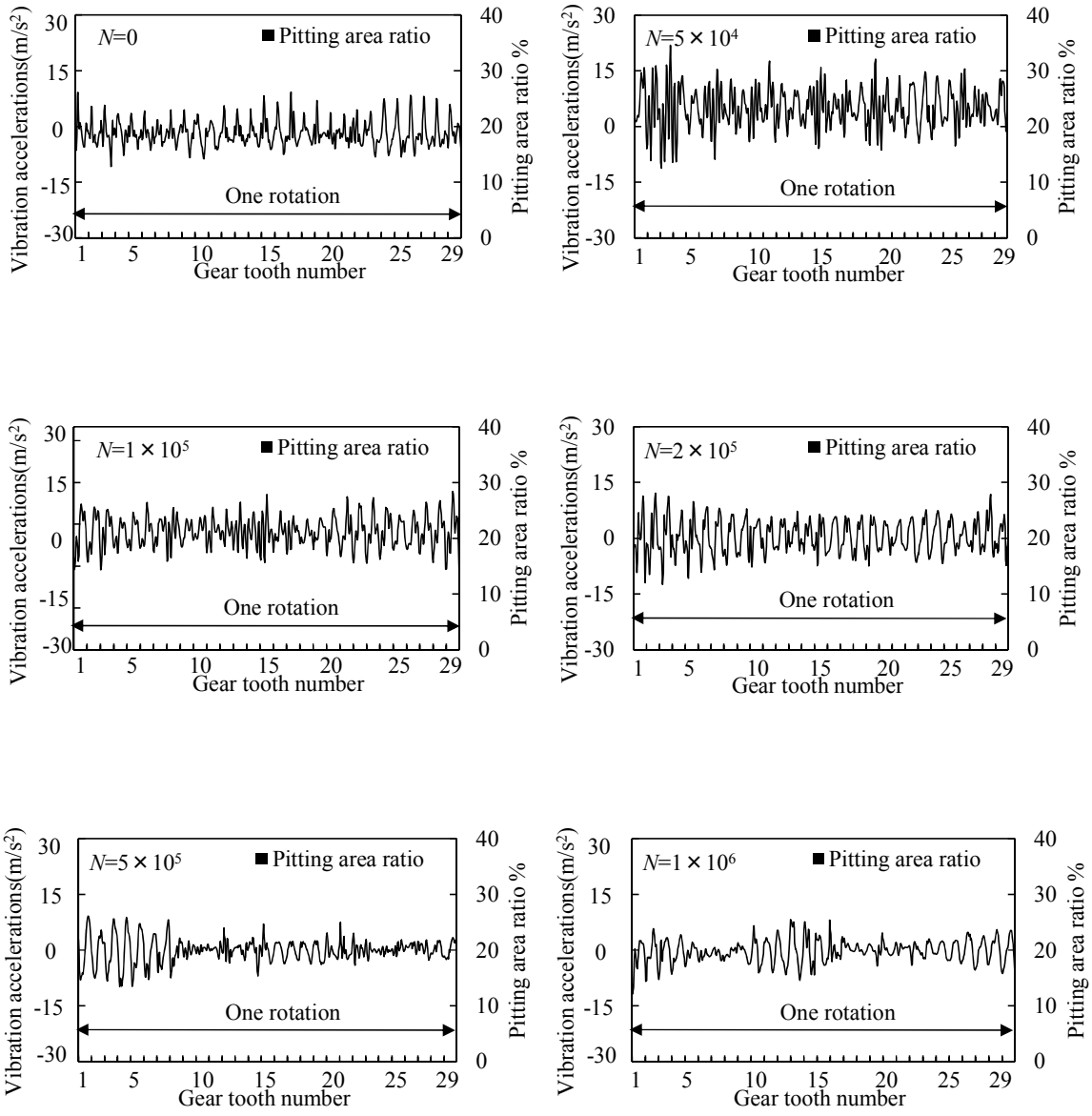

(a) Processed signal on gear box (T=70N-m, n=1800rpm, N=0 ~ 1×10^6)

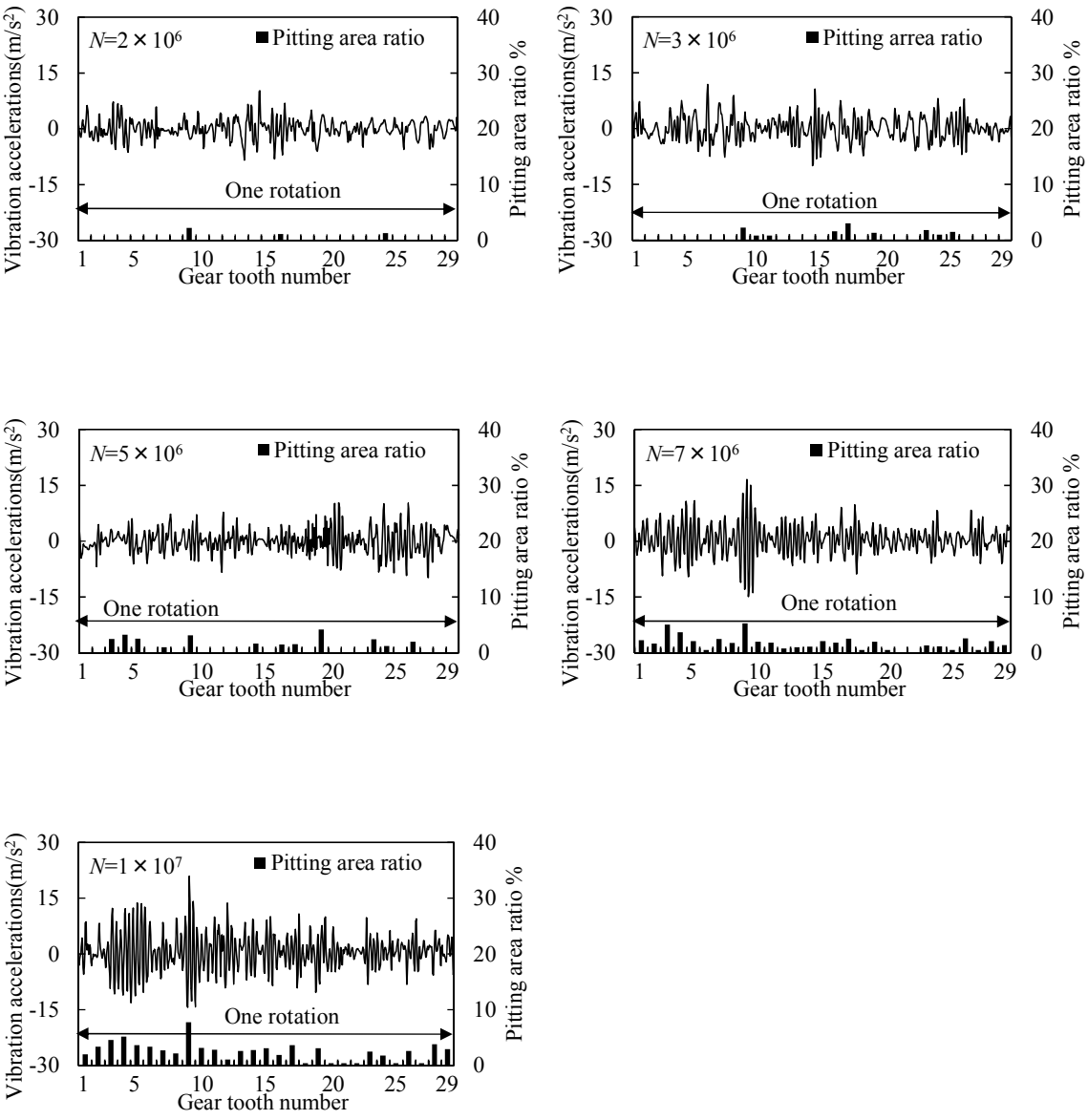

(b) Processed signal on gear box (T=70N-m, n=1800rpm, N=2×10^6 ~ 1×10^7)

Fig. 5.13 Processed signal on gear box in cyclic fatigue test

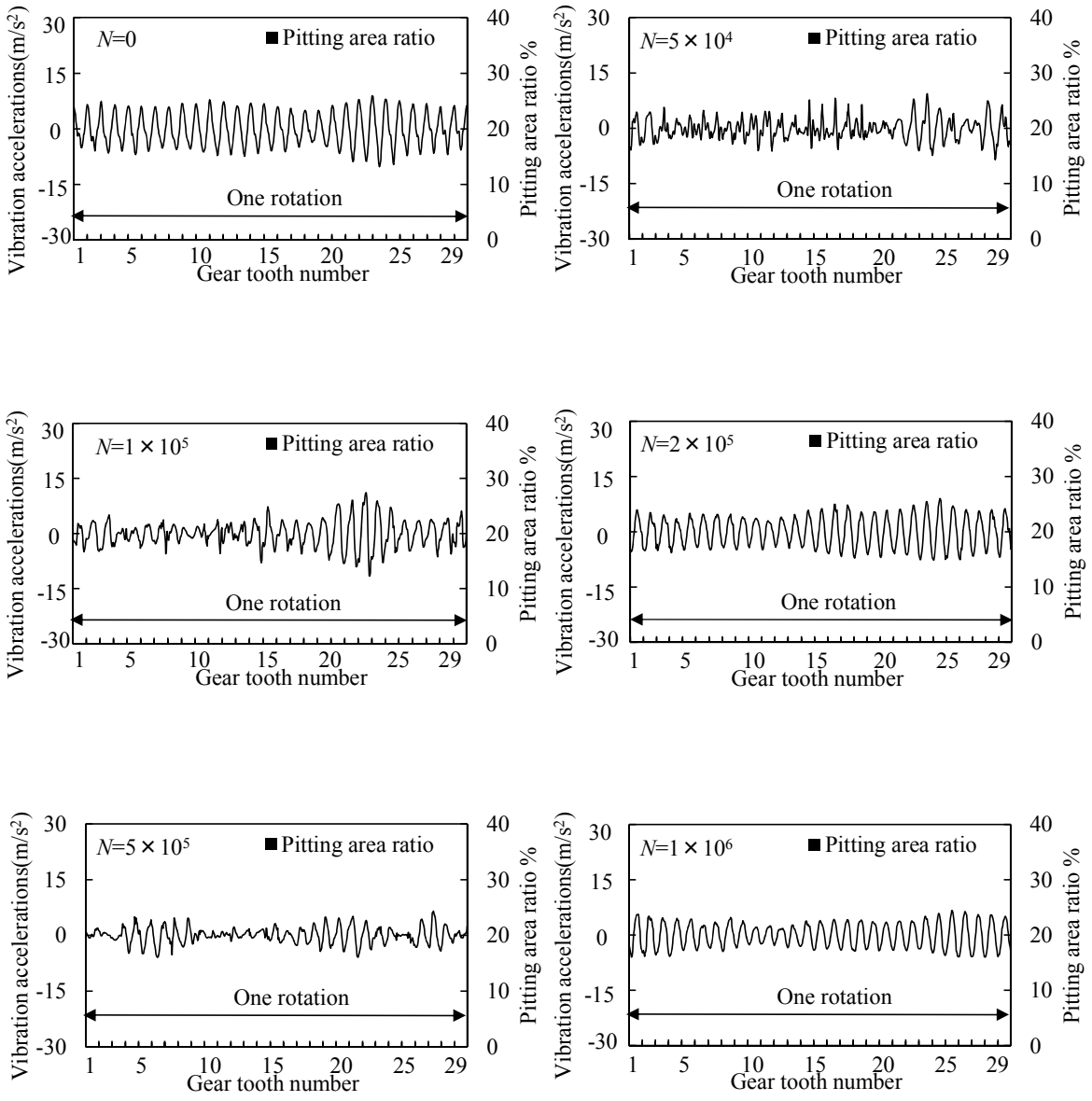

(a) Processed signal on bearing box (T=70N-m, n=1800rpm, N=0 ~ 1×10^6)

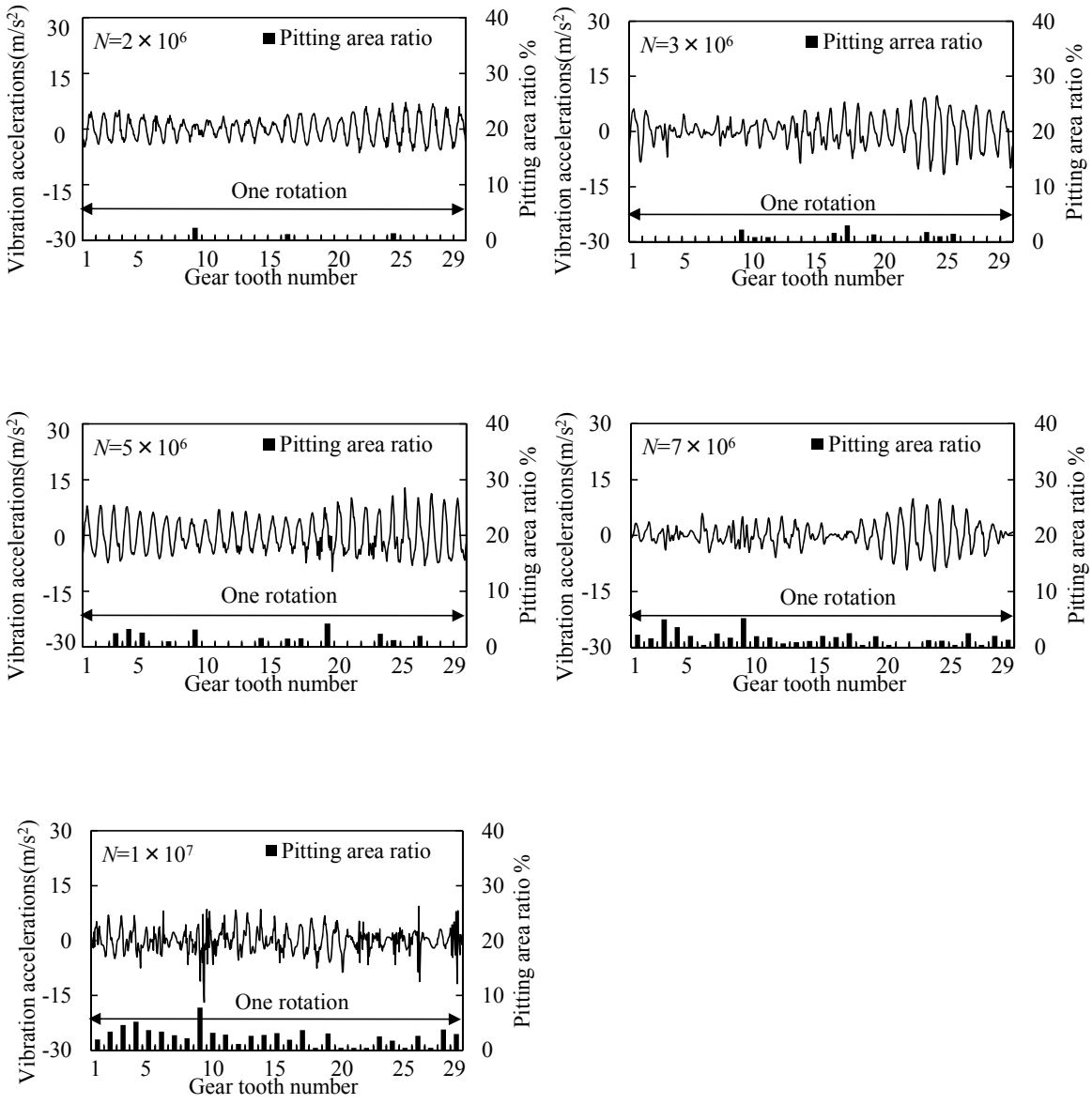

(b) Processed signal on bearing box (T=70N-m, n=1800rpm, N=2×10^6 ~ 1×10^7)

Fig. 5.14 Processed signal on bearing box in cyclic fatigue test

5.5 Summary

In this chapter, the cyclic fatigue test is introduced. The original vibration accelerations on gear box and bearing box are presented and discussed. The frequency spectrum of the original vibration signal is also analyzed. Then, the residual signal and processed signal are acquired using techniques of Fast Fourier Transform and discrete wavelet transform. Conclusions can be summarized as follows:

1. The vibration accelerations gradually become larger and fluctuate more and more strongly as the increase of pitting area. Additionally, comparing with the normal teeth which have no failure on tooth surface, the vibration accelerations of the failure teeth are a little larger and manifest an increasing tendency with the growth of pitting area. The gear condition of severe failure can be diagnosed according to the original signal. However, it is difficult to diagnose the gear condition of slight failure only based on the waveform.

2. In the frequency spectrum for normal, slight failure and severe failure condition, the amplitude of meshing frequency becomes smaller and the amplitudes of the harmonics become stronger with the increase of pitting area. Similarly, the amplitude of sidebands becomes stronger and the band width also becomes broader with the deterioration of gear condition.

3. For normal condition, the amplitude value and waveform of residual signal are more stable than that of the original signal. For slight failure condition, there is no evident indication of gear damage in the residual signal. For severe failure condition, the evident of fault impulse for severe failure is more obvious in residual signals. However, it is still hard to diagnose the early gear faults only through the waveform of residual signal.

4. The waveform of processed signal is much smoother than that of the residual signal, which indicates the noise is reduced from the residual signal. Comparing with the residual signal, the difference of amplitude value of each tooth becomes larger in the processed signal. The fault features are more clearly visualized in processed signals.

6 Diagnosis of Gear Damage Using Support Vector Machines

6.1 Introduction

This chapter proposes a diagnostic method for gear damage using support vector machines (SVMs) with extracting statistical parameters and characteristic amplitude ratios of frequency bands from the vibration signal as failure feature vector. Moreover, the method of empirical mode decomposition is also employed to extract failure feature parameters to represent gear conditions.

The procedure of diagnosis can be summarized as Fig. 6.1. Generally, data acquisition, failure features extraction and diagnosis are the main parts of the procedure. Vibration signals of gear box and bearing box are acquired as original data by testing three kinds of gears namely normal gear, spot damaged gear and pitted gear in the experiment. The original signal is analyzed using Fast Fourier Transform (FFT) and the frequency spectrum is obtained. Then, the characteristic amplitude ratios of frequency bands are extracted from the frequency spectrum. Meanwhile, the residual signal is acquired using FFT. After that, the technique of discrete wavelet transform (DWT) is employed to reduce noise from the residual signal. The coefficients of discrete wavelet transform are reconstructed into the processed signal for the further analysis. Then, statistical parameters are computed from the processed signals. Both of the characteristic amplitude ratios and statistical parameters are together served as failure feature vector for representing characteristics of gear conditions. Additionally, in order to reduce the computational complexity, the method of principal component analysis (PCA) is adopted to reduce the dimensions of failure feature vector. The original features are transformed into a smaller set of parameters as input vector of SVMs classifiers. In the process of diagnosis, the experimental data is separated into training dataset and test dataset. Then, multiple classifiers of SVMs based on binary tree are built using the training data. Finally, the test data is diagnosed by the trained model of SVMs.

In this chapter, techniques of SVMs and PCA are introduced. The characteristic amplitude ratios of frequency bands and statistical parameters are also discussed in the paper. Finally, the diagnostic results are presented. In addition, another technique called empirical mode decomposition is also introduced and is employed to extract failure feature parameter. The results of cyclic fatigue test are adopted to demonstrate the effectiveness of this approach.

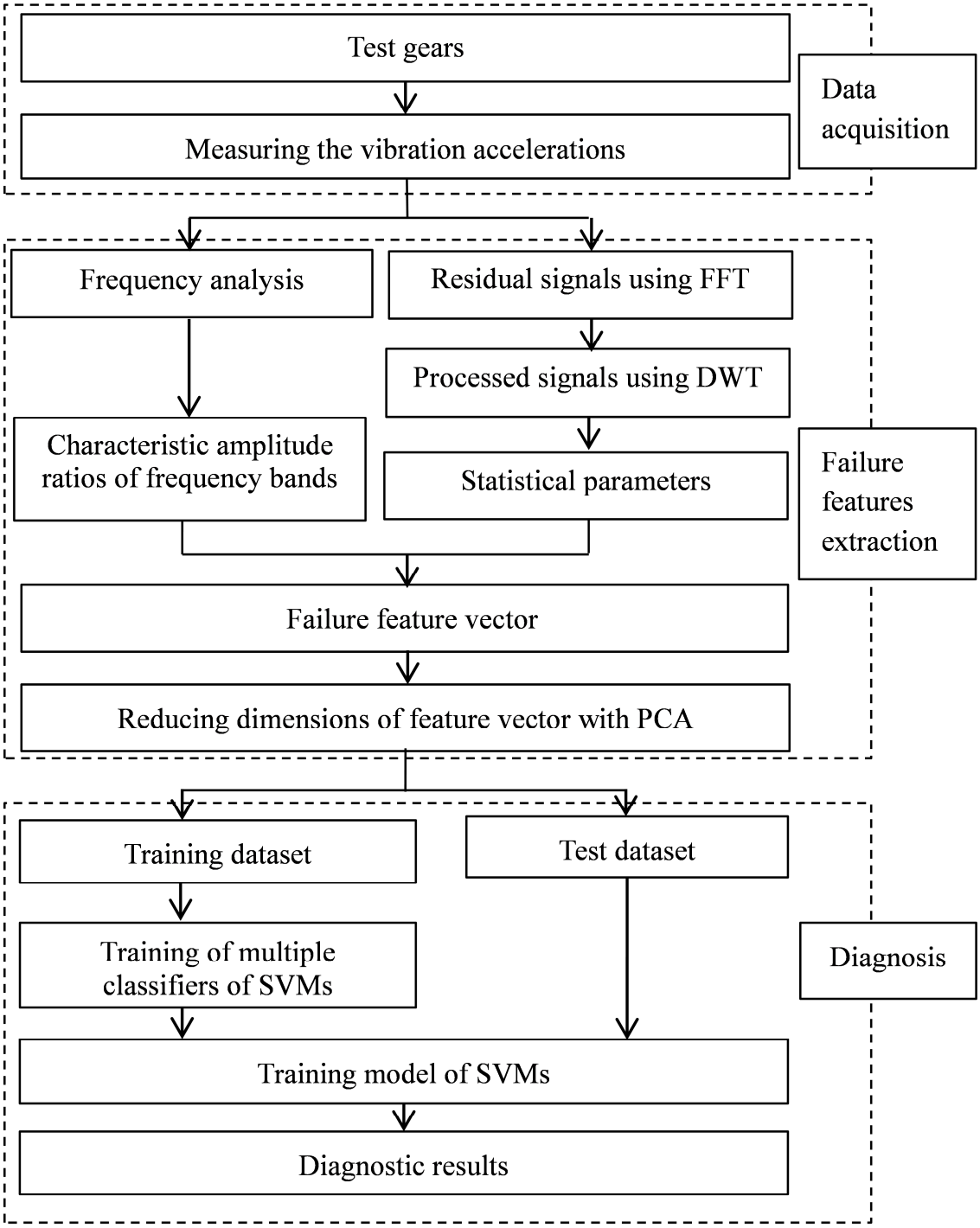

Fig. 6.1 The flow chart of gear damage diagnosis

6.2 Support Vector Machines

6.2.1 Algorithm of Support Vector Machines

Support vector machines (SVMs) are a machine learning method developed from the theory of limited samples Statistical Learning Theory by Vapnik in early 1990s [47]. It is initially dealt with linear classification problems by constructing an optimal separating hyper-plane for high classification accuracy.

In case of linear classification, supposing a data set is $\{(\mathbf{x}_i, y_i)\}$, i = 1, 2, . . ., n, n is the total number of samples, y_i = {1, -1} is the class label of samples. As shown in Fig. 6.2, squares stand for class A and circles stand for class B, x_1 and x_2 are feature parameters value of input vector $\mathbf{x}_i$. SVMs try to search for an optimal linear boundary to identify the two classes precisely and to ensure the margin between two classes is maximum to improve the classification accuracy [48]. The nearest data points used to determine the margin are called support vectors. When the feature space of input vector $\mathbf{x}_i$ is high-dimensional (>2), the boundary is called separating hyper-plane which can be defined as:

$$f(\mathbf{x}) = \langle \mathbf{w} \cdot \mathbf{x} \rangle + b \tag{6.1}$$

Where, $\mathbf{w}$ is a weight vector with the same dimensions of $\mathbf{x}$, $\langle \cdot \rangle$ denotes a scalar product of vectors, b is a scalar threshold, $\mathbf{w}$ and b are used to determine the position of the hyper-plane. $\mathbf{w}$ and b are obtained by training data set. The feature parameters of test data are inputted into the decision function. If sgn(f($\mathbf{x}$))=1, the test data is defined as class A; if sgn(f($\mathbf{x}$))= -1, the test data is defined as class B.

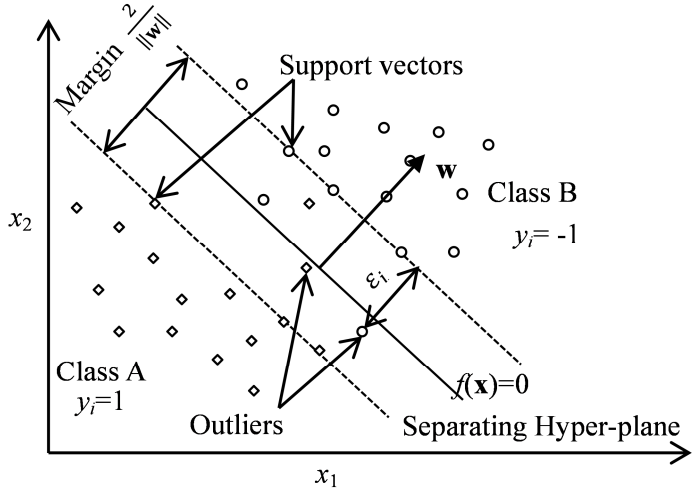

Fig. 6.2 Linear SVMs for two classes

In order to search an optimal separating hyper-plane, one has to find a maximum margin $2/\|\mathbf{w}\|$ by minimizing $2/\|\mathbf{w}\|^2$ subject to the linear constraint as follows [47]:

$$\left.\begin{aligned} &\text{Minimize } J(\mathbf{w}) = \frac{1}{2}\|\mathbf{w}\|^2 \\ &\text{Subject to, } y_i\left(\langle \mathbf{w} \times \mathbf{x}_i \rangle + b\right) \geq 1,\ i = 1,\ldots,n \end{aligned}\right\} \tag{6.2}$$

Therefore, the optimal hyper-plane problem transforms into the quadratic optimization problem. However, samples are usually not perfectly separable in practice, outliers would reduce the margin even affect the determination of separating hyper-plane. To address this problem, slack variable ε_i is introduced to reduce the effect of outliers on the boundary. The optimal hyper-plane can be obtained as a solution to the following quadratic optimization problem:

$$\left.\begin{aligned} &\text{Minimize } J(\mathbf{w}) = \frac{1}{2}\|\mathbf{w}\|^2 + C\sum_{i=1}^{n}\varepsilon_i \\ &\text{Subject to, } y_i\left(\langle \mathbf{w} \times \mathbf{x}_i \rangle + b\right) \geq 1 - \varepsilon_i,\ \varepsilon_i \geq 0, i = 1,\ldots,n \end{aligned}\right\} \tag{6.3}$$

Where n is the number of samples, ε_i is the slack variable measuring the degree of permitted deviation of outliers, C is the penalty constant which controls the weight between objectives of searching the optimal hyper-plane and guarantees the minimum deviation of outliers in the function. In order to solve this convex quadratic programming problem, the calculation can be converted into the equivalent Lagrange dual problem. According to the optimization theory, the Lagrange function is illustrated as follows:

$$L(\mathbf{w}, b, \alpha) = \frac{1}{2}\|\mathbf{w}\|^2 + C\sum_{i=1}^{n}\varepsilon_i - \sum_{i=1}^{n}\alpha_i\left(y_i\left(\langle \mathbf{w} \times \mathbf{x}_i \rangle + b\right) - 1 + \varepsilon_i\right) - \sum_{i=1}^{n}\xi_i\varepsilon_i \tag{6.4}$$

Where, α_i and ξ_i denote Lagrange multipliers. Equation (6.4) can be obtained by partially differentiating L with respect to $\mathbf{w}$, b, ε_i and considering the resulting equations to zero.

$$\left.\begin{aligned} &\frac{\mathrm{d}L}{\mathrm{d}\mathbf{w}} = 0 \Rightarrow\ \mathbf{w} = \sum_{i=1}^{n}\alpha_i y_i \mathbf{x}_i \\ &\frac{\mathrm{d}L}{\mathrm{d}b} = 0 \Rightarrow\ \sum_{i=1}^{n}\alpha_i y_i = 0 \\ &\frac{\mathrm{d}L}{\mathrm{d}\varepsilon_i} = 0 \Rightarrow\ C\text{-}\alpha_i\text{-}r_i = 0\ ,i = 1,\ldots,n \end{aligned}\right\} \tag{6.5}$$

Substituting Eq. (6.5) into Eq. (6.4), the above equality can be transformed into the optimization problem of the dual variable α_i:

$$\left.\begin{aligned}&\text{Maximize } L(\alpha)=\sum_{i=1}^{n}\alpha_i-\frac{1}{2}\sum_{i,j=1}^{n}\alpha_i\alpha_j y_i y_j\left\langle \mathbf{x}_i \times \mathbf{x}_j\right\rangle\\&\text{Subject to, } \sum_{i=1}^{n}\alpha_i y_i=0, 0\le\alpha_i\le C,\ i=1,\ldots,n\end{aligned}\right\} \tag{6.6}$$

After solving the optimization problem of α_i, **w** and b can be acquired through Eqs. (6.1) and (6.5). With $\mathbf{w}=\sum_{i=1}^{n}\alpha_i y_i \mathbf{x}_i$ the optimal separating hyper-plane can be determined as follows:

$$f(\mathbf{x})=\left(\sum_{i=1}^{n}\alpha_i y_i \mathbf{x}_i \times \mathbf{x}\right)+b=\sum_{i=1}^{n}\alpha_i y_i\left\langle \mathbf{x}_i \times \mathbf{x}\right\rangle+b \tag{6.7}$$

Therefore the decision function for linearly classifying the input test data as either belonging to class A or class B is acquired as follows:

$$h(\mathbf{x})=\operatorname{sgn}(f(\mathbf{x}))=\operatorname{sgn}\left(\sum_{i=1}^{n}\alpha_i y_i\left\langle \mathbf{x}_i, \mathbf{x}\right\rangle+b\right) \tag{6.8}$$

The model mentioned above is only for linear classification with two-class labels. For the nonlinear classification, SVMs can also be capable by mapping the input variables into a high-dimensional feature space with kernel functions, where the linear classification is possible [61]. Then, the nonlinear classification function is defined as [47]:

$$h(\mathbf{x})=\operatorname{sgn}\left(\sum_{i=1}^{n}\alpha_i y_i k\left(\mathbf{x}_i, \mathbf{x}\right)+b\right) \tag{6.9}$$

Where, k ($\mathbf{x}_i$, **x**) is the kernel function. There are many types of kernel functions can be used in SVMs, including linear function, Gaussian radial basis function and polynomial function. In this paper, the kernel function of Gaussian radial basis function is adopted for its high flexibility and broad application. The equation is shown as follows:

$$k(x_1, x_2)=\exp\left(-\frac{\|x_1-x_2\|^2}{2\mu^2}\right) \tag{6.10}$$

Where, μ is the width of Gaussian function which can be determined by an iterative program. In SVMs model, the penalty constant C and kernel parameter μ both impact the generalization capability and classification accuracy of SVMs. However, there is not any precise basis to determine the suitable C and μ for the given problem [87]. Therefore, the appropriate C and μ must be selected by some parameter optimization algorithm according to the training data. In present work, the approaches of grid-search and 5-fold cross validation were adopted to identify the most suitable C and μ, within the initial setting range [2^{-8}, 2^{8}] of C and μ. Various pairs of (C, μ) values are tried and the one with the best cross-validation accuracy is picked.

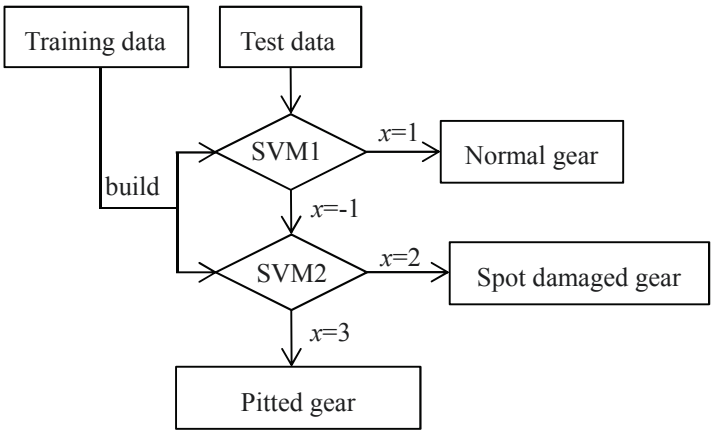

Fig. 6.3 Procedure of gear damage diagnosis using multi-classifiers of SVMs

6.2.2 Multiple Classifiers of Support Vector Machines

Since a basic SVM classifier can only correspond to the classification of two classes, to solve the multi-classes classification problem, many multiple classifiers such as one-against-one, one-against-all and direct acyclic graph have been developed [88, 64]. There are three kinds of gears in this study, called normal gear, spot damaged gear and pitted gear. Thus, two SVM classifiers based on the binary tree are designed to classify the condition of test gear into three types: normal gear, spot damaged gear and pitted gear.

Figure 6.3 illustrates the diagram of diagnosis using classifiers of SVMs. SVM1 and SVM2 are the classifiers built by the training data. Variable x represents output result: x=1 shows the test gear condition is normal gear, x=2 is spot damaged gear, while x=3 is pitted gear. Firstly, the test data is inputted into SVM1, if x=1 the sample is judged as normal gear and the procedure completes; otherwise the sample will be automatically inputted into SVM2. The sample is considered as spot damaged gear when x=2, or else is pitted gear.

6.3 Extracting Failure Feature Vectors

In the automatic diagnosis system for gear damage, extracting appropriate parameters to quantitatively illustrate the representative property of the signal is one crucial step to improve the diagnostic accuracy. In this paper, the statistical parameters of standard deviation (σ), kurtosis (β_1), skewness (β_2), root mean square value (γ) and so on are calculated from the processed signal. Moreover, the characteristic amplitude ratios of frequency bands are acquired from the frequency spectrum of the original signal. The characteristic amplitude ratios of frequency bands and

statistical parameters are together served as failure feature vector to represent the characteristics of gear conditions.

6.3.1 Statistical Parameters

In the time domain, statistical parameters, such as kurtosis, skewness, crest factor and so on, have been proved to be sensitive to the alteration of the signal and can illustrate the characteristic features of the waveform. Wang, et al. (2010) [41] proposed an approach which explores the properties of kurtosis, mean, variance, form factor and crest factor of the mean amplitude of continuous wavelet transform coefficient as quantitative indicators of gear failure, by employing the method of the continuous wavelet transform to analyze the time synchronously averaged residual signals. The statistical parameters are proved to be insensitive to experimental conditions. These indicators have also been applied to the detection of localized damage in many studies [40, 87~89]. In this paper, the statistical parameters like standard deviation (σ), kurtosis (β_1), skewness (β_2) and RMS (γ) described in Table 6.1 are calculated from the processed signal acquired by DWT.

Table 6.1 The expression of statistical parameters

Standard deviation	$\sigma = \sqrt{\frac{1}{n-1}\sum_{i=1}^{n}(x_i - \overline{x})^2}$
Kurtosis	$\beta_1 = \frac{\sum_{i=1}^{n}\left(x_i - \overline{x}\right)^4}{n\sigma^4}$
Skewness	$\beta_2 = \frac{n}{(n-1)(n-2)}\sum_{i=1}^{n}(\frac{x_i - \bar{x}}{\sigma})^3$
Root Mean Square	$\gamma = \sqrt{\frac{1}{n}\sum_{i=1}^{n}{x_i}^2}$
x_i: the data of the signal, $\overline{x}$: the mean value of the signal, n: the data number of the signal	

(a) Statistical Parameters Calculated From the Experimental Results of Damage Contrast Test

The statistical parameters are extracted from the processed signals acquired from the experimental results of damage contrast test under load torque T=70N-m. The parameters for five kinds of test gears are shown in Figs. 6.4~6.7.

Figure 6.4 shows the standard deviation calculated from the processed signal on gear box and on bearing box respectively. The standard deviation stands for the dispersion degree of data distribution. As found from Fig. 6.4, the standard deviation of normal gear is the smallest. The standard deviation of spot damaged gear and pitted gear becomes larger along with the increase of damaged area and gear rotation speed. In addition, the difference of standard deviation among different kinds of test gears is little under the lower speed 1200rpm, but the difference becomes larger with the increase of gear rotation speed. It is because the major factor resulting in the vibration and noise of test gears is the tooth profile error, which becomes larger as the increase of damaged area on tooth surface. The larger the tooth profile error, the stronger the vibrations of gears become. The vibrations of gears also become stronger with the increase of gear rotation speed. Therefore, the scattering of the vibration accelerations becomes larger with the increase of damaged area and gear rotation speed. Comparing Fig. 6.4 (a) with Fig. 6.4 (b), one can find that the standard deviation calculated from the processed signal on gear box is larger than that calculated from the processed signal on bearing box. Moreover, the relative difference of the standard deviation among the normal gear, spot damaged gear and pitted gear shown in Fig. 6.4 (a) is larger than that shown in Fig. 6.4 (b). This is because the vibration accelerations on gear box are larger than those on bearing box.

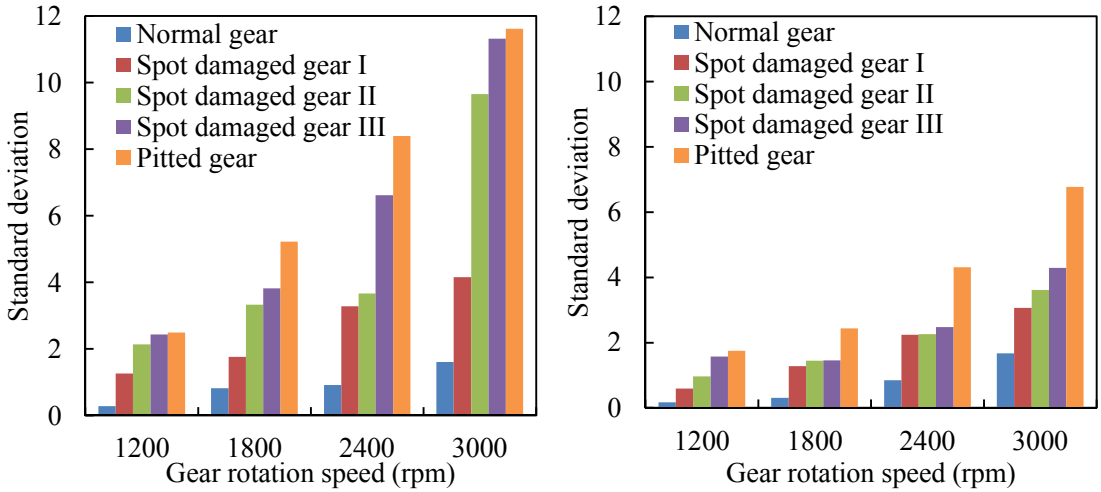

(a) Calculated from the signal on gear box (b) Calculated from the signal on bearing box

Fig. 6.4 Standard deviation calculated from the processed signal (T=70N-m)

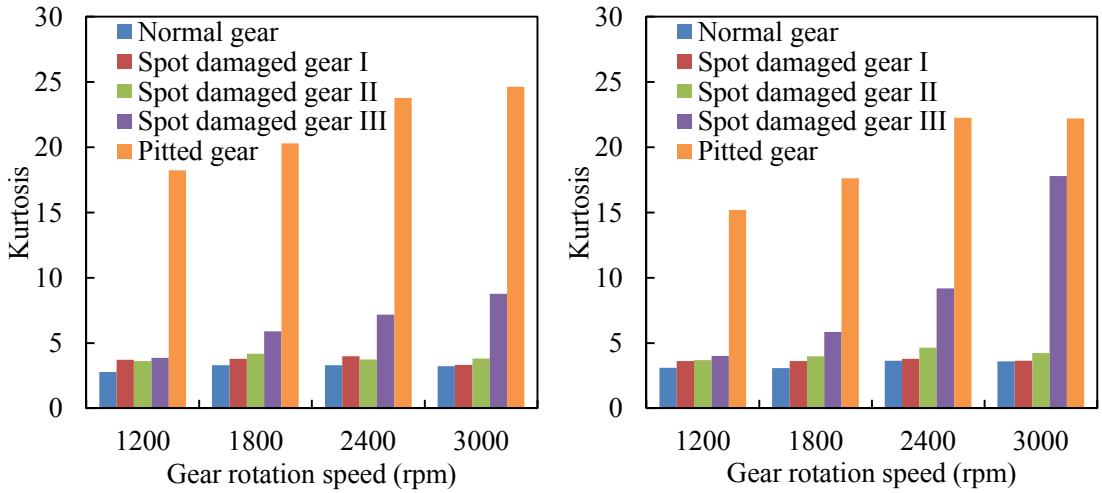

(a) Calculated from the signal on gear box (b) Calculated from the signal on bearing box

Fig. 6.5 Kurtosis calculated from the processed signal (T=70N-m)

Figure 6.5 represents the kurtosis calculated from the processed signal on gear box and on bearing box respectively. Kurtosis is a measurement of whether the data probability distribution is peaked or flat around the mean value, which equals to 3 for a standard normal distribution. From Fig. 6.5, it can be seen that the kurtosis of the normal gear is almost stable and equals to 3 under all the gear rotation speeds. The kurtosis of spot damaged gear I and II is nearly equal with each other and the value is a little larger than that of normal gear. The kurtosis of spot damaged gear III is larger than that of gear I and II. While, the value of kurtosis for pitted gear is the largest. Moreover, for the damaged gear, the larger the gear rotation speed and the damaged area are, the larger the kurtosis is. This is because the vibration accelerations of the normal gear fluctuate slightly under all the gear rotation speeds, but the abnormal vibration accelerations caused by the gear damage fluctuate greatly along with the increase of the damaged area and gear rotation speed. The larger the amplitude of transient abnormal vibration accelerations is, the larger the kurtosis is [90]. Comparing Fig. 6.5 (a) with Fig. 6.5 (b), the kurtosis calculated from the signals on gear box and the difference of kurtosis among various test gears are larger than that shown in Fig. 6.5 (b).

Figure 6.6 depicts the skewness value calculated from the processed signal on gear box and bearing box. Skewness is a measure of asymmetry in a statistical distribution and can be quantified to define the extent to which distribution differs from a normal distribution. If the skewness value is positive, it indicates that the distribution has wide skirts on the right side of the mean value. As shown in Fig. 6.6, the skewness value of normal gear is the smallest, while the value of pitted gear is the largest. The skewness of spot damaged gear I and II is almost as same as each other and the value is a little larger than that of normal gear. The skewness of spot damaged gear III is larger than

that of damaged gear I and II. For spot damaged gear and pitted gear, the skewness increases gradually as the increase of gear rotation speed. This can be explained as the abnormal vibration accelerations caused by the tooth profile error become larger when the gear rotation speed increases, which results in enlarging the deviation of the waveform from the mean value. Additionally, the skewness represented in Fig. 6.6 (a) is larger than that represented in Fig. 6.6 (b). However, the difference of skewness among spot damaged gear I, II and III can be more clearly observed from Fig. 6.6 (b).

Figure 6.7 represents the root mean square value calculated from the processed signal on gear box and bearing box. As one can see from Fig. 6.7, under the same gear rotation speed, the root mean square becomes larger in the order of normal gear, spot damaged gear and pitted gear. Furthermore, along with the increase of gear rotation speed, the root mean square becomes larger. The root mean square value of normal gear change slightly, while the value of spot damaged gear and pitted gear varies obviously. This is because the influence of tooth profile error on the vibrations of gears becomes stronger when the damaged area and gear rotation speed become large. As shown in Fig. 6.7 (a) and Fig. 6.7 (b), the root mean square value calculated from the processed signal on gear box is a larger than that calculated from the signal on bearing box. The difference of value between spot damaged gear I and II is little. However, the difference of root mean square value among spot damaged gear II and III is obvious as presented in Fig. 6.7 (a).

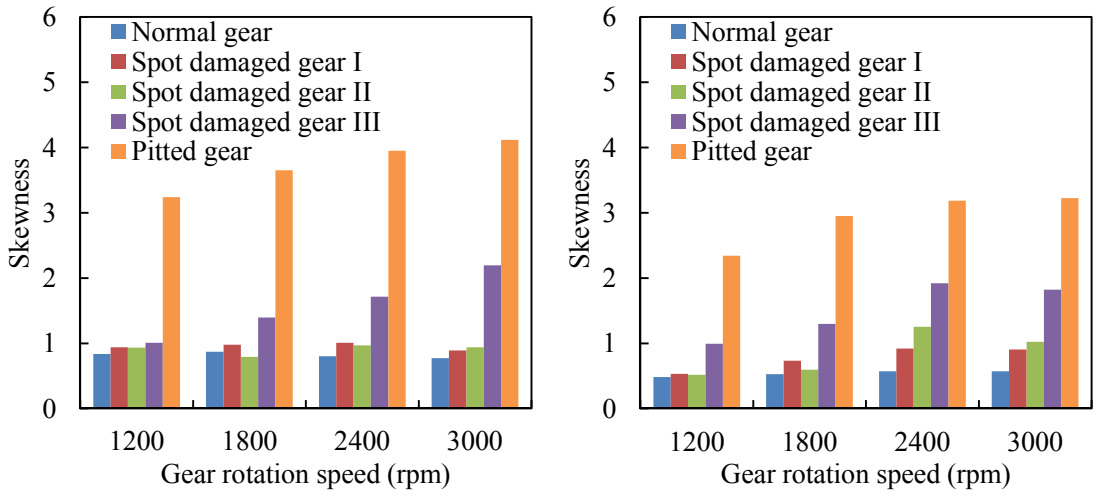

(a) Calculated from the signal on gear box (b) Calculated from the signal on bearing box

Fig. 6.6 Skewness calculated from the processed signal (T=70N-m)

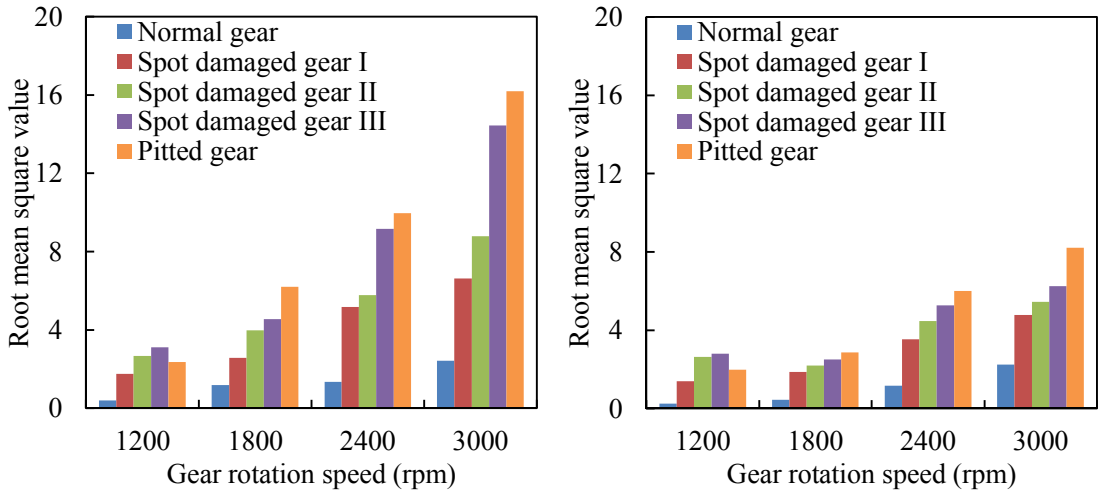

(a) Calculated from the signal on gear box (b) Calculated from the signal on bearing box

Fig. 6.7 Root mean square value calculated from the processed signal (T=70N-m)

(b) Statistical Parameters Extracted From the Experimental Results of Cyclic Fatigue Test

Figure 6.8 shows the statistical parameters of standard deviation (σ), kurtosis(β_1), skewness (β_2) and root mean square value (γ) which are calculated from the processed signals acquired in cyclic fatigue test. When the gear condition is normal from N=0 to 1×10^6, the values of statistical parameters are nearly stable and relatively smaller. After the generation of pitting failure on tooth surface, the values of statistical parameters become larger with the increase of cycles after about N=1×10^6. Particularly after N=3×10^6, the statistical parameters increase obviously. This is because the vibration of gear is considerably influenced by the tooth profile error which becomes larger with the increase of pitting area. The failure area on tooth surface becomes larger as the increase of cycles after the generation of pitting damage, especially after N=3×10^6. Therefore, after the failure occurs on tooth surface, the measured vibration acceleration and its statistical parameters increase with the progression of pitting area. The statistical parameters can be employed to represent characteristic features of various gear conditions.

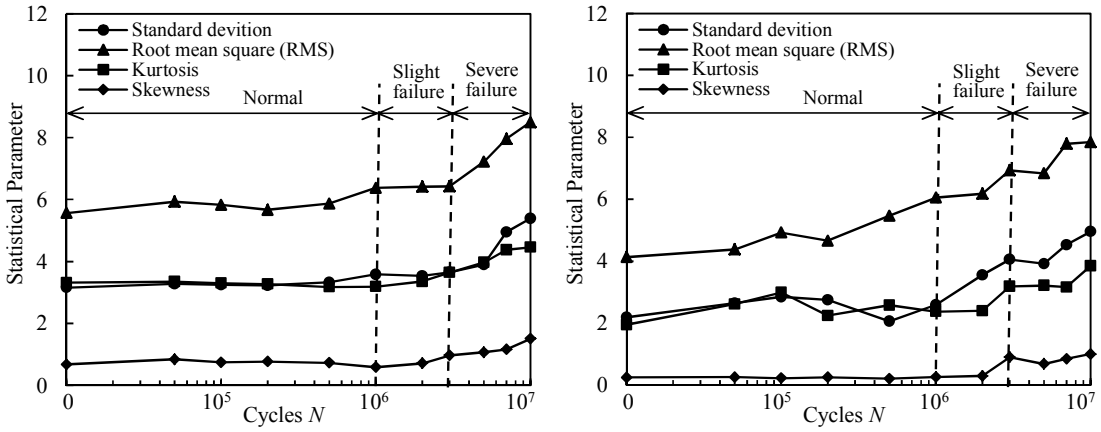

(a) Calculated from the signal on gear box (b) Calculated from the signal on bearing box

Fig. 6.8 Statistical parameters extracted from the processed signal of cyclic fatigue test

6.3.2 Characteristic Amplitude Ratios of Frequency Bands

As described in the frequency analysis of the vibration accelerations, the frequency spectrum changes with different gear conditions. The amplitude of harmonics and sidebands varies with the conditions of test gears. Thus, it is capable to extract failure features from the frequency spectrum based on the amplitude of harmonics and sidebands. We can separate the spectrum into several frequency bands according to the harmonics and their sidebands. Then, the sum-of-squares of amplitudes of each frequency band is computed and normalized to form the vector of characteristic amplitude ratio $\mathbf{R} = (r_1, r_2, \dots, r_i)$. The calculation procedure is shown as follows:

$$T_i = \sum_{j=1}^{n} A_j^{\,2} \tag{6.11}$$

$$T = \sum_{i=1}^{m} T_i \tag{6.12}$$

$$r_i = T_i / T \tag{6.13}$$

Where, A_j is the amplitude of frequency spectrum, T_i is the sum of squares of amplitude, n is the number of samples in each frequency band, m is the number of frequency bands ($m \approx$ analytical frequency / meshing frequency -1), r_i is the characteristic amplitude ratio of i-th frequency band.

The vibration accelerations on gear box under conditions of 70N-m and 1800rpm is employed

to representatively present the characteristic amplitude ratios from its frequency spectrum. The gear rotation speed is n=1800rpm, the meshing frequency is 870Hz and the analysis frequency is 10000Hz. The frequency spectrum is divided into 10 frequency bands (m=10). The range of each frequency band are 0-1000Hz, 1001-2000Hz, 2001-3000Hz, 3001-4000Hz, 4001-5000Hz, 5001-6000Hz, 6001-7000Hz, 7001-8000Hz, 8001-9000Hz and 9001-10000Hz respectively. The frequency interval of the spectrum is 0.5Hz, therefore, each of the frequency bands has 2000 samples (n=2000).

The characteristic amplitude ratios shown in Fig. 6.9 are calculated from the frequency spectrum of the original signal on gear box under 70N-m and 1800rpm in damage contrast test,. Figure 6.9 shows the characteristic amplitude ratios of frequency bands obtained from the frequency spectrum of normal gear, spot damaged gear I, II, III and the pitted gear respectively. From the amplitude ratios of all the test gears, it can be seen that the amplitude ratios of the 3rd and 4th frequency bands are relatively larger than those of the other frequency bands. This is because the resonance frequency of the gear box is about 3000Hz, which is included in the 3rd and 4th frequency bands. As shown in Fig. 6.9 (a), the amplitude ratio of the first frequency band is the largest. The amplitude ratios of the 3rd and 4th frequency bands are relatively larger than that of the other frequency bands. This can be considered as, for the normal gear, the meshing frequency is dominant and is included in the 1st frequency band, and the amplitude of its high-order harmonics is relatively weaker. Comparing with Fig. 6.9 (a), in Fig. 6.9 (b), the amplitude ratio of the 1st frequency band becomes smaller, while the amplitude ratio of the 4th frequency band becomes larger and more dominant. It indicates that the resonance frequency becomes stronger. Figure 6.9 (c) presents the amplitude ratios of frequency bands for spot damaged gear II. Comparing with that of spot damaged gear I, The amplitude ratio of the 3rd frequency band becomes larger. In the amplitude ratio of frequency bands for spot damaged gear III shown in Fig. 6.9 (d), the amplitude ratio of the 4th frequency band becomes significantly larger than that of the other frequency bands. Similarly, the amplitude ratio of the 4th frequency band shown in Fig. 6.9 (e) is also obviously larger than that of the other frequency bands, which indicates the abnormal gear condition. As shown in Fig.6.9, for the spot damaged gear and pitted gear, the amplitude ratio of the 4th frequency band is always dominant and much larger. This shows that the high-order harmonics and the resonance frequency will become stronger with the increase of damaged area.

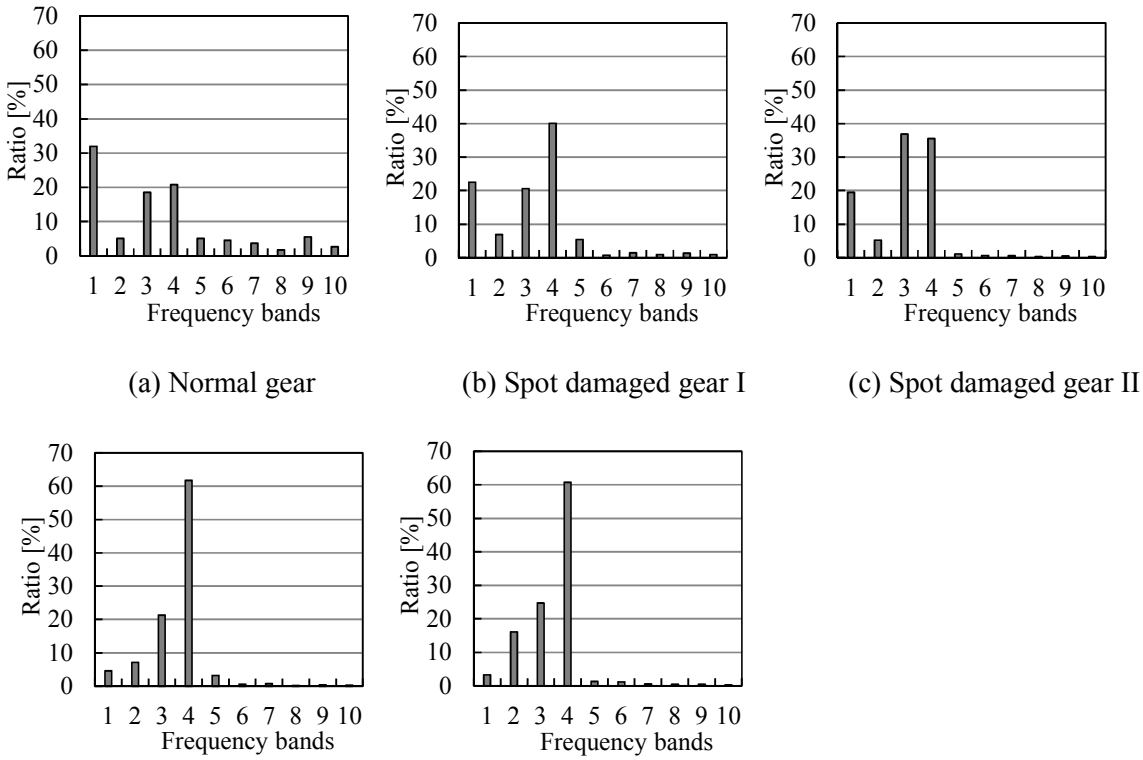

(a) Normal gear (b) Spot damaged gear I (c) Spot damaged gear II

(d) Spot damaged gear III (e) Pitted gear

Fig. 6.9 Characteristic amplitude ratios of frequency bands in damage contrast test

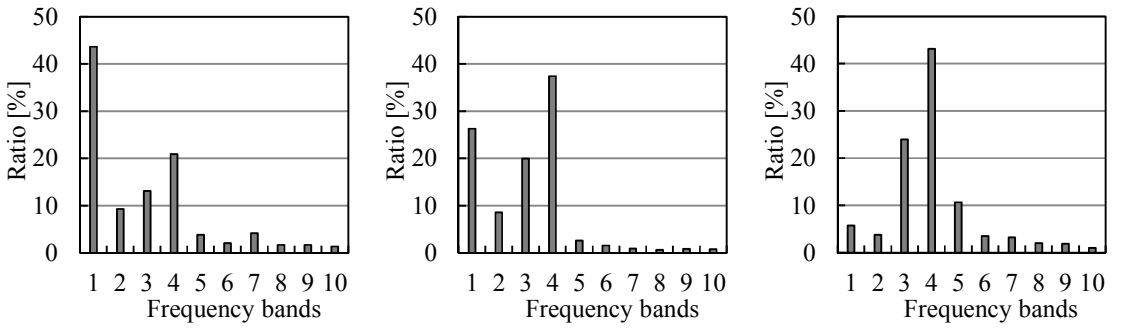

(a) Normal (b) Slight failure condition (c) Severe failure condition

Fig. 6.10 Characteristic amplitude ratios of frequency bands in cyclic fatigue test

Figure 6.10 shows the characteristic amplitude ratios of frequency bands obtained from the frequency spectrum of original signals in cyclic fatigue test. Figures 6.10 (a), (b) and (c) correspondingly illustrate the amplitude ratios of frequency bands for normal gear, slight failure

gear and severe failure gear respectively. In the amplitude ratios of frequency bands for normal gear shown in Fig. 6.10 (a), the amplitude ratio of the first frequency band is the largest. Except for the 3rd and 4th frequency bands, the amplitude ratios of the other frequency bands become weaker in order. Figure 6.10 (b) depicts the amplitude ratio of frequency bands for slight failure gear. The amplitude ratio of the 4th frequency band becomes the largest. In addition, the amplitude ratio of the 3rd frequency band becomes larger. On the contrary, the amplitude ratio of the 1st frequency band becomes smaller. Figure 6.10 (e) illustrates the amplitude ratio of the frequency bands for severe failure gear. The amplitude ratio of the 4th frequency band becomes significantly larger than that of the other frequency bands, which shows the abnormal gear condition.

Overall, the characteristic amplitude ratios shown in Fig. 6.10 are similar with that of normal gear, spot damaged gear I and pitted gear shown in Fig. 6.9. In addition, the amplitude ratios of frequency bands approximately represent the characteristics of frequency spectrum and change with the variation of gear conditions. Consequently, the characteristic amplitude ratios of frequency bands can be adopted to demonstrate features of the vibration signals in frequency domain.

6.4 Features Extraction Using Principal Component Analysis

In order to acquire satisfactory classification accuracy using SVMs, it is necessary to preprocess the extracted feature parameters to preparing the data inputs for classifier of SVMs. The feature parameters extracted from the experimental results can't be directly inputted into classifier because it will decrease the performance of classifier. Moreover, too many features can cause the curse of dimensionality phenomenon since irrelevant and redundant features degrade the performance of classifier [91]. Problem with high-dimensional data, known as the curse of dimensionality in pattern recognition implies that the number of training samples must grow exponentially with the number of features in order to learn an accurate model. Moreover, the high-dimensional data will increase the difficulty and time of calculation. Therefore, we need feature extraction to reduce the number of features for avoiding the redundancy. Feature extraction means transforming the existing features into a lower dimensional space [92].

Many feature extraction techniques have been developed based on principal component analysis, linear discriminant analysis, and independent component analysis. Recently, the use of feature extraction methods for data preprocessing before inputting into classifier has been reported in many literatures. Zang, et al. [93] and Ypma & Pajunen [94] have applied independent component analysis to machine condition monitoring and faults detection. Sohn, et al. [95] and Worden & Manson [96] have employed principal component analysis to enhance the

discrimination features from the undamaged and damaged structures, implemented visualization and dimension reduction for damage detection. They have investigated that the feature extraction methods with the benefits of improving classification accuracy, reducing execution time and more compact understanding knowledge-base.

6.4.1 Principal Component Analysis

Since the high-dimensions of failure feature vector will complicate the calculation and extend the processing time, principal component analysis (PCA) is adopted to reduce dimensions of vectors by synthesizing characteristics of each parameter into one index. PCA is a statistical technique using an orthogonal transformation to convert an original set of variables into a substantially smaller set of uncorrelated variables called principal components.

Supposing a set of original feature vectors $\mathbf{Z}_l$ (l=1, … , n), each of which is of m dimensions $\mathbf{Z}_l = (z_1, \dots, z_m)_{(l)}$. PCA transforms each vector $\mathbf{Z}_l$ into a new one $\mathbf{P}_l = (p_1, \dots, p_m)_{(l)}$by:

$$\mathbf{P}_l = \mathbf{A}^{\mathrm{T}}\mathbf{Z}_l = \begin{bmatrix} a_{11} & \cdots & a_{1m} \\ \vdots & \cdots & \vdots \\ a_{m1} & \cdots & a_{mm} \end{bmatrix} \begin{bmatrix} z_1 \\ \vdots \\ z_m \end{bmatrix} = \begin{bmatrix} p_1 \\ \vdots \\ p_m \end{bmatrix} \tag{6.14}$$

Where $\mathbf{A}$ is the $m \times m$ orthogonal matrix whose i-th column a_i is the eigenvector of the sample covariance matrix, the new components are called principal components [97].

Generally, the first several principal components sorted in descending order of the eigenvalues perform the considerable effect in feature vector $\mathbf{P}_l$ and can be selected to represent almost all the features of the vector. The number of selected principal components can be decided based on a threshold value whichis generally between [0, 100]. If the threshold value is 90, it means that the selected principal components can represent 90% percent features of the original vector. Thus, the number of principal components in $\mathbf{P}_l$ can be reduced and PCA has the characteristic of dimension reduction.

6.4.2 Distribution of Damage Contrast Test Data Based on Principal Components

The characteristic amplitude ratios of frequency bands and statistical parameters are together served as 14-dimensions failure feature vector $\mathbf{V}=(\sigma, \beta_1, \beta_2, \gamma, r_1, \dots, r_{10})$ to represent the characteristics of gear conditions. In order to eliminate the influence of dimensions and to simplify the calculating, firstly, the failure feature vectors are normalized into 0 to 1. Then, the PCA method

is adopted to reduce dimensions of the failure feature vector. The threshold value is set as 95, and 8 principal components are selected to represent the features of the original vector. Therefore, the original features are transformed into a 8-dimensions input vector $\mathbf{P} = (p_1, \ldots, p_8)$ for SVMs classifiers

In order to generally illustrate the distribution of input vector in the feature space, the space diagram was made based on the first 3 principal components of the input vector. The distribution of test samples in damage contrast test is shown in Fig. 6.11. As shown in this figure, the distribution of samples for normal gear, spot damaged gear I and pitted gear is concentrated. While the distribution of spot damaged gear II and III is a little more scattered. The distribution of normal gear and spot damaged gear I is very close, which indicates the difference of failure feature vectors between the spot damaged gear and the normal gear is not obvious. The identification between the normal gear and spot damaged gear I may be difficult. Some samples of spot damaged gear II overlap with the range of spot damaged gear I and III. It would be difficult to clearly separate the types of spot damaged gear. The samples of pitted gear distinguish clearly with the normal gear and the spot damaged gear.

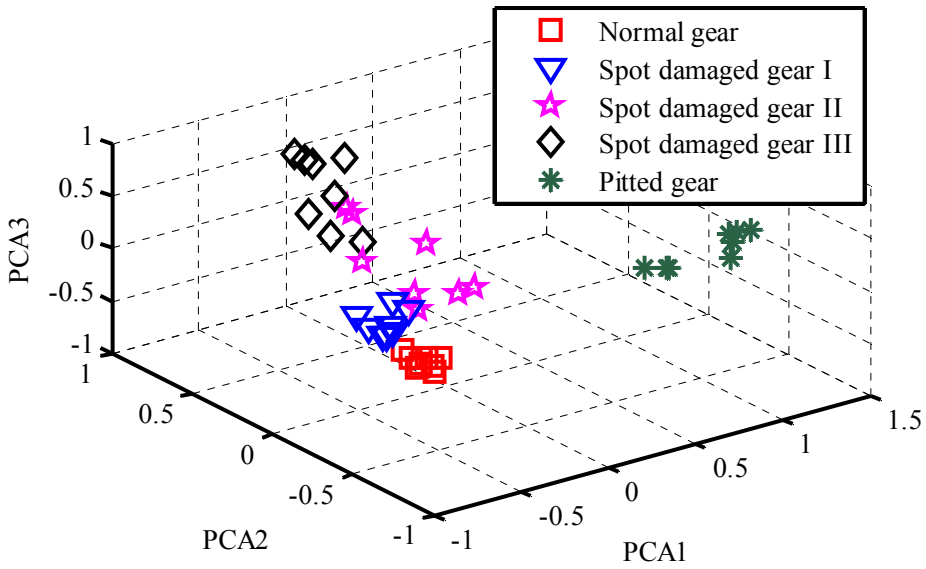

Fig. 6.11 Distribution of test data in damage contrast test based on the first 3 principal components

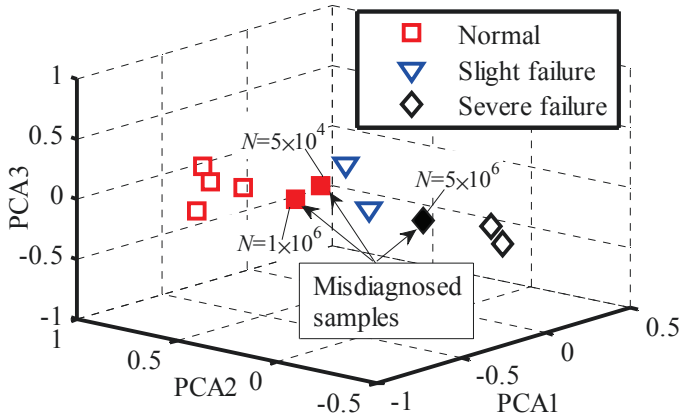

Fig. 6.12 Distribution of test data in cyclic fatigue test based on the first 3 principal components

6.4.3 Distribution of Cyclic Fatigue Test Data Based on Principal Components

Figure 6.12 presents the distribution of test data in cyclic fatigue test based on the first three principal components. PCA1, 2, 3 represent the first three principal components p_1, p_2 and p_3 respectively. In the figure, the painted markers are misdiagnosed samples. The data distribution is a little scattered. The distribution of normal samples and slight failure samples can't be completely separated. Samples at N= 5×10^4 and N= 1×10^6 distribute closely with the samples of slight failure condition. It indicates the differences of failure feature vectors between the normal condition and slight failure condition are not obvious. Samples of severe failure are distinguished clearly from the samples of normal and slight failure. However, sample at N= 5×10^6 nearly distribute in the range of slight failure, which is probably misdiagnosed into slight failure.

6.5 Diagnostic Results

6.5.1 Diagnostic Results of Damage Contrast Test

Support vector machines are employed to diagnose gear damage based on the extracted failure feature vector above. For the damage contrast test, 40 experimental results of normal gear, spot damaged gear I, II, III and pitted gear are selected as test dataset. The training dataset is acquired by performing several experiments on the same testing machine with normal gear spot damaged gear and pitted gear. 40 experimental results are adopted as training dataset, and failure feature vectors are extracted with the same method as that for test data. SVMs classifiers of SVM1 and SVM2 are built by the training dataset. After that, the gear condition is diagnosed by inputting feature vector of test dataset to the trained model. Finally, the diagnostic results are outputted. In

addition, during the training process of SVMs model, the methods of grid-search and 5-fold cross validation are employed to search the best penalty coefficient C and kernel parameter μ based on the training dataset.

The diagnostic results of test gear conditions in damage contrast test are shown in Table 6.2. The number -1, 1, 2 and 3 in table 6.2 represent the diagnostic results. If the output result is 1, it denotes that the test gear condition is normal, and the diagnosis procedure completes. If the output is -1, it means that the gear condition is not normal, and the test data will be inputted into SVM2. The output number 2 represents the gear condition is spot damaged, while 3 shows the gear condition is pitting.

In table 6.2, the 7th sample of normal gear is misdiagnosed into spot damaged gear. Also, the 3rd sample of spot damaged gear I is misdiagnosed into normal gear. This is because the damage on tooth surface of spot damaged gear I is relatively small. The influence of the damage in the vibration accelerations is little, which can be found from the original signal and feature parameters of the spot damaged gear I. Moreover, the vibration signals are always inevitably interfered by the random noise and vibrations from shafts, bearings, or other components. The useful information and characteristics of damage are very weak. The extracted feature parameters of normal gear and spot damaged gear I are very close, which can be seen from Fig. 6.11. In feature space of SVMs, the data distribution of normal gear is close to that of the spot damaged gear I. Therefore, the sample of spot damaged gear I would be probably misdiagnosed into normal gear. Besides, the 4th sample of spot damaged gear III is misdiagnosed into pitted gear. The vibration accelerations and extracted feature parameters of spot damaged gear III is different from that of the pitted gear. In Fig. 6.11, the distribution of samples for spot damaged gear III is also clearly separated with the distribution of pitted gear. Therefore, the diagnosis of the 4th sample of spot damaged gear III may be an error of diagnosis. All the samples of pitted gear are correctly diagnosed by the proposed method. The diagnostic accuracy is 92.5%, which demonstrates that the proposed method can effectively classify the normal gear and damaged gear. The diagnostic accuracy is defined as a ratio of the number of correctly diagnosed samples to the total number of test data.

I try to adopt the proposed method to identify the degree of gear damage. 24 experimental results of spot damaged gear I, II, III in damage contrast test are chosen as testing dataset. 24 experimental results of spot damaged gear are selected as training dataset. SVMs classifiers of SVM1 and SVM2 are built by the training dataset. After that, the gear condition is diagnosed by inputting feature vector of test dataset to the trained model. Table 6.3 shows the diagnostic results of gear conditions. In this table, the output result 1 represents spot damaged gear I, the number 2 stands for spot damaged gear II, while 3 represents spot damaged gear III.

In the diagnostic results, the 5th and 6th samples of spot damaged gear I are misdiagnosed into spot damaged gear II, the second sample of spot damaged gear II is misdiagnosed into spot damaged gear I. This is because the difference of the damaged area between spot damaged gear I and II is not obvious. The vibration accelerations and extracted characteristic parameters value of the two test gears are also similar, which can be seen from the statistical parameters of the signal. In feature space, the distribution of some samples of spot damaged gear II also overlaps with the distribution of spot damaged gear I. Therefore, there is a possibility of misdiagnosis in classifying the spot damaged gear I and II. Moreover, the 5th and 6th samples of spot damaged gear II are misdiagnosed into spot damaged gear III. The extracted feature parameters of spot damaged gear II fluctuates a little larger, which can be seen from Fig. 6.11. In feature space, the data distribution of spot damaged gear II is a little more scattered, and some samples distribute in the range of spot damaged gear III. Consequently, some samples of spot damaged gear II may be misdiagnosed. The diagnostic accuracy is 79%. The results show that the proposed method is able to correctly diagnose most of the damaged gear. However, there is a possibility of misdiagnosis in identifying the degree of damage. The failure feature parameters should be further optimized to improve the diagnostic accuracy.

Table 6.2 Diagnostic results of gear conditions in damage contrast test

Test dataset		SVM classifiers		Diagnostic result
		SVM1	SVM2	
Normal gear		1		normal gear
		1		normal gear
		1		normal gear
		1		normal gear
		1		normal gear
		1		normal gear
		-1	2	spot damaged gear*
		1		normal gear
Spot damaged gear	Spot damage gear I	-1	2	spot damaged gear
		-1	2	spot damaged gear
		1		normal gear*
		-1	2	spot damaged gear
		-1	2	spot damaged gear
		-1	2	spot damaged gear
		-1	2	spot damaged gear
		-1	2	spot damaged gear
	Spot damage gear II	-1	2	spot damaged gear
		-1	2	spot damaged gear
		-1	2	spot damaged gear
		-1	2	spot damaged gear
		-1	2	spot damaged gear
		-1	2	spot damaged gear
		-1	2	spot damaged gear
		-1	2	spot damaged gear
	Spot damage gear III	-1	2	spot damaged gear
		-1	2	spot damaged gear
		-1	2	spot damaged gear
		-1	3	pitted gear*
		-1	2	spot damaged gear
		-1	2	spot damaged gear
		-1	2	spot damaged gear
		-1	2	spot damaged gear
Pitted gear		-1	3	pitted gear
		-1	3	pitted gear
		-1	3	pitted gear
		-1	3	pitted gear
		-1	3	pitted gear
		-1	3	pitted gear
		-1	3	pitted gear
		-1	3	pitted gear
Total diagnostic accuracy		92.5%		

*denotes misdiagnosed sample

Table 6.3 Results of diagnosing the degree of damage

Test dataset	SVM classifiers		Diagnostic result
	SVM1	SVM2	
Spot damage gear I	1		spot damage gear I
	1		spot damage gear I
	1		spot damage gear I
	1		spot damage gear I
	-1	2	spot damage gear II*
	-1	2	spot damage gear II*
	1		spot damage gear I
	1		spot damage gear I
Spot damage gear II	-1	2	spot damage gear II
	1		spot damage gear I*
	-1	2	spot damage gear II
	-1	2	spot damage gear II
	-1	3	spot damage gear III*
	-1	3	spot damage gear III*
	-1	2	spot damage gear II
	-1	2	spot damage gear II
Spot damage gear III	-1	3	spot damage gear III
	-1	3	spot damage gear III
	-1	3	spot damage gear III
	-1	3	spot damage gear III
	-1	3	spot damage gear III
	-1	3	spot damage gear III
	-1	3	spot damage gear III
	-1	3	spot damage gear III
Total diagnostic accuracy	79%		

*denotes misdiagnosed sample

6.5.2 Diagnostic Results of Cyclic Fatigue Test

For cyclic fatigue test, the vibration accelerations on gear box measured in the test are utilized as testing dataset. To acquire the training data set, several times of experiments were performed on a normal gear, slight failure gear and severe failure gear respectively. All the experiments are carried out under the same conditions with cyclic fatigue test. Finally, 40 experimental results are obtained as training dataset. Then, SVMs classifiers of SVM1 and SVM2 are built based on the training data set. Test gear conditions are diagnosed by inputting principal components of test dataset to the training model.

Table 6.4 shows the diagnostic results of test gear conditions in cyclic fatigue test using support vector machines. The number -1, 1, 2 and 3 represent the diagnostic result of classifiers SVM1 and SVM2. If the output result is 1, it means the test gear condition is normal, and the diagnosis procedure completes. The number -1 means the gear condition is not normal, and the test data is inputted into SVM2. The output result 2 represents the gear condition is slight failure, while 3 shows the gear condition is severe failure.

Table 6.4 Diagnostic results of gear conditions in cyclic fatigue test

Cycles	Actual condition	Result		
		SVM1	SVM2	Diagnostic result
N=0	Normal	1		Normal
5×10^4	Normal	-1	2	Slight failure *
1×10^5	Normal	1		Normal
2×10^5	Normal	1		Normal
5×10^5	Normal	1		Normal
1×10^6	Normal	-1	2	Slight failure*
2×10^6	Slight failure	-1	2	Slight failure
3×10^6	Slight failure	-1	2	Slight failure
5×10^6	Severe failure	-1	2	Slight failure*
7×10^6	Severe failure	-1	3	Severe failure
1×10^7	Severe failure	-1	3	Severe failure
Accuracy	73%			

* represents misclassified data.

In Table 6.4, samples of $N=5\times10^4$, $N=1\times10^6$ and $N=5\times10^6$ are misclassified into slight failure. The vibration acceleration at $N=5\times10^4$ may be strongly affected by the operation conditions or environment disturbances during measurement. The vibration acceleration and its statistical parameters acquired at $N=5\times10^4$ are a little larger and close to those of slight failure condition, which can be seen from Fig. 6.12. It is possible to diagnose the condition of this sample into slight failure. The sample of normal condition at $N=1\times10^6$ is also misdiagnosed into slight failure. The damage began to generate on tooth surface between cycles 1×10^6 and 2×10^6. When the test gear working until 1×10^6 cycles, the condition of tooth surface begins to deteriorate and the tooth profile error becomes larger, which will intensify the vibration of gears. Therefore, the vibration acceleration and failure features acquired at $N=1\times10^6$ is a little larger, which would be misdiagnosed into slight failure. For the misdiagnosed sample of $N=5\times10^6$, the reason can be considered as follows. The number of failure teeth of test gear at $N=3\times10^6$, 5×10^6 and 7×10^6 are 9, 12 and 21 respectively. The number of failure teeth at $N=5\times10^6$ is much fewer than that of severe failure at $N=7\times10^6$. Although the condition of test gear at $N=5\times10^6$ is regarded as severe failure according to the average pitting area ratio, the pitting area of most damaged teeth is much smaller than that of severe failure teeth. The vibration accelerations and failure feature vectors acquired at $N=5\times10^6$ are more similar with those of slight failure. Thus, the sample at $N=5\times10^6$ is more likely to misdiagnosed as slight failure.

The diagnostic accuracy of test data is 73%. The proposed method can correctly classify almost all the samples of normal condition and damaged condition. However, the capability of the proposed method in diagnosing the degree of damage is still need to be strengthened.

6.6 Diagnosis of Gear Damage by Empirical Mode Decomposition

In section 6.4, a diagnostic method for gear damage using SVMs was proposed, in which amplitude ratios of frequency bands and statistical parameters were extracted as failure feature parameters. In this section, a diagnostic method based on techniques of empirical mode decomposition and SVMs is proposed to monitor and diagnose gear conditions. I try to employ the empirical mode decomposition method to extract the appropriate failure feature parameters from the vibration acceleration. Because the vibration data on gear box is always non-stationary, and empirical mode decomposition has been proved for effectively dealing with data from non-stationary and nonlinear processes because of its excellent generation capability. The experimental results of cyclic fatigue test are adopted to demonstrate the effectiveness of the proposed approach. The obtained vibration signal is decomposed into a number of intrinsic mode functions using empirical mode decomposition. Then characteristic energy ratios of intrinsic mode

functions and statistical parameters are together served as failure feature vectors for SVMs classifiers to identify gear conditions.

6.6.1 Empirical Mode Decomposition

Local faults in gears always produce transient modifications in vibration signals. Therefore, these signals have to be considered as non-stationary. Empirical mode decomposition (EMD) as a new data processing method was recently introduced by Huang et al. in 1990s [72], especially for analyzing data from nonlinear and non-stationary processes. The main purpose of EMD is to decompose any linear or nonlinear signal into a number of intrinsic mode functions (IMFs), each of which represents a simple oscillatory mode as a counterpart to the simple harmonic function and varies with the variation of the original signal. In contrast to other previous decomposition methods, the EMD approach is intuitive and adaptive, with a posteriori defined basis which is derived from the analytical data [73]. With the recent development on EMD method, the technique has already been employed successfully in wide applications : earthquake, climate variability, analysis of daily surface air temperature data, nonlinear ocean waves, detection of structural damage, health-monitoring and so on [74]. Recently, literatures of its applications on the failure detection of gear, bearing and rotary machine have been reported [75, 77, 81, 82]. Because the vibration signals on gear box is always non-stationary, I try to adopt the EMD method to extract the most suitable feature vectors from the measured signal for fault detection.

The algorithm of EMD is based on a simple assumption that any data consists of different simple intrinsic modes of oscillations which have the same number of extremas and zero-crossings. With the initial processing of EMD, any signal can be decomposed into a finite set of IMFs with frequency bands ranging from high to low, each of which must satisfy the following definitions [74]:

(i) in the whole dataset, the number of extremas and the number of zero-crossings must either equal each other or differ at most by one, and

(ii) at any point, the mean value of the envelopes defined by the local maxima and local minima is zero.

An IMF represents a simple oscillatory mode as a counterpart to the simple harmonic function, however, it is much more general as the IMF can have a variable amplitude and frequency as functions of time. With the definition of IMF, a sifting process is employed for identifying IMFs in time-series signal [98]. Supposing a time-series signal is $S(t)$, it can be decomposed into its

constituent IMFs by the following steps:

(i) Identify all the local extremas, then produce the upper and lower envelops by connecting the local maxima and minima with a spline curve respectively. Their mean value is computed as follows:

$$m_1 = (S(t)_{\max} + S(t)_{\min})/2. \tag{6.15}$$

(ii) The first component h_1 is obtained as the following equation:

$$h_1 = S(t) - m_1 \tag{6.16}$$

(iii) If h_1 is an IMF, the procedure moves to step (iv). Otherwise, if h_1 does not fulfill the criteria defining an IMF, it is treated as data $S(t)$ and the step (i)-(ii) are repeated up to k times until h_{1k} can be considered as an IMF, that is:

$$h_{1k} = h_{1(k-1)} - m_{1(k-1)} \tag{6.17}$$

(iv) The first IMF c_1 and the residual data r_1 are designated as:

$$c_1 = h_{1k} \tag{6.18}$$

$$r_1 = S(t) - c_1 \tag{6.19}$$

(v) The residue r_1 is treated as the new data and iterated as the same sifting process (i)-(iv).

The sifting process is completed until the resulting signal is monotonous or lower than the pre-specified value [99]. Thus the analytical signal consists with n-empirical modes and a residue r_n is achieved as:

$$S(t) = \sum_{i=1}^{n} c_i + r_n \tag{6.20}$$

Note that the sifting process is adaptively and based solely on the analytical data, which is able to find appropriate time-scales that may reveal intrinsic characteristics of the original signal. Furthermore, the IMFs include different frequency bands ranging from high to low and vary with the change of the original signal.

6.6.2 Analysis of Vibration Accelerations Using Empirical Mode Decomposition

The vibration accelerations on gearbox acquired from the cyclic fatigue test are adopted to be analyzed by the method of EMD. With the initial processing of EMD, the vibration signal is decomposed into 6 IMFs with frequency bands ranging from high to low. An IMF represents a simple oscillatory mode as a counterpart to the simple harmonic function, but it is much more general as the IMF can have a variable amplitude and frequency as functions of time. The original signal can be constituted of several IMFs, each of which contains different frequency component of the original signal from high to low. Therefore, an IMF is also a modulation signal of the original signal and varies with the change of original signal. The characteristics of local fault on tooth surface can be extracted from the IMFs.

Figure 6.13 shows the decomposed IMFs of original signal for different gear conditions in cyclic fatigue test. Figure 6.13 (a) shows the decomposed IMFs of vibration accelerations at cycles N=0, which is for normal gear condition. Figure 6.13 (b) illustrates the decomposed IMFs of vibration accelerations at cycles $N = 2\times10^6$ for slight failure gear condition. Figure 6.13 (c) presents the decomposed IMFs of vibration accelerations at cycles $N = 1\times10^7$ for severe failure gear condition. Each of the IMFs corresponds to one wheel rotation of the signal. In Fig. 6.13, figures from top to bottom are arranged in order of frequency from high to low. IMFs 1-3 contain the high frequency bands components of the raw signal, while IMFs 4-6 mainly contain signals of low frequency bands. Moreover, amplitudes of IMFs become weaker and more stable from IMF1 to IMF6. This is because the high-order harmonics and interference signals mainly concentrate in high frequency bands and attenuate rapidly with the decrease of frequency. The interference signals are usually caused by the vibration of other components on the testing machine, the environmental disturbances or the error of measurement system. The signals in low frequency bands are usually periodic and stable, such as signals with meshing frequency in IMF5. In IMF1, the amplitudes are relatively flat throughout the whole rotation under normal condition. The fluctuation of the waveform can be observed under slight failure condition and the fluctuation becomes stronger under severe failure condition. Additionally, comparing with the raw signal, IMF1 of severe failure magnifies the variation of the signal, which can more clearly manifests the characteristic of pitting fault. The IMF2 of severe failure is stronger than that of normal and slight failure, while IMF3 of normal is a little larger than that of other conditions. In IMFs4-6, the signal periodicity of normal and slight failure is more stable and clearer than that of severe failure. However, the magnitude of vibration acceleration is nearly the same among three conditions. Generally, the whole IMFs are relatively stable in normal case, in addition, their fluctuation becomes stronger with the increase of pitting area. Consequently, IMFs can be employed to represent intrinsic features of the vibration signal.

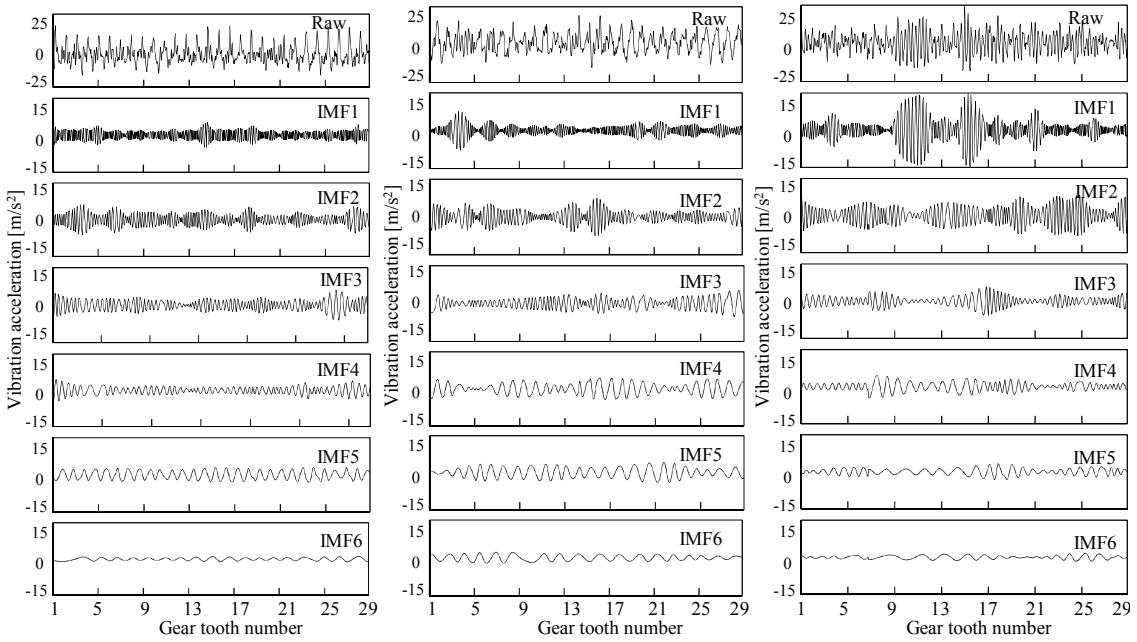

(a) Normal (N=0) (b) Slight failure ($N = 2\times10^6$) (c) Severe failure ($N = 1\times10^7$)

Fig.6.13 Intrinsic mode functions of vibration acceleration in cyclic fatigue test

6.6.3 Extracting Failure Feature Vectors

From the analysis of section 6.5.2, the method of EMD can decompose the original signal into a number of IMFs, each of which corresponds to various frequency bands from high to low and represents the local characteristics of the original signal. Since the IMFs are adaptively derived from the measured data, the amplitude of each IMF also changes along with the variation of gear conditions. Thus, the energy of IMFs from first to n-th can be served as representative parameters to demonstrate characteristics of various gear conditions. The energy of IMFs is computed as:

$$E_i = \sum_{j=1}^{M} \left| Ac_i(j) \right|^2 \tag{6.21}$$

Where, E_i is the energy of i-th IMF, M is the discrete data length of i-th IMF and $Ac_i(j)$ is the sample amplitude of i-th IMF. In order to eliminate the impact of dimension and make convenience for the following data processing, the energy of IMFs are normalized by using the total energy $E = \sum_{i=1}^{n} E_i$. Thus, the characteristic energy ratios of IMFs E_R are computed as representative parameters of gear conditions as follows:

$$E_R = (e_{r1}, e_{r2}, \ldots, e_{ri}) = (E_1/E\,, E_2/E, \cdots, E_i/E) \tag{6.22}$$

Energy of each IMF is computed to constitute the characteristic energy ratios by Eq. 6.22. Figure 6.14 shows the characteristic energy ratios of IMFs for normal, slight failure and severe failure gear conditions respectively. A_p is the damaged area ratio of the test gear. The condition of test driving gear at N=0 is normal, at N=2×10^6 is slight failure, and is severe failure at N=1×10^7. In this figure, the energy ratios of IMFs for normal, slight failure and severe failure are different from each other. In addition, the energy ratio of the first IMF becomes larger in order of normal, slight failure and severe failure. This is because most part of the first IMF is comprised of high frequency bands of vibration accelerations. The vibration acceleration and its high order harmonics become stronger with the increase of damaged area.

As shown in section 6.2.1, statistical parameters of standard deviation (σ), kurtosis(β_1), skewness (β_2) and root mean square value (γ) are calculated from the processed signal of the vibration acceleration. The obtained statistical parameters characteristic energy ratios of IMFs are combined as failure feature vector $\mathbf{V} = (\sigma, \beta_1, \beta_2, \gamma, e_{r1}, \ldots, e_{r6})$ for the diagnosis of gear conditions. Since the high-dimensionality of feature vector complicates the calculation and extends the processing time, the method of principal component analysis is adopted to transform the original feature vector into a new smaller-dimensions vector **P** consisted of several principal components. The first 7 principal components contribute 95% effect in vector **P**. Thus, components ($p_1, \ldots, p_7$) are selected as reduced input vector for SVM.

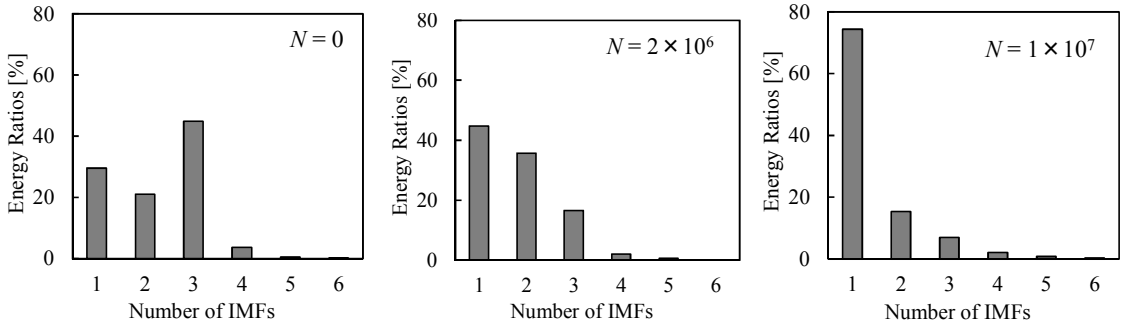

(a) Normal (A_p= 0) (b) Slight failure (A_p= 0.54%) (c) Severe failure (A_p= 3.65%)

Fig. 6.14 Characteristic energy ratios of IMFs for various gear conditions

6.6.4 Diagnostic Results

The test data and training data are as same as that in section 6.4. The vibration accelerations on gear box measured in cyclic fatigue test are utilized as test dataset. 36 experimental results are obtained as training dataset by performing tests on a normal gear, slight failure gear and severe failure gear with the same condition as cyclic fatigue test. Then, SVMs classifiers of SVM1 and SVM2 are built with the training data set. Test gear conditions are diagnosed by inputting principal components of test dataset to the training model.

Figure 6.15 presents the distribution of test data based on the first three principal components acquired with EMD method. PCA1, 2, 3 represent the first three principal components p_1, p_2 and p_3 respectively. The painted markers are misdiagnosed samples. In this figure, the distribution of normal samples and slight failure samples is a little closer, which indicates the differences of failure feature vectors between the normal condition and slight failure condition are not obvious. Samples of severe failure are distinguished clearly from the samples of normal and slight failure. However, samples at N= 5×10^4 and 5×10^6 nearly distribute in the range of slight failure, which are probably misdiagnosed into slight failure. Comparing with the data distribution without EMD method shown in Fig. 6.12, the data distribution with EMD method is a little more concrete and clearly separated with each other.

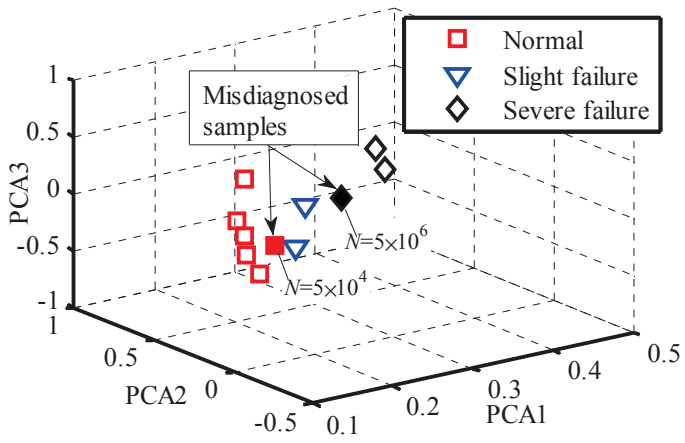

Fig. 6.15 The distribution of test data based on the first 3 principal components

Table 6.5 shows the diagnostic results of test gear conditions with EMD method. In the results, samples for N =5×10^4 and N =5×10^6 are misclassified into slight failure. The reason is that the vibration acceleration at N =5×10^4 may be strongly affected by the operation conditions or environment disturbances during measurement. Therefore, the vibration acceleration and its statistical parameters acquired at N =5×10^4 are a little larger and close to those of slight failure condition, which is possible to be misdiagnosed. The sample for N =5×10^6 is misdiagnosed into slight failure. This is because the vibration accelerations and failure feature vectors acquired at N =5×10^6 are more similar with those of slight failure. The number of failure teeth of test gear at N =3×10^6, 5×10^6 and 7×10^6 are 9, 12 and 21 respectively. The number of failure teeth at N =5×10^6 is much fewer than that of severe failure at N =7×10^6. Although the condition of test gear at N =5×10^6 is regarded as severe failure according to the average pitting area ratio, the pitting area of most damaged teeth is much smaller than that of severe failure teeth. Thus, the sample at N =5×10^6 is more likely to misdiagnosed as slight failure. The diagnostic accuracy is 82%. The diagnostic results show that the proposed method can detect gear damage with satisfactory accuracy. In addition, the diagnostic accuracy acquired with the EMD method is better than that acquired with the previous method, which indicates that the EMD method is effective for gear damage diagnosis and classification, even can improve the accuracy of diagnosis.

Table 6.5 Diagnostic results of gear conditions

Cycles	Actual condition	Result		
		SVM1	SVM2	Diagnostic result
N=0	Normal	1		Normal
5×10^4	Normal	-1	2	Slight failure *
1×10^5	Normal	1		Normal
2×10^5	Normal	1		Normal
5×10^5	Normal	1		Normal
1×10^6	Normal	1		Normal
2×10^6	Slight failure	-1	2	Slight failure
3×10^6	Slight failure	-1	2	Slight failure
5×10^6	Severe failure	-1	2	Slight failure*
7×10^6	Severe failure	-1	3	Severe failure
1×10^7	Severe failure	-1	3	Severe failure
Accuracy	82%			

* represents misclassified data.

6.7 Summary

In this chapter, a diagnostic method of gear damage using support vector machines with extracting failure feature vector from the vibration signal is proposed. The characteristic amplitude ratios of frequency bands and statistical parameters are extracted from the signals as failure feature vector. Then, support vector machines is adopted to diagnose gear conditions based on the extracted feature vector. Moreover, the method of empirical mode decomposition is also employed to extract failure feature parameters to represent gear conditions. The algorithm of support vector machines, principal component analysis and empirical mode decomposition are also introduced. The following conclusions can be concluded from the performed work.

1. Statistical parameters of standard deviation, root mean square value, kurtosis and skewness are extracted from the processed signal. The value of statistical parameters becomes larger along with the increase of the gear rotation speed and damaged area. Especially, the value of statistical parameters of normal gear is the smallest and changes slightly with the variation of gear rotation speeds. While, the parameters' value of spot damaged gear and pitted gear varies obviously with the variation of gear speeds. The difference of parameters value between different kinds of gears is little when the damaged area is small.

2. The amplitude ratios of frequency bands approximately represent the characteristics of frequency spectrum and change with the variation of gear conditions. The amplitude ratio of the first frequency band becomes smaller with the increase of damaged area, while the amplitude ratios of 3rd and 4th frequency bands become larger. The statistical parameters and characteristic amplitude ratios of frequency bands can be adopted to demonstrate features of gear conditions.

3. The method of principal component analysis can transform the extracted failure feature vector into a fewer-dimensional inputting vector for classifiers of support vector machines. The distribution of samples in feature space can be generally illustrated based on the first three principal components. The data distribution of normal gear and failure gear with small damage area is a little closer. The samples of severe failure gear or pitted gear are clearly separate with the other samples.

4. By using the method of support vector machines, most of the samples in damage contrast test are correctly classified into three types, called normal gear, spot damaged gear and pitted gear. The diagnostic accuracy is 92.5%. The diagnostic accuracy of test data in cyclic test is 73%. The proposed method can correctly classify almost all the samples of normal condition and damaged condition. However, the capability of the proposed method in diagnosing the degree of damage is still need to be strengthened.

5. By the technique of empirical mode decomposition, the original signal can be decomposed

into a number of intrinsic mode functions, each of which represents the local characteristics of the original signal and changes along with the variation of gear conditions. Therefore, the characteristic energy ratios can be extracted from the intrinsic mode functions as failure features to be input to the support vector machine classifiers. The diagnostic accuracy of test data in cyclic fatigue test is 82%. It is confirmed that the empirical mode decomposition method is effective for gear damage diagnosis and classification, even can improve the accuracy of diagnosis.

7 Conclusions

This study proposes an intelligent method for diagnosing gear tooth surface damage by analyzing the vibration accelerations of gear box and bearing box. To investigate the validity of the proposed method, damage contrast test has been carried out in this study. Three kinds of gears namely normal gear, spot damaged gear and pitted gear are tested under different loads and gear rotation speeds on the power circulating type gear testing machine. The vibration accelerations of gear box and bearing box are measured in the experiment. Moreover, in order to illustrate the progression of gear failures and to demonstrate the effectiveness of the proposed approach, the cyclic fatigue test also has been implemented on the power circulating type gear testing machine. A test gear is driven continually with the same rotation speed and load torque. During the cyclic fatigue test, the vibration accelerations on gear box and bearing box are measured at different cycles. The acquired vibration accelerations are analyzed by techniques of Fast Fourier Transform and discrete wavelet transform. In order to quantitatively illustrate the characters of vibration accelerations, statistical parameters and characteristic amplitude ratios of frequency bands are extracted from the vibration accelerations. Both of the characteristic amplitude ratios and statistical parameters are together served as failure feature vector for representing different gear conditions. Finally, the technique of support vector machine is employed to diagnose gear condition based on the extracted failure feature vector. The diagnostic results demonstrate the effectiveness of the proposed method. Although a diagnostic method for gear damage based on support vector machines has been proposed, I try to adopt another technique of empirical mode decomposition to extract failure feature vector for gear damage diagnosis. By the technique of empirical mode decomposition, the original signal is decomposed into several intrinsic mode functions. Then, the characteristic energy ratios of intrinsic mode functions and statistical parameters are extracted as failure feature vectors to be input to the support vector machines classifiers for diagnosis. The validity of the proposed approach is demonstrated by experimental results.

In Chap. 4 **[Damage Contrast Test]**, the damage contrast test is performed. The vibration accelerations on gear box and bearing box and the sound level signal are presented and discussed. The original vibration accelerations are analyzed using Fast Fourier Transform and discrete wavelet transform. The frequency spectrum, residual signal and processed signal are obtained from the vibration accelerations. The following conclusions can be drawn from the previous work.

1. The large damage on tooth surface will cause transient larger amplitude in the original vibration signals, based on which the abnormal gear condition can be diagnosed. However, the

abnormal amplitude is invisible when the damaged area is small. Therefore, the slight gear damage would not be detected based on the original waveform. The vibration accelerations acquired under T=70N-m is a little stronger than that acquired under T=40N-m. In addition, along with the increase of rotation speeds, the vibration accelerations become larger and the indication of damage also becomes more and more obvious in the original signal. The influence of varying loads on the vibration accelerations is weaker than the influence of varying gear rotation speed on the vibration accelerations.

2. In the frequency spectrum of various gear conditions, the amplitudes of high-order harmonics and the natural frequency become larger with the increase of damaged area. Moreover, the sidebands also become stronger and broader. The frequency spectrum can represent particular characteristics of different gear conditions. Representative failure features can be extracted from the spectrum.

3. Comparing with the original signal, the method of residual signal can emphasize the abnormal amplitude generated by the gear damage. The evidence of fault impulse is a little more obvious in residual signals on gear box. Although the residual signal can strengthen the failure features of gear damage to some extent, it is still hard to diagnose the early gear faults only based on the residual signal.

4. The noise can be effectively reduced from the residual signal by employing the method of discrete wavelet transform. The processed signal is acquired by reconstructing the coefficients of discrete wavelet transform. In the processed signals of spot damaged gear and pitted gear, the difference of amplitude value is enlarged. Therefore, the fault indications are more clearly visualized in processed signals. It is confirmed that the method of discrete wavelet transform can contribute to emphasize the characteristics of gear damage.

In Chap. 5 **[Cyclic Fatigue Test]**, the cyclic fatigue test is introduced. The original vibration accelerations on gear box and bearing box are presented and discussed. The frequency spectrum of the original vibration signal is also analyzed. Then, the residual signal and processed signal are acquired using techniques of Fast Fourier Transform and discrete wavelet transform. Conclusions can be summarized as follows:

1. The vibration accelerations gradually become larger and fluctuate more and more strongly as the increase of pitting area. Additionally, comparing with the normal teeth which have no failure on tooth surface, the vibration accelerations of the failure teeth are a little larger and manifest an increasing tendency with the growth of pitting area. The gear condition of severe failure can be diagnosed according to the original signal. However, it is difficult to diagnose the gear condition of

slight failure only based on the waveform.

2. In the frequency spectrum for normal, slight failure and severe failure condition, the amplitude of meshing frequency becomes smaller and the amplitudes of the harmonics become stronger with the increase of pitting area. Similarly, the amplitude of sidebands becomes stronger and the band width also becomes broader with the deterioration of gear condition.

3. For normal condition, the amplitude value and waveform of residual signal is more stable than that of the original signal. For slight failure condition, there is no evident indication of gear damage in the residual signal. For severe failure condition, the evidence of fault impulse for severe failure is more obvious in residual signals. However, it is still hard to diagnose the early gear faults only through the residual signal.

4. The waveform of processed signal is much smoother than that of the residual signal, which indicates the noise is reduced from the residual signal. Comparing with the residual signal, the difference of amplitude value of each tooth becomes larger in the processed signal. The fault features are more clearly visualized in processed signals.

In Chap. 6 **[Diagnosis of Gear Damage Using Support Vector Machines]**, a diagnostic method of gear damage using support vector machines with extracting failure feature vector from the vibration signal is proposed. The characteristic amplitude ratios of frequency bands and statistical parameters are extracted from the signals as failure feature vector. Then, support vector machines is adopted to diagnose gear conditions based on the extracted feature vector. Moreover, the method of empirical mode decomposition is also employed to extract failure feature parameters to represent gear conditions. The algorithm of support vector machines, principal component analysis and empirical mode decomposition is also introduced. The following conclusions can be concluded from the performed work.

1. Statistical parameters of standard deviation, root mean square value, kurtosis and skewness are extracted from the processed signal. The value of statistical parameters becomes larger along with the increase of the gear rotation speed and damaged area. Especially, the value of statistical parameters of normal gear is the smallest and changes slightly with the variation of gear rotation speeds. While, the parameters' value of spot damaged gear and pitted gear varies obviously with the variation of gear speeds. The difference of parameters value between different kinds of gears is little when the damaged area is small.

2. The amplitude ratios of frequency bands approximately represent the characteristics of frequency spectrum and change with the variation of gear conditions. The amplitude ratio of the first frequency band becomes smaller with the increase of damaged area, while the amplitude ratios

of the 3rd and 4th frequency bands become larger. The statistical parameters and characteristic amplitude ratios of frequency bands can be adopted to demonstrate features of gear conditions.

3. The method of principal component analysis can transform the extracted failure feature vector into a fewer-dimensional inputting vector for classifiers of support vector machines. The distribution of samples in feature space can be generally illustrated based on the first three principal components. The data distribution of normal gear and slight failure gear with small damaged area is a little closer. The samples of severe failure gear or pitted gear are clearly separate with the other samples.

4. By using the method of support vector machines, most of the samples in damage contrast test are correctly classified into three types, called normal gear, spot damaged gear and pitted gear. The diagnostic accuracy of damage contrast test is 92.5%. The diagnostic accuracy of test data in cyclic test is 73%. The proposed method can correctly classify almost all the samples of normal condition and damaged condition. However, the capability of the proposed method in diagnosing the degree of damage is still need to be improved.

5. By the technique of empirical mode decomposition, the original signal can be decomposed into a number of intrinsic mode functions, each of which represents the local characteristics of the original signal and changes along with the variation of gear conditions. Therefore, the characteristic energy ratios can be extracted from the intrinsic mode functions as failure features to be input to the support vector machine classifiers. The diagnostic accuracy of test data in cyclic fatigue test is 82%. It is confirmed that the empirical mode decomposition method is effective for gear damage diagnosis and classification, even can improve the accuracy of diagnosis.

References

[1] Ishigawa, J., Machine Element (Revised Edition), Vol. 2, (1990), pp.129, Corona Publishing CO., LTD, (in Japanese).

[2] Yamazaki, K., Abnormal detection and prediction-diagnostic technology for sensor and equipment, (1998), pp. 239-265, Industrial investigation committee.

[3] Feng, F., Toyota, T. and Chen, P., Dynamics and diagnosis method on gear drive: 1st report, vibration equation and solution for faulty gear drive, Joint Symposium of JSME and ASJ Conference, 2001, pp. 195-198 (in Japanese).

[4] Loutridis, S., A local energy density methodology for monitoring the evolution of gear faults, NDT&E International, Vol.37, No.6, (2004), pp.447-453.

[5] Dalpiaz, G., Rivola, A. and Rubini, R., Gear fault monitoring: Comparison of vibration analysis techniques, Proceedings of the 3rd international conference on acoustic and vibration survey method and diagnosis technology (1998), pp.623-637.

[6] Toutountzakis T., Tan C.K., Mba D., Application of acoustic emission to seeded gear fault detection, NDT&E International, Vol. 38, (2005), pp. 27-36.

[7] Singh A, Houser D.R, Vijayakar S. Early detection of gear pitting Power transmission and gearing conference, ASME, DE, vol. 88, (1996), pp. 673-678.

[8] Singh A, Houser DR, Vijayakar S. Detecting gear tooth breakage using acoustic emission: a feasibility and sensor placement study, Journal of Mechanical Design, Vol. 121, (1999), pp.587-593.

[9] Al-Balushi, K. R., and Samanta, B., Gear fault diagnosis using energy-based features of acoustic emission signals, Proceedings of the Institution of Mechanical Engineers, Part I: Journal of Systems and Control Engineering, Vol. 216, No. 3, (2002), pp. 249-263.

[10] Board, D. B., Gear diagnosis by stress wave analysis, Proceedings of ASME 9th International Power Transmission and Gearing Conference, (2003), pp. 635-644.

[11] Tanaka, E., Nagamura, K., Ikejo, K., and Nemoto, R., In situ diagnosis of a gear-tooth surface damage using laser scattering, Journal of Advanced Mechanical Design, Systems, and Manufacturing, Vol.5, No.3.(2011), pp.199-213.

[12] Mafadden P. D., Examination of a technique for the early detection of failure in gears by signal processing of the time domain average of the meshing vibration, Mechanical Systems and Signal Processing, Vol.1, No. 2, (1987), pp. 173-183.

[13] Mafadden P. D., Detecting fatigue cracks in gear by amplitude and phase demodulation of the meshing vibration, ASME Journal of Vibration and Acoustics, Vol. 108, No.2, (1986), pp. 165-170.

[14] Dalpiaz G., Early detection of fatigue cracks in gears by vibration analysis techniques, Osterreichische Ingenieur- und Architekten-Zeitschrift (OG IAZ), Vol.135, (1990), pp. 312-317.

[15] Mafadden P. D., Determining the location of fatigue crack in a gear from the phase of the change in the meshing vibration, Mechanical Systems and Signal Processing, Vol. 2, No.4，(1988), pp. 403-409.

[16] Randall R.B., A new method of modeling gear faults, Journal of Mechanical Design, Vol. 104, No. 2, (1982), pp.259-267.

[17] Randall R.B., Gearbox fault diagnosis using cepstrum analysis, Proceedings of Fourth World Congress on T. of M. and M., Newcastle u. Tyne, Vol.1, (1975), pp. 169-171.

[18] Dalpiaz, G., Rivola, A. and Rubini, R., Effectiveness and sensitivity of processing techniques for fault detection in gears, Mechanical Systems and Signal Preprocessing, Vol. 14, No. 3, (2000), pp. 387-412.

[19] Capdessusa C., Sidahmedb M. and Lacoumec J.L., Cyclostationary processes: application in gear faults early diagnosis, Mechanical Systems and Signal Processing, Vol. 14, No. 3, (2000), pp. 371-385.

[20] Antonia J., Bonnardotb F., Raada A. and El Badaouib M., Cyclostationary modelling of rotating machine vibration signals, Mechanical Systems and Signal Processing, Vol. 18, No. 6, (2004), pp. 1285-1314.

[21] Lin J., Zuo M.J., Extraction of Periodic Components for Gearbox Diagnosis Combining Wavelet Filtering and Cyclostationary Analysis, Journal of Vibration and Acoustics, Vol. 126, No. 3, (2004), pp. 449-451.

[22] Drouiche K., Sidahmed M. and Srenier Y., Fault detection in gears using advanced signal processing techniques, Proceedings of the 3rd International Machinery Monitoring & Diagnostics Conference, (1991), pp. 65-71.

[23] Wang, W. J., Applications of wavelets to gearbox vibration signals for fault detection, Journal of Sound and Vibration, Vol. 192, No. 5, (1996), pp. 927-939.

[24] Grossmann A. and Morlet J., Decomposition of Hardy functions into square integrable wavelets of constant shape, SIAM Journal of Mathematical Analysis, Vol.15, No.4, (1984), pp. 723-736.

[25] Combes, J. M., Grossmann, A., & Tchamitchian, P., Wavelets, time-frequency methods and phase space. Proceedings of International Conference, Marsellie, France, December 1987, Eds. (1989), Berlin: Springer-Verlag, pp. 315.

[26] Mallat, S. G., Transactions on Pattern Analysis on Machine Intelligent, IEEE, 11-17, (1989), pp. 674-693.

[27] Meyer, Y., Wavelets and applications, Proceedings of the Marsellie Workshop on Wavelets, Research Notes in Applied Mechanics, France, May 1989, (Ed.) (1992), Berlin: Springer-Verlag.

[28] Daubechies, I., Ortho-normal bases of compactly supported wavelets, Communications on Pure and Applied Mathematics, Vol. 41, (1988), pp. 909-996.

[29] Wang, W. J. and McFadden, P. D., Application of the Wavelet transform to gearbox vibration analysis, American Society of Mechanical Engineers Petroleum Division, (1993), pp. 13-20.

[30] Peng, Z.K. and Chu, F.L., Application of the wavelet transform in machine condition monitoring and fault diagnostics: a review with bibliography, Mechanical Systems and Signal Processing, Vol.18, No.2, (2004), pp.199-221.

[31] Staszewski W. J. and Tomlinson G. R., Application of the Wavelet transform to fault detection in a spur gear, Mechanical Systems and Signal Processing, Vol. 8, (1994), pp.289-307.

[32] Mcfadden P. D., Application of the wavelet transform to early detection of gear failure by vibration analysis, Proceedings of an International Conference on Condition Monitoring, (1994), pp.172-183.

[33] Wu J. D., Hsu C. C., Fault gear identification using vibration signal with discrete wavelet transform technique and fuzzy-logic inference, Expert Systems with Applications, Vol. 36 (2009), pp. 3785-3794.

[34] Saravanan N. and Ramachandran K.I., Incipient gear box fault diagnosis using discrete wavelet transform (DWT) for feature extraction and classification using artificial neural network (ANN), Expert Systems with Applications, Vol. 37, (2010), pp. 4168-4181.

[35] Zheng H., Li Z. and Chen X., Gear fault diagnosis based on continuous wavelet transform, Mechanical Systems and Signal Processing, Vol. 16(2-3), (2002), pp. 447-457.

[36] Nikolaou N. G., Antoniadis I. A., Rolling element bearing fault diagnosis using wavelet packet, NDT&E International, Vol. 35, (2002), pp. 197-205.

[37] Yen G.G., Lin K. C., Wavelet packet feature extraction for vibration monitoring, IEEE Transactions on Industrial Electronics, Vol.47, (2000), pp. 650-667.

[38] Feldman M., Non-linear free vibration identification via the Hilbert transform, Journal of Sound and Vibration, Vol. 208 (3), (1997), pp. 475-489.

[39] Fan, X.F., and Zuo, M.J., Gearbox fault detection using Hilbert and wavelet packet transform, Mechanical Systems and Signal Processing, Vol.20, No.4, (2006), pp.966-982.

[40] Pachaud, C., Salvetat, R. and Fray, C., Crest factor and kurtosis contributions to identify defects inducing periodical impulsive forces, Mechanical Systems and Signal Process, Vol.11, No.6, (1997), pp.903-916.

[41] Wang, X.Y., Viliam, M. and Yang, M., A wavelet approach to fault diagnosis of a gearbox under varying load conditions, Journal of Sound and Vibration, Vol.329, No.9, (2010), pp.1570-1585.

[42] Chui C.H.K., Wavelets Analysis and its Applications, vol. 1: An Introduction to Wavelets, 1992, Academic Press, Boston.

[43] Paya B. A., Esat I. I., Artificial neural network based fault diagnostics of rotating machinery using wavelet transform as a preprocessor, Mechanical Systems and Signal Processing, Vol. 11, No. 5, (1997), pp. 751-765.

[44]Saravanan, N., Kumar Siddabattuni, V.N.S. and Ramachandran, K.I., Fault diagnosis of spur bevel gear box using artificial neural network (ANN) and proximal support vector machine (PSVM), Applied Soft Computing, Vol.10, No.1, (2010), pp. 344-360.

[45] Staszewski W. J., Gearbox vibration diagnostics-an overview, The 7th International Congress on Condition Monitoring and Diagnostic Engineering Management, 1996.

[46] Staszewski W. J., Worden K. and Tomlinson G. R., Time-frequency analysis in gearbox fault detection using the wigner-ville distribution and pattern recognition, Mechanical Systems and Signal Processing, Vol. 11, No. 5, (1997), pp. 673-692.

[47] Vapnik, V.N., Statistical Learning Theory, (1998), pp.401-440, John Wiley & Sons Inc.

[48] Samanta, B., Gear fault detection using artificial neural networks and support vector machines with genetic algorithms, Mechanical Systems and Signal Processing, Vol.18, No.3, (2004), pp.625-644.

[49] Saravanan, N. and Ramachandran, K.I., A case study on classification of features by fast single-shot multiclass PSVM using Morlet wavelet for fault diagnosis of spur bevel gear box, Expert Systems with Applications, Vol.36, No.8, (2009), pp.10854-10862.

[50] Wang W. J. and McFadden P. D., Application of wavelets to gearbox vibration signals for fault detection, Journal of Sound and Vibration, Vol. 192, (1996), pp. 927-939.

[51] Wang W. J. and McFadden P. D., Application of orthogonal wavelets to early gear damage detection, Mechanical System and Signal Processing, Vol. 9(1995), pp. 497-507.

[52] Butler-Purry, K. L., Bagriyanik, M., Characterization of transients in transformers using discrete wavelet transforms. IEEE Transactions on Power System, Vol. 18, (2003), pp. 648-656.

[53] Donoho D.L., Denoising by soft-thresholding, IEEE Trans. Information Theory, Vol. 41, No. 3, (1995), pp.613-627.

[54] Lin, J. and Qu, L.S., Feature extraction based on Morlet Wavelet and its application for mechanical fault diagnosis, Journal of Sound and vibration, Vol. 234, No.1, (2000), pp.135-148.

[55] Pasti L., Walczak B., Massart D.L. and Reschiglian P., Optimization of signal denoising in discrete wavelet transform, Chemometrics and Intelligent Laboratory Systems, Vol. 48, (1999), pp.21-34.

[56] Littler T.B., Morrow D.J., Signal enhancement and de-noising of power system disturbances using the wavelet method, Proceedings of the Universities Power Engineering Conference, Vol.2, (1996), pp.590-593.

[57] Menon S., Schoess J.N., Hamza R. and Busch D., Wavelet-based acoustic emission detection method with adaptive thresholding, Proceedings of SPIE, 3986 (2000), pp.71-77.

[58] Vapnik, V.N., The Nature of Statistical Learning Theory, (1995), pp.123-223, Springer -Verlag.

[59] Yang, Y., Yu, D.J. and Cheng, J.S., A fault diagnosis approach for roller bearing based on IMF envelope spectrum and SVM, Measurement, Vol.40, No.9-10, (2007), pp.943-950.

[60] Paya, B.A., Esat, I.L. and Madi, M.N.M., Artificial neural network based fault diagnostics of rotating machinery using wavelet transforms as a processor, Mechanical Systems and Signal Processing, Vol.11, No.5, (1997), pp.751–765.

[61] Chen, F.F., Tang, B.P. and Chen, R.X., A novel fault diagnosis model for gearbox based on wavelet support vector machine with immune genetic algorithm, Measurement, Vol.46, No.1, (2013), pp.220-232.

[62] Guo, G.D., Li, S.Z. and Chan, K.L., Support vector machines for face recognition, Image and Vision Computing, Vol.19, No.9-10, (2001), pp.631-638.

[63] Kim, H.C., Pang, S.N., Je, H.M., Kim, D. and Bang, S.Y., Constructing support vector machine ensemble, Pattern Recognition, Vol.36, No.12, (2003), pp.2757-2767.

[64] Bo, C.M., Qia, X., Zhang, G.M., Bai, Y.J. and Zhang, S., An integrated method of independent component analysis and support vector machines for industry distillation process monitoring, Journal of Process Control, Vol.20, No.10, (2010), pp.1133-1140.

[65] Tandon, N. and Nakra, B.C., A review of vibration and acoustic monitoring techniques for the detection of defects in rolling element bearings, Shock and Vibration Digest, Vol.24, No.3, (1992), pp.3-11.

[66] Thissen, U., Van Brakel, R., De Weijer, A.P., Melssena, W.J. and Buydens, L.M.C., Using support vector machines for time series prediction, Chemometrics and Intelligent Laboratory Systems, Vol.69, No.1, (2003), pp.35-49.

[67] Yuan, S.F. and Chu, F.L., Support vector machines-based fault diagnosis for turbo-pump rotor, Mechanical Systems and Signal Processing, Vol.20, No.4, (2006), pp.939-952.

[68] Samanta, B., Al-Balushi, K.R. and Al-Araimi, S.A., Artificial neural networks and support vector machines with genetic algorithm for bearing fault detection, Engineering Applications of Artificial Intelligence, Vol.16, No.7-8, (2003), pp.657-665.

[69] Sugumaran, V., Muralidharan, V. and Ramachandran, K.I., Feature selection using Decision Tree and classification through Proximal Support Vector Machine for fault diagnostics of roller bearing, Mechanical Systems and Signal Processing, Vol. 21, No.2, (2007), PP. 930-942.

[70] Xue, H.T., Wang, H.Q., Chen, P., Li, K. and Song, L.Y., Automatic diagnosis method for structural fault of rotating machinery based on distinctive frequency components and support vector machines under varied operating conditions, Neurocomputing, Vol.116, (2013), pp.326-335.

[71] Cao, L. J., Chua, K. S., Chong, W. K., Lee, H. P. and Gu, Q. M., A comparison of PCA, KPCA and ICA for dimensional reduction in support vector machine, Neurocomputing, Vol. 55, (2003), pp. 321-336.

[72] Huang, N.E., Shen, Z., Long, S.R., Wu, N.C., Shih, H.H., Zheng, Q., Yen, N.C., Tung, C.C., Liu, H.H., The empirical mode decomposition and the Hilbert spectrum for nonlinear and non-stationary time series analysis, Proceedings of the Royal Society of London A, 454 (1998), pp. 903-995.

[73] Huang, N.E. and Shen, S.S., Hilbert-Huang Transform and Its Applications, (2005), pp. 289-303, World Scientific Publishing Co. Pte. Ltd.

[74] Huang, N.E. and Attoh-Okine, N.O., The Hilbert-Huang Transform in Engineering, (2005), pp. 59-298, CRC Press.

[75] Loutridis, S.J., Damage detection in gear systems using empirical mode decomposition, Engineering Structures, Vol.26, No.12, (2004), pp. 1833-1841.

[76] Liu, B., Riemenschneider, S., Xu, Y., Gearbox fault diagnosis using empirical mode decomposition and Hilbert spectrum, Mechanical Systems and Signal Processing, Vol. 20, (2006), pp.718-734.

[77] Parey, A., Badaoui, M. El., Guillet, F., and Tandon, N., Dynamic modelling of spur gear pair and application of empirical mode decomposition-based statistical analysis for early detection of localized tooth defect, Journal of Sound and Vibration Vol.294, No.3 (2006), pp. 547-561.

[78] Parey, A., Tandon, N., Impact velocity modeling and signal processing of spur gear vibration for the estimation of defect size, Mechanical Systems and Signal Processing, Vol. 21, (2007), pp.234-243.

[79] Yu, D., Chen, J. and Yang, Y., Application of EMD method and Hilbert spectrum to the fault diagnosis of roller bearings, Mechanical Systems and Signal Processing, Vol.19, (2005), pp. 259-270.

[80] Yang, Y., Yu, D. and Chen, J., A roller bearing fault diagnosis method based on EMD energy entropy and ANN, Journal of Sound and Vibration, Vol. 294, (2006), pp. 269-277.

[81] Rai, V.K., and Mohanty, A.R., Bearing fault diagnosis using FFT of intrinsic mode functions in Hilbert – Huang transform, Mechanical Systems and Signal Processing, Vol. 21, No.6,

(2007), pp. 2607-2615.

[82] Gao, Q., Duan, C., Fan, H., and Meng, Q., Rotating machine fault diagnosis using empirical mode decomposition, Mechanical Systems and Signal Processing, Vol. 22, No.5, (2008), pp. 1072-1081.

[83] JGMA STANDARD, JGMA 7001-01 (1990).

[84] Djebala, A., Ouelaa, N., Benchaabane, C. and Laefer, D.F., Application of the Wavelet Multi-resolution Analysis and Hilbert transform for the prediction of gear tooth defects, Meccanica, Vol.47, No.7, (2012), pp.1601-1612.

[85] Boulahbal, D., Golnaraghi, M.F. and Ismail, F., Amplitude and phase wavelet maps for the detection of cracks in geared systems, Mechanical Systems and Signal Processing, Vol. 13, (1999), PP. 423-436.

[86] Omar, F.K. and Gaouda, A.M., Gear tooth diagnosis using wavelet multi-resolution analysis enhanced by Kaiser's windowing, Transactions of the Institute of Measurement and Control, Vol.33, No.5, (2011), pp.573-590.

[87] Zhan, Y.M., Makis, V. and Jardine, A.K.S., Adaptive state detection of gearboxes under varying load conditions based on parametric modeling, Mechanical Systems and Signal Processing, Vol.20, No.1, (2006), pp.188-221.

[88] Saravanan, N., Kumar Siddabattuni, V.N.S., and Ramachandran, K.I., A comparative study on classification of features by SVM and PSVM extracted using Morlet wavelet for fault diagnosis of spur bevel gear box, Expert Systems with Applications, Vol.35, No.3, (2008), pp.1351-1366.

[89] Widodo, A., Kim, E.Y. and Son, J.D., Fault diagnosis of low speed bearing based on relevance vector machine and support vector machine, Expert Systems with Applications, Vol.36, No.3, (2009), pp.7252-7261.

[90] Komura, H., Shimomura, K. and Shibata, K., Failure survey diagnosis of bearing using the equivalent RMS of vibration wave form, Transactions of the Japan Society of Mechanical Engineers. C 67(664), (2001), pp. 3696-3701. (in Japanese).

[91] Widodo, A., Yang, B.S. and Han, T., Combination of independent component analysis and support vector machines for intelligent faults diagnosis of induction motors, Expert Systems with Applications, Vol.32, No.2, (2007), pp.299 - 312.

[92] Yang, B. S., Han, T. and Yin, Z. J., Fault diagnosis system of induction motors using feature extraction, feature selection and classification algorithm, JSME International Journal Series C Mechanical Systems, Machine Elements and Manufacturing, Vol. 9, No. 3, (2006), pp. 734-741.

[93] Zang, C., Friswell, M. I., & Imregun, M., Structural damage detection using independent components analysis, Structural Health Monitoring, Vol. 3, No. 1, (2004), pp. 69-83.

[94] Ypma, A. and Pajunen, A. P., Rotating machine vibration analysis with second order independent components analysis, Proceeding of the Workshop on ICA and Signal Separation, (1999), pp. 37-42.

[95] Sohn, H., Czarnecki, J. A. and Farrar, C. R., Structural health monitoring using statistical process control. Journal of Structural Engineering, Vol. 126, No. 1, (2000), pp. 1356-1363.

[96] Worden, K. and Manson, G., Visualization and dimension reduction of high-dimensional data for damage detection, IMAC, Vol.17, (1999), pp. 1576-1585.

[97] Shen, Z.J., Chen, X.F., Zhang, X.L. and He, Z.J., A novel intelligent gear fault diagnosis model based on EMD and multi-class TSVM, Measurement, Vol.45, No.1, (2012), pp.30-40.

[98] De Lima, E.R., Andrade, A.O., Pons, J.L., Kyberd, P. and Nasuto, S.J., Empirical mode decomposition: a novel technique for the study of tremor time series, Medical and Biological Engineering and Computing, Vol.44, No.7, (2006), pp.569-582.

[99] Cheng, G., Cheng, Y.L., Shen, L.H., Qiu, J.B. and Zhang, S., Gear fault identification based on Hilbert–Huang transform and SOM neural network, Measurement, Vol.46, No.3, (2013), pp.1137-1146.

Acknowledgements

I would like to express my sincere thanks to all who have helped me to complete this work. The completion of this work would be impossible without their support and advice.

Above all, I would like to express gratitude to my supervisor Prof. Nagamura for his guidance and advice. He has given me so much help and advice in my subject research, writing papers, Japanese learning, even daily life in Japan during all my doctoral course. I admire him for his rigorous working amplitude, preciseness and patience in teaching. I would like to thank our Assistant Prof. Ikejo for his valuable help and advice to my research. He has given me so much help and advice in writing journal papers. I have learned much from their experience and knowledge about the academic, work and social life. I would also like to thank our team members Mr. Yamamoto, Mr. Kawada, Mr. Hashimoto and Mr. Okada. They helped me to perform the experiments, and taught me the basic knowledge about our research and the measurement method in the experiment. Without them, I would not successfully complete the doctoral course according to the schedule. I also want to thank the graduated Chinese students, also my friends, Mr. Liu and Mr. Shen. They have done a lot of efforts for me to be enrolled in Hiroshima University. They also helped me to start the new life and research in Japan. I would also like to thank all the laboratory mates. They are a group of young men with good abilities, enthusiasm, outgoing personality and optimism. They helped me to learn Japanese language and culture through conversations or some activities, like seminar travel, drinking parties and so on.

I would like to express my sincere gratitude to my parents, brother, sisters and other families. Their love, support and encouragement keep me going forward. All my families support and encourage me to have a further study in Japan. Without their support, I would not have the courage to pursue the doctoral degree and study abroad. I would also like to sincerely thank my sweet lover Mr. Guo. For accompanying me to study in Japan, he gave up the decent job in China. His love, careful attention, support and encourage make my life in Japan become happy and give me full of confidence in completing the doctoral course. I also want to thank all my dear friends in Japan. We came together like a big family. Their selfless friendship and help make the life rich in Japan.

Last and not least, I would like to thank the staff in Hiroshima University and all the Japanese around us. They provided nice, peaceful environment and help for us to research and living in Japan.

Publications

Journal Papers and Conference Papers

1. Qingrong FAN, Kiyotaka IKEJO, Kazuteru NAGAMURA, Masato KAWADA, Mitsuo HASHIMOTO, **Application of statistical parameters and discrete wavelet transform to gear damage diagnosis**. *JSME: Journal of Advanced Mechanical Design, Systems, and Manufacturing*, Paper No. 14-00057, Vol.8, No.2, 2014.

2. Qingrong FAN, Kiyotaka IKEJO, Kazuteru NAGAMURA, Masato KAWADA, Mitsuo HASHIMOTO, **Gear damage diagnosis and classification based on support vector machines**. *JSME: Journal of Advanced Mechanical Design, Systems, and Manufacturing,* Paper No. 14-00058, Vol.8, No.3, 2014.

3. Qingrong FAN, Kiyotaka IKEJO, Kazuteru NAGAMURA, Masato KAWADA, Mitsuo HASHIMOTO, **Diagnosis for gear tooth surface damage by empirical mode decomposition in cyclic fatigue test**. *JSME: Journal of Advanced Mechanical Design, Systems, and Manufacturing*, Paper No. 14-00260, Vol.8, No.3, 2014.

4. Qingrong FAN, Kazuteru NAGAMURA, Kiyotaka IKEJO, Masato KAWADA, Mitsuo HASHIMOTO, **A Statistical Approach to Damage Diagnosis of Gear**. *No.13-204 proceedings of the 3rd Japan-Korea Joint Symposium on Dynamics & Control,* Kyushu Sangyo University, Fukuoka, Japan, August 27-28, 2013, pp. 227-230.

5. Qingrong FAN, Kazuteru NAGAMURA, Kiyotaka IKEJO, Masato KAWADA, Mitsuo HASHIMOTO, **A diagnosis method for gear damage based on empirical mode decomposition and support vector machines**. *The 14th Machine Design and Tribology Division Meeting in JSME*, Nagano, Japan, April 21-22, 2014, pp.67-70.

6. Qingrong FAN, Kiyotaka IKEJO, Kazuteru NAGAMURA, **Detection of damaged tooth by support vector machines**. *Proceedings of 2014 2nd Asia Conference on Mechanical and Materials Engineering (ACMME 2014), Applied Mechanics and Materials*, Taipei, Taiwan, July 28-29, 2014, Vol. 627, pp.79-83.

Vita

Qingrong Fan, daughter of Xuecai Fan and Aiying Xin, was born on September 20th, 1986, in Juancheng, Shandong Province, China. She enrolled in Daqing Petroleum Institute and majored in Process Equipment and Control Engineering in September 2004, and was awarded the Bachelor Degree of Engineering in July 2008. Then she entered the Graduate School, Huazhong University of Science and Technology in September 2008 and majored in Mechanical Design and Theory. She was awarded the Master Degree of Engineering in June 2011. Then, she was awarded a scholarship under the State Scholarship Fund to pursue her study in Japan and entered Hiroshima University as a PhD student in October 2011.